Master's thesis

NTNU
Norwegian University of Science and Technology
Faculty of Information Technology and Electrical Engineering
Department of Electric Power Engineering

Trude Birgitte Byre

Modelling and Stability Analysis of Diode-Bridge Rectifier-Synchronous Generator Systems

Master's thesis in Energy and Environmental Engineering
Supervisor: Kjetil Uhlen
Co-supervisor: Atle Rygg
June 2021

NTNU
Norwegian University of Science and Technology

Trude Birgitte Byre

Modelling and Stability Analysis of Diode-Bridge Rectifier-Synchronous Generator Systems

Master's thesis in Energy and Environmental Engineering
Supervisor: Kjetil Uhlen
Co-supervisor: Atle Rygg
June 2021

Norwegian University of Science and Technology
Faculty of Information Technology and Electrical Engineering
Department of Electric Power Engineering

NTNU
Norwegian University of
Science and Technology

Preface

The following master's thesis concludes my Master of Science degree in Energy and Environmental Engineering at the Department of Electric Power Engineering at the Norwegian University of Science and Technology.

The work carried out in this thesis is based on the foundation developed during my years in Trondheim and Lausanne. I can now look back at a five-year-long journey filled with challenges, victories and defeats, joy and disappointments. This journey has made me grow, both as a person and as an academic. I feel privileged by achieving knowledge about such an important field of study: electrical power systems, stability and control theory, electrical machines and power electronics. The submission of this thesis marks the end of these five years, but also the beginning of my discovery within these matters.

Even though I am the author behind this thesis report, there are several people to whom I owe my gratitude. First, I would like to thank my supervisor, Professor Kjetil Uhlen, for his guidance and for sharing his extensive knowledge within power system stability. Without his support and wisdom, all my struggle with model development would have gone to waste.
Second, I would like to thank my co-supervisor, Atle Rygg in Siemens, for providing me system data and for his availability for discussions regarding to the system under study. In addition, I am truly grateful because Siemens was giving me the opportunity to study such an exciting topic.
Third, I will show my gratitude to Dosent Emeritus Trond Leiv Toftevaag, as an interlocutor, for his support, assistance, and for sharing his experiences within electrical machines.

Last, but not least, I would like to thank my friends, my family and my boyfriend for all their support, love and motivating words throughout the course of this work.

Trude Birgitte Byre
Trondheim, June 14, 2021

Abstract

The shipping industry is under social and regulatory pressure to decarbonize its operation and reduce greenhouse gas emissions. Electrification is a fundamental factor in achieving this goal, especially when the amount of renewable power delivered to the transmission grid grows at the same rate as the power consumed. Concerning electrification of the shipping industry, power electronics converters and electric motor drives are being used at an increasingly rapid rate. However, with new technology follows complications regarding system reliability and stability. Synchronous generators in combination with three-phase diode-bridge rectifiers exist in shipboard power systems today. However, not well-understood instabilities are discovered by previous literature in such kind of systems.

In this thesis, a synchronous generator connected to a battery through a three-phase diode bridge rectifier is under study. A simplified model is developed, that facilitates studying and aiding the understanding of the addressed unstable behaviour. The new model was implemented with the idea of keeping it as simple as possible, only including the system components which are believed to be necessary in order to study the unstable phenomenon. The simplified model contains a fifth-order synchronous machine model, an average-value rectifier model, and a DC circuit. The mechanical part of the machine is neglected. The DC circuit consists of a battery, modelled as an ideal DC voltage source connected in series to an internal battery resistance, which is further connected in parallel with a filter capacitor. The simplified model is validated and compared to a detailed simulation model implemented using Simulink/Matlab system blocks and is shown to follow it quite well.
The simplified model is further linearized, and modal analysis techniques are performed. An unstable pair of complex eigenvalues are detected, participation factors are calculated, and sensitivity analysis is conducted. Five different synchronous generator sets are considered during the sensitivity analysis. Moreover, varying combinations of synchronous generators, three-phase diode-bridge rectifiers, and a battery, are studied to explore how the presence of system components affect the presence of the unstable behaviour.

This thesis shows that the unstable phenomenon occurs independently of an AVR and a Governor system. It also shows that instability occurs even though the generator is operated in the absence of a mechanical system. Thus, well-known rotor oscillations are not a part of the underlying problem, and the instability is considered an electromagnetic phenomenon, not an electromechanical phenomenon. Further, based on the fact that the simplified model became unstable, despite that the dynamics associated with diode switching were removed, this indicates that the diode commutation as such is not part of the underlying problem.

The sensitivity analysis conducted indicates x'_d, x'_q and x_q to be the system parameters influencing the real part of the complex pair of unstable eigenvalues the most, followed by T''_{qo} and x''_d. Furthermore, the sensitivity analysis results show that the system improves stability by moving in a specific direction with respect to the d- and q-axis components, either by increasing the q-axis component and decreasing the corresponding d-axis component, or the opposite. As an example, in order to positively affect the system stability, the system wants to increase x'_d and T''_{qo} and decrease x'_q and T''_{do}, respectively. Increasing x'_d such that x'_d is sufficient close to the value of x'_q, solves the challenge concerning low-frequency system oscillations. These observations are in accordance with the stability criteria, $\frac{x_\mathrm{q}}{2x'_\mathrm{d}} \leq 1$, proposed by previous literature for synchronous generators satisfying $x'_q = x_q$.

This study has further shown that an unfavourable type of DC load, not contributing with sufficient damping, needs to be present for the unstable phenomenon to occur. This further indicates that the characteristics associated with the DC load, in addition to an unfavourable relationship between the d-axis and q-axis parameters in the generator, are important parts related to the instability.

To conclude, regardless of the underlying reason causing the instability, the unstable phenomenon can be considered a transient electromagnetic phenomenon that primarily depends on the transient reactances and time constants.

Sammendrag

Skipsfartsindustrien er under sosialt og regulatorisk press for å redusere karbonisering av drift og klimagassutslipp. Elektrifisering er en grunnleggende faktor for å oppnå dette målet, spesielt når mengden fornybar kraft levert til overføringsnettet øker i samme hastighet som mengden kraft forbrukt. Når det gjelder elektrifisering av skipsindustrien, brukes kraftelektronikk og elektriske motordrifter i økende grad. Imidlertidig, med ny teknologi følger komplikasjoner med hensyn til systemets pålitelighet og stabilitet. Synkrongeneratorer i kombinasjon med trefasede diode-likerettere finnes i kraftsystemer om bord på skip i dag. Imidlertid har tidligere litteratur oppdaget ustabilitet, som er lite forstått, knyttet til slike systemer.

I dette studiet er en synkron generator koblet til et batteri gjennom en trefaset diode-likeretter under utredning. En forenklet modell er utviklet som forenkler studiet og hjelper til med forståelsen av adressert ustabil oppførsel. Den nye modellen ble implementert med ideen om å holde den så enkel som mulig, ved å kun inkludere systemkomponentene som antas å være nødvendige for å studere det ustabile fenomenet. Den forenklede modellen inneholder en femteordens synkron maskinmodell, en likeretter modell for gjennomsnittsverdi og en DC-krets. Den mekaniske delen av maskinen er neglisjert. DC-kretsen består av et batteri, modellert som en ideell DC-spenningskilde seriekoblet til en intern batterimotstand, og videre koblet parallelt med en filterkondensator. Den forenklede modellen er validert og sammenlignet med en detaljert simuleringsmodell implementert ved bruk av Simulink/Matlab systemblokker og har vist å etterligne den ganske bra.
Den forenklede modellen er videre linearisert og modal-analyseteknikker utføres. Et ustabilt par av komplekse egenverdier oppdages, deltakelsesfaktorer beregnes og følsomhetsanalyse utføres. Fem forskjellige synkrongeneratorsett vurderes under følsomhetsanalysen. Videre studeres forskjellige kombinasjoner av synkrongeneratorer, trefasede diode-likerettere og et batteri for å undersøke hvordan tilstedeværelsen av systemkomponenter påvirker tilstedeværelsen av ustabil oppførsel.

Dette studiet viser at det ustabile fenomenet forekommer uavhengig av en AVR og et Governor system/turbinregulerende system. Det viser også at ustabilitet oppstår selv om generatoren drives i fravær av et mekanisk system. Dermed er ikke velkjente rotorsvingninger en del av det underliggende problemet, og ustabiliteten betraktes som et elektromagnetisk fenomen, ikke et elektromekanisk fenomen. Videre, basert på det faktum at den forenklede modellen ble ustabil, til tross for at dynamikken knyttet til diodebryting ble fjernet, indikerer at diodekommuteringen som sådan ikke er en del av det underliggende problemet.

Følsomhetsanalysen som er utført indikerer at x'_d, x'_q og x_q er de systemparameterene som mest påvirker den reelle delen av det komplekse paret av ustabile egenverdier, etterfulgt av T''_{qo} og x''_d. Videre viser resultatene fra følsomhetsanalysen at systemet forbedrer stabiliteten ved å bevege systemet i en bestemt retning med hensyn til d- og q-akse-komponentene, enten ved å øke q-akse komponent og redusere d-akse komponent tilsvarende , eller motsatt. For eksempel, for å kunne påvirke systemstabiliteten positivt, ønsker systemet henholdsvis å øke x'_d og T''_{qo} og redusere x'_q og T''_{do}. Økning av x'_d slik at x'_d er tilstrekkelig nær verdien av x'_q, løser utfordringen angående lavfrekvente systemoscillasjoner. Disse observasjonene er i samsvar med stabilitet-skriteriene, $\frac{x_\mathrm{q}}{2x'_\mathrm{d}} \leq 1$, foreslått av tidligere litteratur for synkrongeneratorer som tilfredsstiller $x'_q = x_q$.

Dette studiet har videre vist at en ugunstig type DC-belastning, som ikke bidrar med tilstrekkelig demping, må være til stede for at det ustabile fenomenet skal oppstå. Dette indikerer videre at karakteristikkene knyttet til DC-belastningen, i tillegg til et ugunstig forhold mellom d-aksen og q-akse parameterene i generatoren, er sentrale når denne ustabiliteten vurderes.

For å konkludere, uavhengig av den underliggende årsaken som forårsaker ustabiliteten, kan det ustabile fenomenet betraktes som et forbigående elektromagnetisk fenomen som først og fremst avhenger av de forbigående reaktansene og tidskonstantene.

Contents

List of Tables

List of Figures

List of Abbreviations

AC Alternating Current

AVR Automatic Voltage Regulator

d-axis direct axis

DC Direct Current

EMF Electromotive Force

GHG global greenhouse gas

IMO International Maritime Organization

PF power factor

q-axis quadrature axis

RMS root mean square

THD total harmonic distortion

THD total harmonic distortion

Chapter 1

Introduction

1.1 Motivation and Background

The maritime industry, like any other transportation system, is dominated by the use of fossil fuels, which has a negative impact on the climate change [1]. The International shipping worldwide is responsible for about 2.5% of the total global greenhouse gas (GHG) emissions [2]. Consequently, the maritime industry is experiencing an increasing pressure to decarbonize its operations and to reduce emissions to air [3; 4]. The International Maritime Organization (IMO) agreed in 2018 on a strategy that included to reducing a total amount of at least 50% annually, of GHG emissions until 2050 [5]. Norway has decided to achieve zero-emissions in world heritage fjords within 2026 with respect to cruise ships and ferry vessels [6]. In this context, the global interest has increased regarding turning the marine industry from fossil fuels into electricity [7].

The electric power system of ships has primarily been based on the Alternating Current (AC) system for a long time [8; 9]. However, the rapid development of modern power electronic technologies seems to facilitate a future utilizing DC based shipboard power systems [7; 9; 10; 11]. The DC based power system is claimed to improve the electrical performance, to be more fuel efficient and to save weight and space [11; 12; 13].

In addition to space and weight, costs are of high priority on shipboard power systems. Considering DC shipboard power systems, the synchronous generator in combination with a three-phase diode-bridge rectifier is an existing solution today. The synchronous generators enables the use of the passive diode-bridge rectifier, which is cheap. In addition to their low cost, diode rectifiers occupies less volume, they have a high electromagnetic compatibility as well as reliability and are therefore often to prefer compared to PWM rectifiers [14]. However, previous papers and reports have addressed not-well understood instabilities in such kinds of systems [15; 16; 17; 18]. Low frequency oscillations are detected in the output current, power and voltage and makes a normal operation of the system unpleasant.

1.2 Objective

The aim of this thesis is to better understand why a synchronous generator connected to a battery through a diode-bridge rectifier, or multiple synchronous generator-rectifier system connected in parallel at the dc side becomes unstable. Previous literature studying this unstable phenomenon exist, but a complete explanation of the physics behind is still not completely known.

The specific objective of this thesis is to develop a simplified model that facilitates studying and aiding the understanding of this unstable phenomenon.

1.3 Scope of Work

- Present a brief state-of-the art related to unstable behavior of diode-bridge rectifier-synchronous generator systems.
- Present relevant theory and mathematical equations.
- Establish a model of a synchronous generator connected to a battery through a diode-bridge rectifier, able to reproduce the unstable behaviour, in a proper simulation tool.
- Investigate whether the Automatic Voltage Regulator (AVR) or the Governor is the reason itself to the instability associated with diode-bridge rectifier-synchronous generator systems.
- Investigate whether the instability is an electromagnetic or electromechanical phenomenon.
- Develop a simplified mathematical model of the unstable system in a proper software development tool. The aim is to keep the model simple, but accurate enough to reproduce the unstable behavior.
  Remove components that seem not to be causing the unstable phenomenon.
- Validate the simplified mathematical model against the detailed Simulink model.
- Perform linear analysis techniques on the simplified mathematical model.
- Investigate how different system parameters influence the instability. This for different synchronous generators, both salient pole rotor, and cylindrical pole rotor.
- Explore how the presence of system components affect the presence of the unstable behaviour.
- Perform discussion, conclusion and suggestions for further work.

1.4 Approach to Analysis

This section aims to present the appropriate process used to develop a simplified model that facilitates studying and aiding the understanding of this unstable phenomenon.

The models used during this thesis were developed based on the idea of keeping them as simple as possible, only including system components that are believed to be necessary in order to study the unstable phenomenon. This was done in order to facilitate a better understanding of the underlying phenomenon. First, a *detailed* simulation model was implemented by the use of Simulink/Matlab system blocks from the ”Simscape Electrical Specialized Power Systems” library. This model did not contain an AVR or a governor system and the generator was operated with constant rotor speed. When the model yielded reasonable responses, the model was investigated to understand whether the model contains enough system components to be able to study the unstable phenomenon. This was investigated by performing simulations based on previous experiences of triggering the unstable behaviour. When this simulation model enabled to reproduce the instabilities, a new simplified mathematical model was derived based on this detailed model.

The new simplified model contains mathematical equations describing the system under study. This model is based on a fifth-order synchronous generator, the mechanical system is removed, and the diode rectifier is presented by an average value model. The dynamic associated with diode-switching is neglected. Numerical simulations of the mathematical equations were performed until reasonable responses were achieved. Also here, simulations based on previous experiences of triggering the unstable behaviour were performed. When the simplified model enabled to reproduce the instabilities, it was validated and compared to the detailed model.

The simplified model, which is continuous and non-linear, was further linearized to facilitate linear analysis techniques. The mathematical equations were implemented in Matlab code and further linearized by calculating the state matrix $\mathbf{A}$. To ensure that the model was correctly linearized another method was used for calculating $\mathbf{A}$. This was further used to verify the first obtained matrix. Next, the system eigenvalues were calculated for different operation points in order to understand whether linear analysis techniques are an appropriate tool to further study the unstable phenomenon. The eigenvalues were evaluated based on whether it was possible to detect a complex pair of unstable eigenvalues that corresponded to the time-domain responses, achieved by executing the simplified mathematical model for the corresponding operating cases.

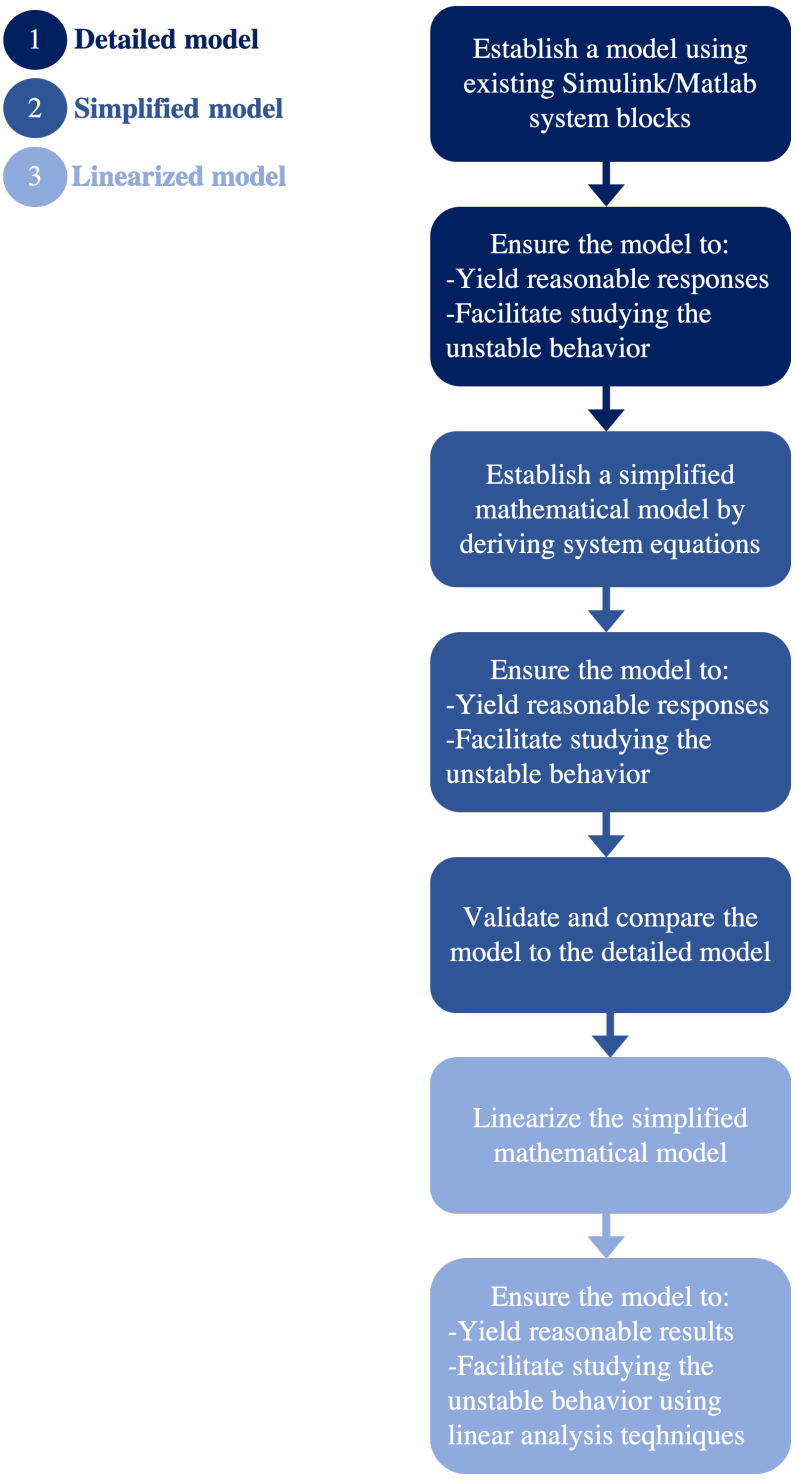

Figure 1.1: Flow chart summarizing the approach used in the thesis work. First, the detailed simulation model was implemented. Second, based on the detailed model, a simplified mathematical model was derived. Third, the simplified mathematical model was linearized.

1.5 Relationship to Previous Work

This master thesis is related to the specialisation project report [19] written in the fall of 2020. This specialisation project report contains a literature review about unstable behaviour of diode-bridge rectifier-synchronous generator systems and a model implementation of parallel connected diode-bridge rectifier-loaded synchronous generators, in Matlab/Simulink, able to reproduce the unstable phenomenon highlighted by the previous literature. This master thesis is a continuation of the specialisation project work, but to make this thesis a complete and independent unit in and of itself, some sections have been included and some of the content have been rewritten and reworded. This will be explicitly marked at the beginning of the respective chapters, where applicable.

1.6 Outline

The master's thesis is divided into 8 chapters where the first chapter is the introduction. The remaining chapters are structured as follows:

Chapter 2 presents the problem description. This includes a description of the system under study, a brief state-of-the-art review, existing methods for modelling the studied system as well as the main results from the specialisation project work carried out in the fall of 2020.

Chapter 3 forms the theoretical foundation on which to form the remaining thesis. It builds the necessary understanding of stability analysis methods and includes a description of the three-phase diode-bridge rectifier and the synchronous generator to be modelled.

Chapter 4 describes the process of modelling the studied system, both the detailed simulation model and the simplified numerical model. It further includes the model validation and the linearization processes, limitations and simplifications made, the cases to be studied in addition to the methods used.

Chapter 5 contains the results obtained when the cases presented in 4 are conducted. The results are further discussed in Chapter 6, together with other remarks made during the thesis.

The conclusions drawn from the thesis are presented in Chapter 7. Chapter 8 contains suggestions for further work based on the remarks made in the thesis. Thereafter, the bibliography and appendices are found.

Chapter 2

Problem Description

Disclaimer: Some of the contents in Section 2.1, 2.2 and 2.4 are retrieved from [19] while some are only based on what was done in [19], but have been rewritten and reexplained.

This chapter aims to introduce the system under study, a state-of-the-art review, existing methods for modelling the studied system as well as the main results from the specialisation project work carried out in the fall of 2020.

2.1 The System Under Study

Previous literature has detected unstable behaviour related to diode-bridge rectifier-synchronous generator systems. Two examples of such systems are depicted in Figure 2.1a and Figure 2.1b. A diode-bridge rectifier-synchronous generator is operated in parallel with another set (Figure 2.1a), or in parallel with a battery (Figure 2.1b), feeding a common Direct Current (DC)-load. Such topologies could typically be found as a part of a shipboard power system today. The propulsion loads represent the main DC load, and they are usually tightly regulated by the use of motor drives and power electronic converters. However, the DC-load do not have to be a propulsion drive in order to create the unstable behaviour, it could be a pure resistive load. Shipboard power system is an example of a isolated and independent power system. The topology shown in Figure 2.1a was studied during the specialisation project work [19], fall 2020, while the topology shown in Figure 2.1b is to be further studied during this master thesis.

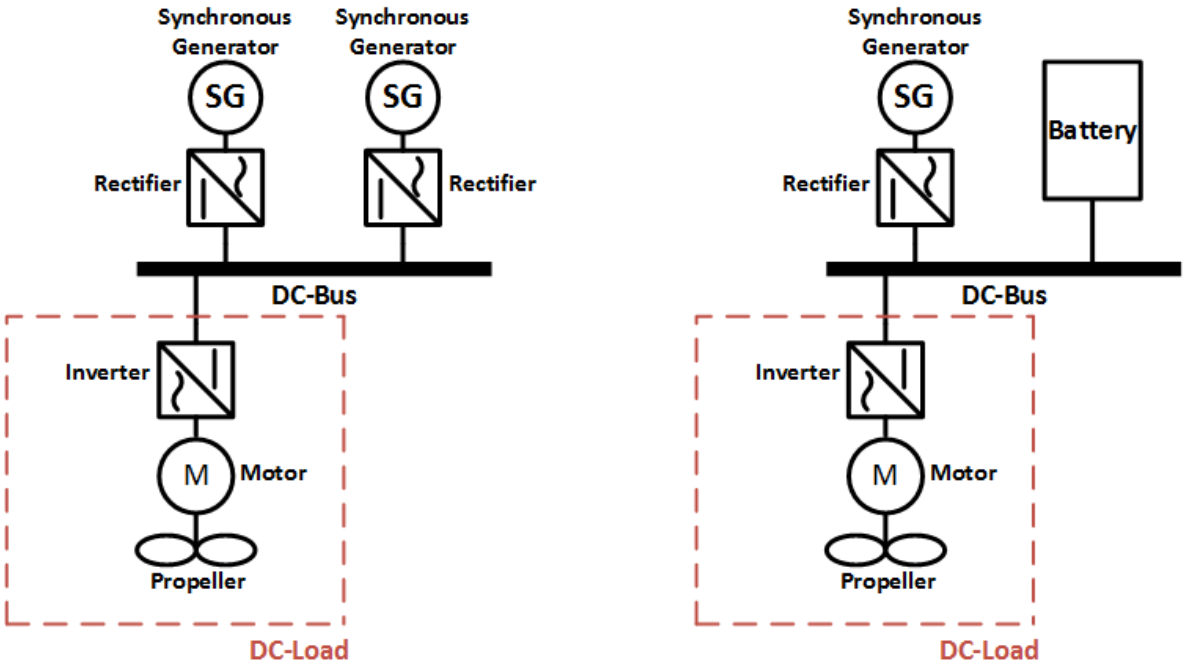

Figure 2.1: Principle schematics of unstable systems to be further analyzed. (a) Two rectifier synchronous generator sets operate in parallel feeding a common DC-load, here modeled as a propulsion load. (b) A rectifier synchronous generator set operates in parallel with a battery feeding a common DC-load, here modeled as a propulsion load.

The operation of a generator connected to a diode rectifier is characterized by the fact that the current can only flow if the instantaneous value of the generator voltage level is higher than the voltage at the output of the rectifier. The current in the generator will then start flowing abruptly. The course of the current is largely determined by the characteristics of the DC load and can be understood as a transient process, at least for the start of the current flow. The voltage at the output of the rectifier is created by batteries and capacitors arranged in the DC circuit, by AC drives or by other parallel connected generator-rectifier systems.

2.2 State-of-the-Art

Instabilities are addressed when a diode-bridge rectifier-synchronous generator system, both salient-pole and round rotor structure, operates in parallel with each other or in parallel with a battery, on an isolated power system. The instability occurs during normal load and it is detected by low frequency oscillations (1-5 Hz) in the output current, power and voltage [15], [17], [20]. The following subsection summaries literature concerning this unstable behaviour. However, existing literature about this type of instability is limited.

Two master thesis at NTNU from 2015, [21], and 2016, [22], as well as their corresponding specialisation projects from 2014 and 2015 have examined instabilities related to this kind of

system. Unstable operation in a diesel-electric propulsion system on a tugboat is the reason behind their studies. Their main findings are listed below:

- The synchronous generator is believed to operate in the transient state due to the constant switching caused by the diode-bridge rectifier.
- Replacing the diode-bridge rectifier with a thyristor rectifier does not get rid of the unstable oscillations itself. However, the stability was improved by reducing the the gain of the AVR in addition to the DC voltage (by increasing the firing angle α). Reducing the DC voltage leads to a reduced time delay for the system currents. Therefore, by using thyristors instead of diodes, one can control these unstable behaviours.
- What is connected to the DC-side is an influencing factor. It was found that the system, with a battery connected to the DC terminals, regains its stability when the synchronous generator was supplying a load close to the rated capacity of the synchronous generator.
- The frequency of the undamped oscillations is about 1.2 Hz $-$ 2.7 Hz.
- The generator parameters, synchronous-, transient- and subtransient reactances, have an important impact on the system stability. The system is only unstable for certain values and combination of parameter values.
- The instabilities are believed to be related to poorly damped synchronous generators.
- Increasing the inertia constant or installing an additional q-axis damper winding on the rotor of the synchronous generator improves the system stability.

Weiming [17] asserts that researchers studying generator-rectifier systems tend to model the generator as an ideal voltage source and focus on the performance of the rectifier and the connected load. For the system described in last subsection, 2.1, rectifier-loaded generator systems become strongly nonlinear due to the presence of the diode-bridge rectifier, thus making the stability analysis rather complicated. This system operates isolated with the absence of a stiff grid and thus, by considering the generator as an ideal voltage source, factors related to the generator that might influence the system stability are lost. Therefore, it is important to study the synchronous generator as well. During the commutation of a three-phase diode-bridge rectifier synchronous generator, the generator is briefly loaded by a suddenly applied 2-phase short circuit and the machine flux is appropriate to this condition. Due to this, transient and subtransient reactances should be taken into account when studying this system. [23]

Auinger [15; 16], states that compared to a conventional stiff grid connection, a diode-bridge rectifier causes the subtransient and transient reactances to participate during stationary operation. This because of the switching operation in the diodes, that for a three-phase diode-bridge rectifier occurs six time each period. He further states that oscillations are observed in the output voltage and that they might originate from physical well-known rotor angle oscillations.

Auinger suggests that these rotor-oscillations are amplified by the rectifier due to the one side blocking effect of the rectifier, which occurs when the voltage at the rectifier output is larger than the instantaneous value of the generator voltage. Therefore, when an active load, such as a battery, is presented on the DC-side, a counter DC voltage is present and impulse behaved current flow with large oscillations might take place and might make a normal operation of the system unpleasant. This phenomenon is studied in [15] and Figure 2.2 is showing this undesirable phenomenon. The rectifier current, I_g, oscillates with a frequency about 1.43 Hz. Auinger [15, p.2-3] motivates his hypothesis by the following explanation;

"Power can only be delivered to the DC side when the generator voltage is at least equal to the counter DC voltage. While the current is driven by the full generator voltage with a passive load, only the (vector) difference between generator and counter DC voltage is effective when connected to an active load. An increase in load leads to a deceleration of the pole wheel, δ, and at the same time to a "compounding" process in the q-axis. Depending on the machine constants, this transient behaviour usually takes place in a damped oscillation. In the case of unfavorable relationship of the transient time constants of the d- and q-axis, however, an undamped oscillation can also arise (Figure 2.2). With small oscillation amplitudes, a DC current is generated on the load side, on which an alternating component of low frequency is superimposed. However, if the oscillation amplitudes of the current are greater than the DC component, the diode in the rectifier blocks when the current tries to go through zero and the voltage u_d, induced by the windings in the q-axis, goes to zero. The voltage u_q, induced by the the d-axis windings, increases with a time constant T'_{d0} until it becomes equal to the DC counter voltage again, and the current can thus start flowing again."

Moreover, in [15, p.3] Auinger expresses that large current amplitudes can occur especially in machines without a damper cage, because their q-axis field can rise almost instantly. With the usual dimensioned damper cage, the build-up of the field in the q-axis is only slightly delayed. The oscillating behavior is similar to that of a machine without a damper cage with the difference that the current increases a little more slowly which further leads to a less abruptly start of the oscillations.
Synchronous generators designed for rectifier operation are often designed without such damper cage such that the diodes of the power rectifier are less endangered in the event of a short circuit on the DC side. The maximum short-circuit current is reduced by an increased subtransient reactance, which can be achieved most easily by omitting the damper cage.

Auinger [15] concludes that under certain boundary conditions, during transient state, the synchronous generator experiences an increase in output voltage, although the machine is operated with constant excitation and constant stationary load. The increase in voltage with a constant - or even increasing - current has the consequence that a negative internal resistance must be assigned to the generator and thus an unstable operating state is present. Auinger believes that these instabilities occur in relationship with the well-known rotor angle oscillations and that

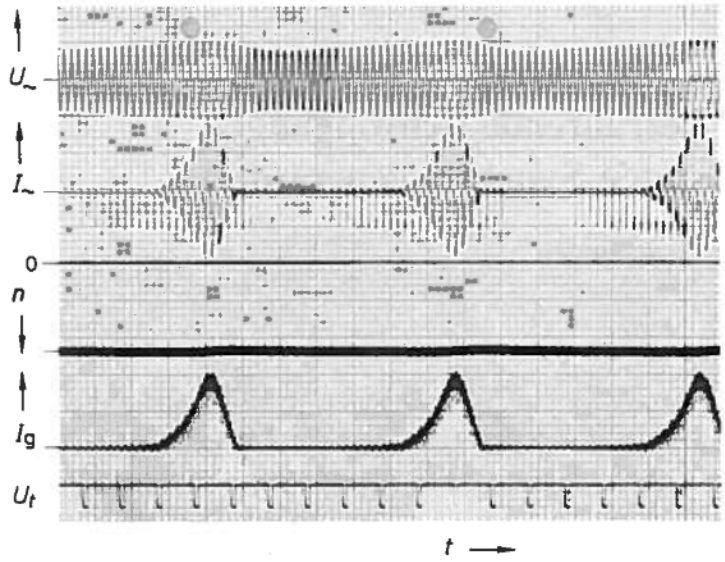

Figure 2.2: Unstable response of a diode-bridge rectifier synchronous generator connected to a battery. U , I represents the generator voltage and current while n is the rotation per minute and I_g is the rectifier current. Each mark on the bottom line marks 0.1 s [15]

these will lead to oscillations of the output voltage. Differences between the transient d- and q-axis time constants are also believed to be a part of the problem.

Weiming and Auinger ([15], [17], [16]) have highlighted $\frac{X_q}{X'_d}$ as a critical relationship when considering stable operation of diode-bridge rectifier-synchronous generator systems. When this relationship becomes greater than or equal to 2, instability may occur for synchronous generators that satisfies $x'_q = x_q$. Because this is not always the case for round rotor structure, these generators needs to be assessed more critically with regard to this ratio, $\frac{X'_q}{X'_d} = \frac{X_q}{X'_d}$.
The same criteria, $\frac{X_q}{X'_d} \leq 2$, is also investigated in [21] and it is verified both by simulations and by real life experiences in shipboard power systems. The criteria is summarised in Equation 2.1 and rewritten in Equation 2.2.

$$\frac{X_q}{X'_d} \leq 2 \tag{2.1}$$

$$\frac{X_q}{2X'_d} \leq 1 \tag{2.2}$$

Weiming [17] states that Equation 2.1 is too harsh for conventional generator design and provides an alternative for generators with short circuited q-axis windings. This alternative is given by Equation 2.3.

$$\frac{1}{X_q} + \frac{1}{X'_q} \geq \frac{1}{X'_d} \tag{2.3}$$

Because $x'_q \leq x_q$, 2.3 will be easier to fulfil compared to 2.1. Weiming namely concludes that installing a short circuited q-axis winding on the machine rotor will improve the system stability by getting rid of the low-frequency current oscillations. Auinger [16] also argues for

installation of an additional short circuited q-axis winding, able to delay the field-build-up in the generator quadrature axis (q-axis). Installing a short-circuited rotor winding in the q-axis, with a sufficiently large time constant, capable to act against changes in the induced q-axis magnetic field, should according to Auinger ensure that the undamped oscillations no longer occur. A special design of the exciter winding is also believed to solve the problem [16, p.86].

Hoeijmakers derives a fourth order model for the synchronous machine connected to a three phase bridge rectifier in [24]. The model derived is further investigated in [18]. The system is linearized and factors influencing the stability of a diode-bridge rectifier-loaded synchronous generator are examined. Hoeijmakers experiences the following:

- Increasing the q-axis damper resistance, the q-axis inductance, the commutation inductance and the DC inductance move the poles in the complex plane towards the right, thus reducing the damping properties which have a negative impact on the system stability.
- Increasing the d-axis damper resistance and the field resistance move the poles in the complex plane towards the left, thus increasing the damping properties which have a positive impact on the system stability.

Further, Hoeijmakers [18, p.87] attempt to explain the physical behaviour of the instability in the following way:

”By having in mind that the considered DC system can remind of synchronous machine with resistor loading, a sudden loading will result in a rapid increase of the q-axis current. As a consequence, the q-axis flux increases suddenly due to the small q-axis damper time constant. On the other hand, the resulting decrease of the direct axis (d-axis) flux follows slowly due to the relative large excitation winding time constant. As a result, the total machine flux as well as the generator voltage and the DC current will experience an increase following by a decrease back to its steady-state value, which is lower compared to its original value.”

Hoeijmakers [18, p.87], further states that a stable system may be achieved by increasing the q-axis time constant (decreasing the q-axis damper resistance) or by decreasing the excitation time constant (increasing the excitation winding resistance). He concludes that all system parameters influence the dynamic behaviour and that the q-axis damper winding resistance is considered as the most importance when consider system stability.
Damper windings prevent changes in armature flux from entering the rotor during subtransient state. In the transient state, the air-gap flux, which rotates at the synchronous speed, is no longer prevented from entering the damper windings and it induces and emf and current whenever the rotor speed deviates from the synchronous speed which further produces a damping torque that tries to restore the synchronous speed [25]. The installation of such additional q-axis damper winding was performed in [22] and resulted in a stable system.

[21] presents some modification to the stability criterion given by Equation 2.1, originally introduced by Auinger [15; 16]. Auinger believes that the output oscillations were caused by oscillations in the rotor angle and amplified due to the switching of the diodes in the rectifier. However, [21] performed simulations with various values for rotor inertia in order to detect these rotor angle oscillations, but whatever value used the output oscillations were still present. As a consequence, an assumption that the voltage oscillations origins from transient currents was made. It is further believed that the transient changes in angle (load angle δ) and magnitude of the induced driving voltage are a result of the transient currents which further leads to output voltage oscillations.

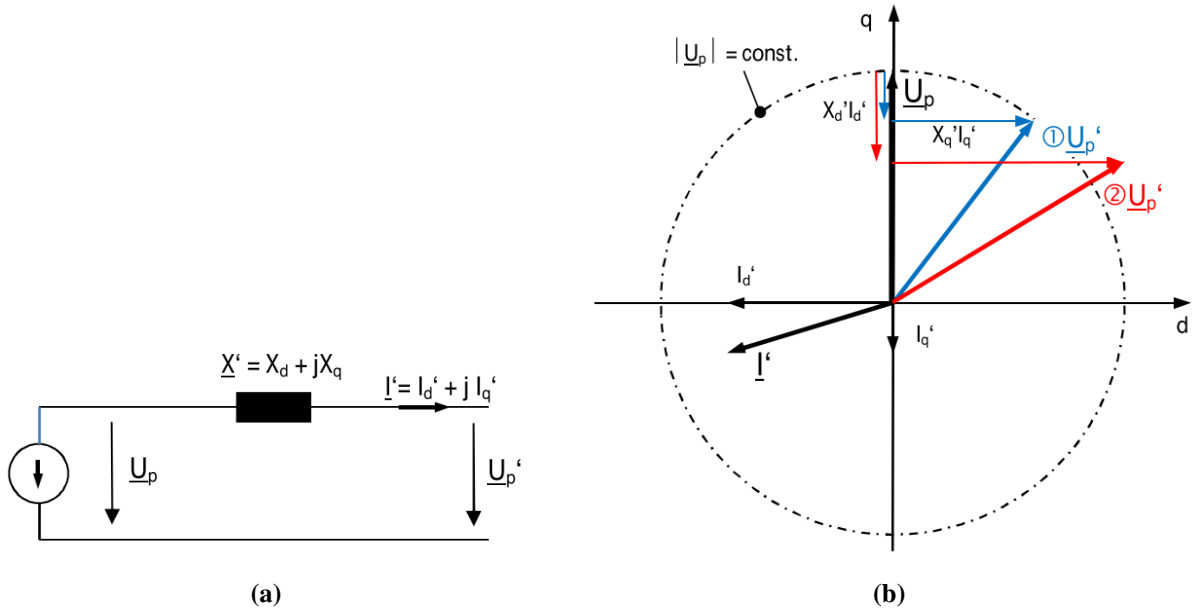

Figure 2.3: (a) Simplified equivalent circuit of the studied system. The synchronous machine operates in generator mode. (b) Vector diagram corresponding to the simplified equivalent circuit. U_p and U_p' represents the steady state source voltage and transient voltage respectively. X' represents the sum of the d-axis and q-axis transient reactance and I' the sum of the d-axis and q-axis transient current. [21]

A simplified schematic of the studied system circuit are presented in Figure 2.3a and its corresponding phasor diagram are presented in Figure 2.3b. Based on these, the following conditions are derived [21]:

- For any presence of transient current, I', transient voltage, U_p', will change with respect to the steady state source voltage, U_p.
- When the transient current, I', causes the transient voltage, U_p', to be larger than the steady state source voltage, U_p, instability occurs.

The latter leads to the following stability criteria:

$$U'_p \leq U_p$$

$$U'_p = \sqrt{(U_p - X'_d I'_d)^2 + (X'_q I'_q)^2} = \sqrt{U_p^2 \underbrace{-2X'_d I'_d U_p + X'^2_d I'^2_d + X'^2_q I'^2_q}_{\text{Must be} \leq 0 \text{ to avoid voltage increase}}} \tag{2.4}$$

$$X'^2_d I'^2_d + X'^2_q I'^2_q - 2X'_d I'_d U_p \leq 0 \tag{2.5}$$

Equation 2.5 shows that the system stability not only depends on the transient reactance, X' (X'_d, X'_q), and the transient current, I' (I'_d, I'_q), but also on the stationary operating point, U_p, before the transient behaviour takes place. The stationary operating point is expressed by the voltage U_p, which, in terms of its magnitude $|U_p|$ and angle (load angle δ), is derived from the stationary values of the terminal voltage U_{LM}, the stationary current I (I_d, I_q) and the synchronous reactance X (X_d, X_q). The amount of voltage U_p= $|U_p|$ is in turn dependent on the excitation of the generator, which must be set in stationary operation such that the desired terminal voltage is set based on the required load.

Due to to differences in time constants, the transient current will change faster than the excitation current which further makes it complicated utilizing the exciter to control the magnetizing current in order to eliminate these oscillations. [21] further states that experiences from real power systems on ships shows that the detected unstable oscillation can not be eliminated by regulating the excitation current. To stabilize the system, [21] suggests to control the transient current, I', or to replace the diode-bridge rectifier with a controlled rectifier, such as thyristors or IGBTs, which can achieve a deadtime lower than the generator transient time constant.

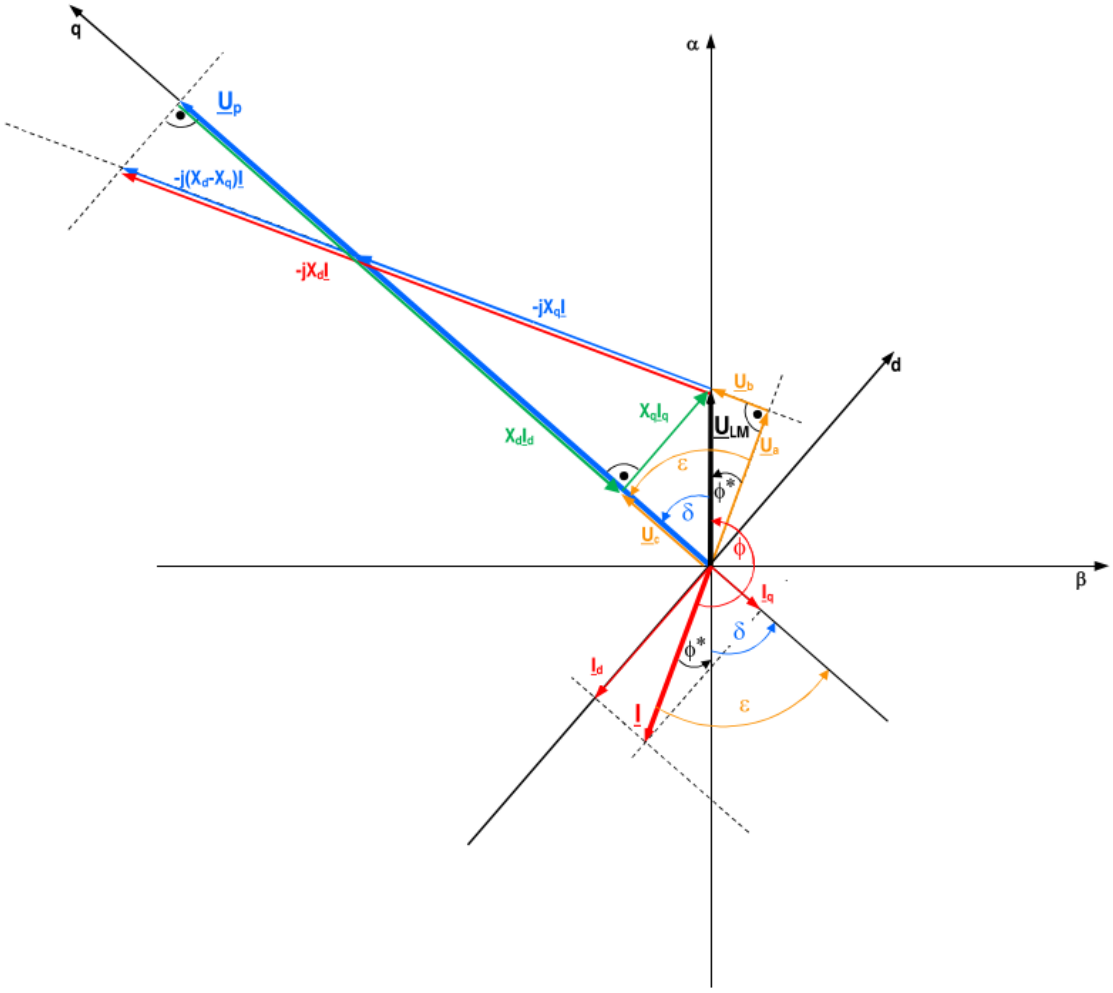

Figure 2.4: Steady state vector diagram of the studied system [21].

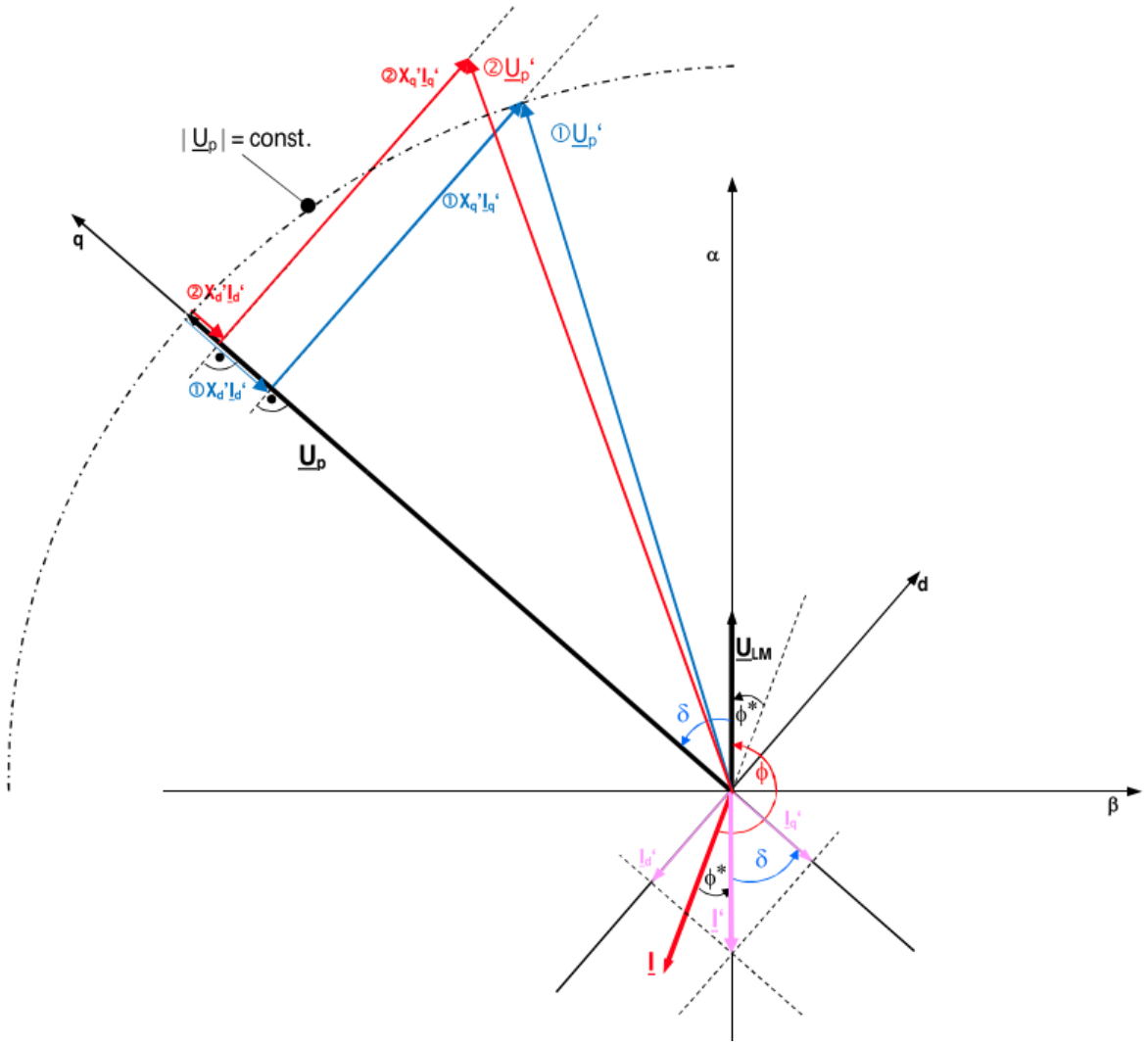

Figure 2.5: Transient vector diagram of the studied system [21].

Based on Equation 2.5 and Figure 2.4 and 2.5, [21] presents three different stability criteria for three different operating scenarios. First, by assuming $X'_q = X_q$, $\frac{X'_q}{X'_d} = \frac{X_q}{X'_d} > 1$ and that $\frac{I}{I'} = 1$, Equation 2.5 is rewritten as:

$$\frac{X'_q}{X'_d} \leq \frac{I}{I'}\left(\frac{X_d}{X_q}\frac{sin(\delta+\phi^*)sin\delta}{cos^2\delta} + \frac{cos(\delta+\phi^*)}{cos\delta}\right) \pm \sqrt{\left(\frac{I}{I'}\left(\frac{X_d}{X_q}\frac{sin(\delta+\phi^*)sin\delta}{cos^2\delta} + \frac{cos(\delta+\phi^*)}{cos\delta}\right)^2 - tan^2\delta\right)} \tag{2.6}$$

The two first assumptions yields for most synchronous machines.
Equation 2.6 is further used as a base when deriving the three following stability criteria:

Operating scenario 1

By assuming $\frac{I}{I'} = 1$, $cos\phi = cos\phi^* = 1$ $(\phi^* = 0)$, Equation 2.7 is derived. A three-phase full-bridge diode rectifier has a power factor equal to 0.995 [26] and assuming a unity power factor is therefore not too imprecise.

$$\frac{X'_q}{X'_d} = \frac{X_q}{X'_d} \leq 1 + \frac{X_d}{X_q} tan^2\delta + \sqrt{\left(1 + \frac{X_d}{X_q} tan^2\delta\right)^2 - tan^2\delta} \tag{2.7}$$

This equation shows that the rotor angle, δ, is an factor contributing to the system stability.

Operating scenario 2

By assuming $\delta \to 0°$, Equation 2.7 becomes:

$$\frac{X'_q}{X'_d} = \frac{X_q}{X'_d} \leq 2 \tag{2.8}$$

Equation 2.8 is identical to the criteria presented in Equation 2.1 investigated by Auinger and Weiming ([15], [17] and [16]). [21] states that it is experienced that this relationship yields for all loads connected to a salient-pole generators while [15] assumes it to yield for arbitrarily small loads, only.

Operating scenario 3

If instead assuming medium loading, $\delta \to 45°$, Equation 2.7 becomes:

$$\frac{X'_\mathrm{q}}{X'_\mathrm{d}} = \frac{X_\mathrm{q}}{X'_\mathrm{d}} \leq 1 + \frac{X_\mathrm{d}}{X_\mathrm{q}} + \sqrt{\left(\frac{X_\mathrm{d}}{X_\mathrm{q}}\right)^2 + 2\frac{X_\mathrm{d}}{X_\mathrm{q}}} \tag{2.9}$$

Equation 2.9 shows that the critical relationship $\frac{X_q}{X'_d}$ only depends on the generator parameters.

As this subsection has shown, some literature studying the stability of the synchronous generator-rectifier system exists, factors influencing the stability are examined, and some stability criteria are proposed. $\frac{X_q}{X'_d}$ is highlighted as a critical relationship by several studies, and the same are the proposal of installing an additional q-axis damper winding. The switching of the diodes in the full-bridge rectifier introduces transient disturbances in the internal components of the generator d- and q-axis. This, in addition to differences between the q- and d-axis transient time constants, T'_{d0}, T'_{q0}, may have a role in causing undesired output oscillations. However, due to the system complexity, a complete explanation of the physics behind the output oscillations is still not completely known.

2.3 Modelling Approaches

Modelling these diode-bridge rectifier-synchronous generator systems are of crucial importance, both for understanding the instability that occurs and for designing compensators to enhance stability and performance. The strong nonlinear and time varying characteristics of a 6-pulse diode-bridge rectifier-synchronous generator system makes the modelling process quite difficult. As mentioned in previous subsection, 2.1, because these diode-bridge rectifier-synchronous generator systems operates isolated, with the absence of a stiff grid, it is important to include a dynamical model of the synchronous generator in order to ensure that critical parameters in the machine, which might influence the unstable behaviour addressed by previous literature, are not lost.

A detailed simulation model could be used in order to investigate the dynamic behaviour as well as the stability and design of non-linear power electronic-based systems. Several methods used for this relays upon extracting an equivalent system impedance, and based on its sign, positive or negative, conclude if the system is stable or not [27; 28; 29; 30]. A positive incremental impedance tries to restore the steady-state operation point and thus acts like negative feedback and influence the system stability in a positive manner. On the other hand, a negative incremental impedance moves the system further away from the steady-state operation point thus acts like positive feedback and influence the system stability in a negative manner [31; 32]. The traditional method of extracting impedance information include frequency sweep techniques and injection of non-sinusoidal signals [33; 34; 35]
However, an effective procedure, determining the impedance over a wide range of frequencies is very time consuming, particularly when using a computationally intensive detailed simulation model that includes diode switching and obtaining many data points at very low frequencies. It might be too large for normal use. In addition, using such a detailed model will complicate stability analysis, because it will be more difficult to understand which parameters being the core of the problem, making a system unstable and which parameters to be a consequence of someone else. Moreover, a detailed switching model of a system is not suitable for small-signal analysis due to the non-time-continuity of the switching elements. For these reasons, a simplified numerical or analytical model of power electronic-based systems may be preferable.

Simplifying or eliminating the switching action of the diode-bridge rectifier is the main problem when establishing simplified numerical or analytical models of power electronic-based systems [17; 36; 37]. By eliminating the switching actions, a time-invariant model is achieved, and classical linear control theory can be applied for system analysis and design. Some commonly used methods for eliminating the switching action is the generalized state-space averaging (GSSA) modelling method, the average-value (AV) modelling method and the DQ-transformation modelling method [38; 39]. The GSSA modelling method has been used for analysis of both DC converter system [37; 39; 40; 41; 42], uncontrolled and controlled rectifiers in single-phase AC distribution systems [43; 44], and of 6- and 12- pulse diode-bridge rectifier in three-phase sys-

tems [17; 24; 14]. The AV modelling method has been used for analysis of both 6- and 12- pulse diode rectifiers [45; 46; 47; 48], and for systems containing generators with line-commutated rectifiers [47; 49; 50]. The DQ-transformation modelling method is another technique used for analysis of AC systems, including both controlled and uncontrolled three-phase diode-bridge rectifier systems, and it can treat the power converters as transformers [38; 39; 51; 52; 53].

An other modelling method is introduced by Wang in [36]. It introduces a periodic orbit model of diode-bridge rectifier-synchronous machine system by using the trapezoidal integration method. This modelling method makes it possible to study the small signal stability of a diode rectifier-synchronous machine systems through orbitally asymptotical stability of its periodic orbit so as to lay a foundation for isolated power system analysis and its control design. The choice of this model is motivated by an increased accuracy when analysing small signal stability rather than using a state space averaging model. Simulations illustrates that the model is effective and practicable.

2.4 Main Results from specialisation Project Work Fall 2020

As mentioned in subsection 1.5, this master thesis is a continuation of the work done in the specialisation project report [19] written in the fall of 2020. The specialisation project work included a model implementation, in Matlab/Simulink, of parallel operation of two diode-bridge rectifier-loaded synchronous generator sets, feeding a common constant current load, able to reproduce the unstable phenomenon highlighted by the literature mentioned in subsection 2.2. Different relationships of the stability criteria proposed by previous studies, $\frac{X_q}{2X'_d} \leq 1$, were simulated by scaling the d-axis transient reactance, X'_d. A threshold limit is found between 2.3125 and 2.4000. Undamped oscillations in the DC output currents was detected for $27\% - 50\%$ load with frequencies in the range of 2 Hz $-$ 3 Hz depending on the scaling of X'_d. The simulation results did further show that the unstable phenomenon is a function of load and that the worst-case scenario occurs when both generators are loaded about 33% load at the same time.

Figure 2.6 and 2.7 shows this unstable phenomenon, reproduced by the model developed during the specialisation project work. The DC current responses are shown in Figure 2.6 when the voltage reference of the second generator is set to 0.1% below the first generator and the DC load is increased linearly from 10% to 100% where an additional square wave with small current steps are superimposed onto the ramp in order to excite possible oscillations in the system. The relationship $\frac{X_q}{2X'_d}$ is increased from its original value by scaling the transient d-axis reactance, X'_d by a factor equal to 0.963542 such that the stability criteria presented by previous literature, Equation 2.2, is equal to 2.4. Undamped oscillations in the generator currents are observed between $27\% - 41\%$ load and the parallel operation is therefore considered unstable. The frequency of the oscillations are about 2.30 Hz $-$ 2.67 Hz. Figure 2.7 shows a zoomed version of Figure 2.6, between 14 s $-$ 32 s.

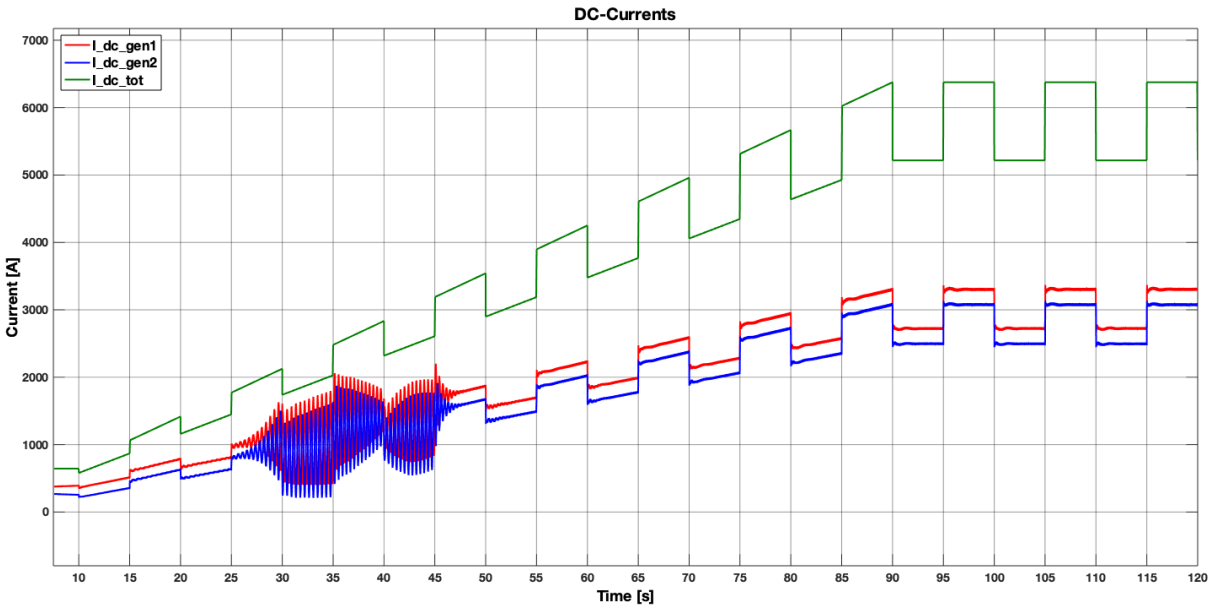

Figure 2.6: DC current responses when two rectifier-generator sets powers a common constant current load. $\frac{X_q}{2X'_d} = 2.4$ and the voltage reference set to 0.1% below the first generator. The DC load is increased linearly from 10% to 100% where an additional square wave with small current steps are superimposed onto the ramp in order to excite possible oscillations in the system. [19]

The specialisation project concludes that these undamped oscillations needs to be further analysed in order to better understand the phenomenon behind, if they origins from a electromechanical or electromagnetic phenomenon and from there on how to control them.

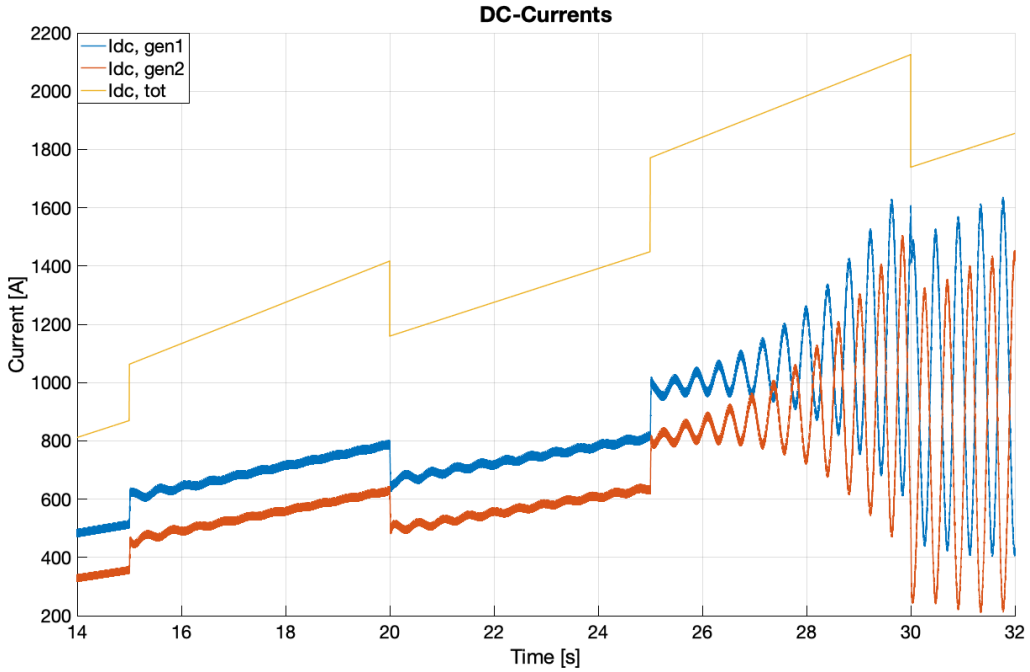

Figure 2.7: DC current responses when two rectifier-generator sets powers a common constant current load. $\frac{X_q}{2X'_d} = 2.4$ and the voltage reference of the second generator is set to 0.1% below the first generator. The DC load is increased linearly from 10% to 100% where an additional square wave with small current steps are superimposed onto the ramp in order to excite possible oscillations in the system. [19]

Chapter 3

Theoretical Background and Mathematical Description

Disclaimer: Section 3.4, 3.5.1 and 3.5.3 are retrieved from [19].

This chapter aims to be a theoretical foundation on which to form the remaining thesis. This includes a review of small-signal-stability, state-space representation, linear analysis tools for stability analysis, a three-phase diode-bridge rectifier, as well as the synchronous generator.

3.1 Small-Signal-Stability

Power system stability is the ability of an electric power system, for a given initial operating condition, to regain a state of operating equilibrium after being subjected to a physical disturbance, with most system variables bounded so that practically the entire system remains intact [54].

Small signal stability is defined as the ability of the power system to remain stable when subjected to small disturbances [55]. Such disturbances occur continuously in power systems due to small variations in load and generation. Instability of small signal stability is of the following two forms:

- Steady increase in generator angle due to lack of synchronising torque.
- Rotor oscillations of increasing amplitude due to lack of sufficient damping torque.

How a system response to a small disturbances depends on the initial condition, the strength of the grid and the type of generator excitation controls used. Figure 3.1a and Figure 3.1b depicts typical responses for generators not equipped with an AVR and equipped with an AVR, respectively. For the first case, instability is typical due to lack of sufficient synchronising torque while for the latter case typical due to lack of sufficient damping torque. In today´s practical

power systems, the small-signal stability problem is usually one of insufficient damping of system oscillations.

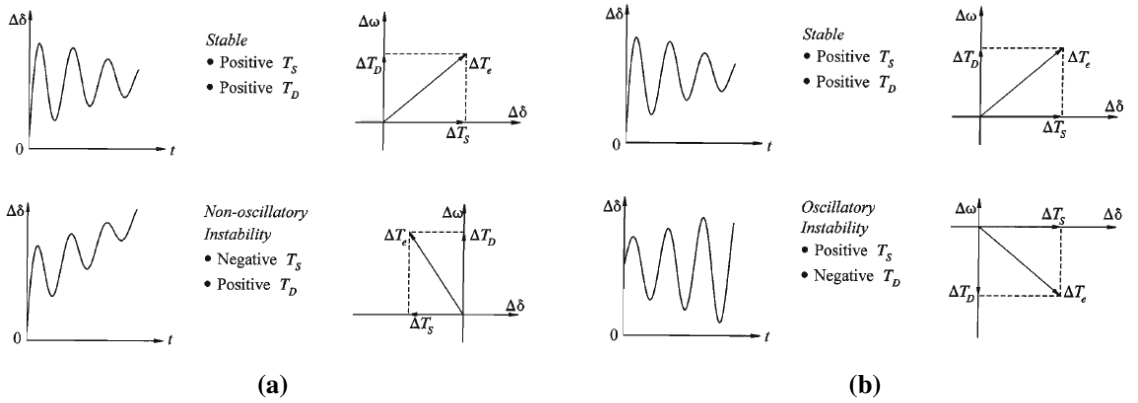

Figure 3.1: Nature of small-disturbance response [56, p. 24]. (a) With the absence of AVR (constant field voltage). (b) With the presence of AVR.

As seen in Figure 3.1a and 3.1b, both T_s and T_d needs to be positive in order to achieve a stable condition.

Because the disturbances that occurs when studying small signal stability are considered to be sufficiently small, linearization of system equations can be applied for stability analysis studies [56]. The use of such linear analysis techniques provide valuable information about the inherent dynamic characteristics of the power system and assists in its design.

3.2 State-Space Representation and Linearization

The behaviour of a dynamic system, such as a power system, may be described by a set of n first order nonlinear ordinary differential equations of the following form:

$$\dot{x}_i = f_i(x_1, x_2, \cdots, x_n; u_1, u_2, \cdots, u_r; t) \qquad i = 1, 2, \cdots, n \tag{3.1}$$

where n is the order of the system and r is the number of inputs [56]. In vector-matrix notation this becomes:

$$\dot{\mathbf{x}} = \mathbf{f}(\mathbf{x}, \mathbf{u}, t) \tag{3.2}$$

where **x**, **u** and **f** are presented by 3.3.

$$\mathbf{x} = \begin{bmatrix} x_1 \\ x_2 \\ \vdots \\ x_n \end{bmatrix} \qquad \mathbf{u} = \begin{bmatrix} u_1 \\ u_2 \\ \vdots \\ u_r \end{bmatrix} \qquad \mathbf{f} = \begin{bmatrix} f_1 \\ f_2 \\ \vdots \\ f_n \end{bmatrix} \tag{3.3}$$

x is called the *state vector* and its entries, x_i, are called state variables. A state variable is a variable in the system that has to be time-derived through a simulation [57]. The state of a system represents the minimum amount of information about the system at any instant in time t_0 that is necessary so that its future behaviour can be determined without reference to the input before t_0 [56]. The vector **u** (do further) represents the system inputs and its entries, u_i, are the input variables and define the external signals that influence the performance of the system. t denotes the time and $\dot{x}$ denotes the derivative of state variables with respect to time. When the derivatives are not explicit a function of time, Equation 3.2 becomes:

$$\dot{\mathbf{x}} = \mathbf{f}(\mathbf{x}, \mathbf{u}) \tag{3.4}$$

One can further relate state and input variables to observed output variables of the system in the following form:

$$\mathbf{y} = \mathbf{g}(\mathbf{x}, \mathbf{u}) \tag{3.5}$$

where

$$\mathbf{y} = \begin{bmatrix} y_1 \\ y_2 \\ \vdots \\ y_m \end{bmatrix} \qquad \mathbf{g} = \begin{bmatrix} g_1 \\ g_2 \\ \vdots \\ g_m \end{bmatrix} \tag{3.6}$$

y is the output vector while the vector **g** contains nonlinear functions relating state and input variable to output variables [56]. Figure 3.2 visualizes such a described dynamic system.

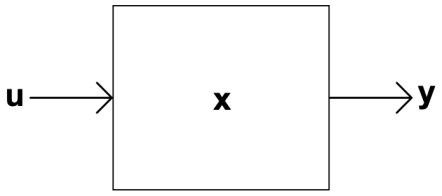

Figure 3.2: A dynamic system.

Linearization is the process of taking the gradient of a nonlinear function with respect to all variables and creating a linear representation at that point [58]. Linearization of the nonlinear system equations makes it possible to better understand how a dynamic system behaves near equilibrium points, whether the point is stable or unstable, and how the system approaches (or moves away from) the equilibrium point when being subjected to small disturbances. By disturbing the system in Figure 3.2 with minor deviations in both the state vector **x** and the input vector **u**, the linearized form of Equation 3.4 and 3.5 is obtained:

$$\boldsymbol{\Delta}\dot{\mathbf{x}} = \mathbf{A}\boldsymbol{\Delta}\mathbf{x} + \mathbf{B}\boldsymbol{\Delta}\mathbf{u} \tag{3.7}$$

$$\boldsymbol{\Delta}\mathbf{y} = \mathbf{C}\boldsymbol{\Delta}\mathbf{x} + \mathbf{D}\boldsymbol{\Delta}\mathbf{u} \tag{3.8}$$

where

$$\mathbf{A} = \begin{bmatrix} \frac{\partial f_1}{\partial x_1} & \cdots & \frac{\partial f_1}{\partial x_n} \\ \cdots & \cdots & \cdots \\ \frac{\partial f_n}{\partial x_1} & \cdots & \frac{\partial f_n}{\partial x_n} \end{bmatrix} \qquad \mathbf{B} = \begin{bmatrix} \frac{\partial f_1}{\partial u_1} & \cdots & \frac{\partial f_1}{\partial u_n} \\ \cdots & \cdots & \cdots \\ \frac{\partial f_n}{\partial u_1} & \cdots & \frac{\partial f_n}{\partial u_n} \end{bmatrix}$$

$$\mathbf{C} = \begin{bmatrix} \frac{\partial g_1}{\partial x_1} & \cdots & \frac{\partial g_1}{\partial x_n} \\ \cdots & \cdots & \cdots \\ \frac{\partial g_n}{\partial x_1} & \cdots & \frac{\partial g_n}{\partial x_n} \end{bmatrix} \qquad \mathbf{D} = \begin{bmatrix} \frac{\partial g_1}{\partial u_1} & \cdots & \frac{\partial g_1}{\partial u_n} \\ \cdots & \cdots & \cdots \\ \frac{\partial g_n}{\partial u_1} & \cdots & \frac{\partial g_n}{\partial u_n} \end{bmatrix} \tag{3.9}$$

The above partial derivatives are evaluated at the equilibrium point about which the small perturbation is being analyzed.

3.3 Linear Analysis

Small-signal analysis using linear analysis techniques provide valuable information about system dynamic properties, responses and assists in its robust system design. Linear analysis covers a broad range of methods, which use linear behavior to study power system dynamic performance. Some of these methods includes eigenvalues calculation, eigenvectors and participation factors calculation and sensitivity analysis. Their practical value resides in the insights they provide into the dynamic characteristics of a power system; such insights are often not easily inferred from time domain simulations alone. [59; 60]

3.3.1 Eigenvalues

A systems corresponding eigenvalues contains compact information about its dynamic behaviour and are useful for determining the system stability [57; 61]. The matrix $\mathbf{A}$, presented in Equation 3.9, is called *state matrix* and consists of size [*nxn*]. The poles of the corresponding dynamic system can be found as the roots of the so called *characteristic equation*, which is presented by Equation 3.10 [56].

$$\det(\mathbf{A} - \lambda\mathbf{I}) = \mathbf{0} \tag{3.10}$$

The number of eigenvalues are always the same as the dimension of matrix $\mathbf{A}$. Some of them can be multiple and some can be complex and it is therefore beneficial to represent them in the complex plane [57]. Real eigenvalues corresponds to non-oscillatory modes where a negative value represents a decaying mode whereas a positive value represents aperiodic instability [56]. Complex eigenvalues occur in conjugate pairs where each pair corresponds to an oscillatory mode. Power system oscillations usually contain multiple frequency components which are determined by the system elements. These frequency components are referred to as modes or eigenvalues. A complex pair of eigenvalues can be described by the following equation:

$$\lambda = \sigma \pm j\omega \tag{3.11}$$

where the real part, σ, and the imaginary part, ω, contains information about the damping and frequency of oscillation, respectively. A negative real part represents damped oscillation whereas a positive real part represents oscillation of increasing amplitude [56]. When a power system is subjected to a sufficiently small disturbance at steady-state operation, the disturbance can approach zero with time, or it can increase infinitely with time. The first case corresponds to a power system where all the roots of its corresponding state matrix have negative real parts and the system is considered asymptotically stable (in sense of Lyapunov stability) for this specific operating point. However, for the latter case, at least one of the roots of its corresponding state matrix has to contain a positive real value and the system is considered unstable for this specific operating point [60]. Eigenvalues with negative real part are located in the left-half plane in the complex plane whereas eigenvalues with positive real part are located in the right-half plane. The more negative σ, the better the eigenvalue is damped and the faster the time-response decays to zero. On the other hand, the more positive σ, the more unstable mode and the faster the time-response will increase to infinity. [57]

Based on Equation 3.11 one can determine the damped frequency in Hz:

$$f = \frac{\omega}{2\pi} \tag{3.12}$$

the naturally frequency in Hz:

$$f_0 = \frac{\omega_0}{2\pi} = \frac{\sqrt{\sigma^2 + \omega^2}}{2\pi} \tag{3.13}$$

and the damping ratio:

$$\zeta = \frac{-\sigma}{\sqrt{\sigma^2 + \omega^2}} \tag{3.14}$$

The damping ratio, ζ determines the rate of decay of the amplitude of the oscillation [56].

3.3.2 Eigenvectors

For any eigenvalue λ there exists two eigenvectors, a right column vector $\boldsymbol{\phi}$ and a left row vector $\boldsymbol{\psi}$ such that following relationships are fulfilled:

$$\mathbf{A}\boldsymbol{\phi}_i = \lambda_i \boldsymbol{\phi}_i \qquad i = 1, 2, ..., n \tag{3.15}$$

$$\boldsymbol{\psi}_i^T \mathbf{A} = \lambda_i \boldsymbol{\psi}_i^T \qquad i = 1, 2, ..., n \tag{3.16}$$

All the n eigenvectors can be expressed in two common matrices:

$$\boldsymbol{\Phi} = [\boldsymbol{\phi}_1 \;\; \boldsymbol{\phi}_2 \;\; \cdots \;\; \boldsymbol{\phi}_n]$$
$$\boldsymbol{\Psi} = [\boldsymbol{\psi}_1^T \;\; \boldsymbol{\psi}_2^T \;\; \cdots \;\; \boldsymbol{\psi}_n^T]^T$$

The left and the right eigenvectors corresponding to different eigenvalues are orthogonal:

$$\boldsymbol{\psi}_j \boldsymbol{\phi}_i = 0$$

while eigenvectors corresponding to the same eigenvalue:

$$\boldsymbol{\psi}_i \boldsymbol{\phi}_i = C_i$$

where C_i is a non-zero constant. Eigenvectors are determined only to within a scalar multiplier, it is common practise to normalize these vectors such that:

$$\boldsymbol{\psi}_i \boldsymbol{\phi}_i = 1$$

Furthermore, the matrices containing all the left and the right eigenvectors are inverse of each other:

$$\boldsymbol{\Psi}\boldsymbol{\Phi} = \mathbf{I} \qquad\qquad \boldsymbol{\Psi} = \boldsymbol{\Phi}^{-1}$$

The left eigenvector, $\boldsymbol{\psi}_i$, weights the contribution of the activity of the state variables to the *i*th mode [62; 56]. It gives information about how able a state variable is to influence an eigenvalue [57]. The information obtained from the left eigenvector can therefore be utilized in order to control the corresponding eigenvalue. For example, if an eigenvalue is found in the right-half plane, information from the right eigenvector can be used to force the corresponding eigenvalue to the left-half plane and in turn make the system stable.

On the other hand, the right eigenvector, $\boldsymbol{\phi}_i$, measures the relative activity of the state variables in the *i*th mode and it is said to give the mode shape, i.e. the relative activity of the state variables when a particular mode is excited [62; 56]. It contains information about how observable an eigenvalue is among the state variables [57]. For example, the degree of activity of the state variable x_k in the ith mode is given my the element ϕ_{ki} in the right eigenvectormatrix $\boldsymbol{\Phi}$.

Based on this, the kth element of the right eiegenvector $\boldsymbol{\phi}_i$ measures the activity of the state variable x_k in the ith mode, and the kth element of the left eigenvector ψ_i weights the contribution of this activity to the ith mode [56].

3.3.3 Participation Factors

A participation matrix, **P**, combines the right and the left eigenvectors and is defined in the following way:

$$\mathbf{P} = [\mathbf{p}_1 \quad \mathbf{p}_2 \quad \cdots \quad \mathbf{p}_n]$$

$$\mathbf{p}_i = \begin{bmatrix} p_{1i} \\ p_{2i} \\ \vdots \\ p_{ni} \end{bmatrix} = \begin{bmatrix} \phi_{1i}\psi_{i1} \\ \phi_{2i}\psi_{i2} \\ \vdots \\ \phi_{ni}\psi_{in} \end{bmatrix}$$

p_{ki} measures the relative participation of the kth state variable in the ith mode. The elements in the matrix are dimensionless and are referred to as *participation factors* [56]. A partcipation factor is similiar to the sensitivity of an eigenvalue λ_i to the diagonal element a_{kk} of the state matrix **A** and is given by the following equation:

$$p_{ki} = \frac{\partial \lambda_i}{\partial a_{kk}} = \psi_{ik}\phi_{ki} \tag{3.17}$$

For normalized eigenvectors, the sum of the participation factors associated with any mode or with any state is equal to 1:

$$\sum_{i=1}^{n} p_{ki} = 1 \tag{3.18}$$

If the absolute value of p_{1i} is greater than p_{2i} it means that state variable 1 participates more in eigenvalue i than state variable 2. Another explanation is that eigenvalue i is more sensitive to changes in element a_{11} compared to changes in element a_{22}. Participation factors can be used to better understand which state variables that contribute to the different modes. It is therefore a valuable tool considering stability analysis.

3.3.4 Sensitivity Analysis

Sensitivity analysis is a tool used to better understand how different system parameters influence the different eigenvalues. For example, if some eigenvalues are found in the right-half plane in the complex plane or at the left-half plane, but close to the imaginary axis, further investigations of which parameters influence these modes the most will be of great importance. One method is to change one parameter at the time, keeping the other parameters unchanged, and measure how the real value of the corresponding eigenvalue has change compared to the base case situation where all parameters are unchanged and equal to its original value. To be able to compare the effect of changing the different parameters, it is important to change each of the parameters by the same percentage change.

3.4 Three-Phase Diode-Bridge Rectifier

A three-phase, six-pulse, full-bridge diode rectifier and its corresponding waveforms are depicted in Figure 3.3. This circuit assumes a constant output DC voltage which is an approximation to a resistive DC-load connected in parallel with a large filter capacitor [26].

The rectifier consists of diodes, each conducting 120°. A diode starts to conduct when the voltage across it becomes positive and the diode stops to conduct when the current drops to zero. The diodes are conducting in pair, one from the top group and one from the bottom group. In the top group, the diode with is anode (indicated by the widest side of the diode symbol) at the highest potential will conduct while the other two will be reversed biased, and thus not conduct. In the bottom group, the diode with its cathode (indicated by a line on the diode symbol) at the lowest potential (most negative) will conduct and the other two will be reversed biased. The fact that only two diodes conduct at any given time is an other assumption drawn by this circuit waveform which further makes the DC output current to flow discontinuous [26]. The term ”six-pulse” comes from the fact that the output DC voltage contains six segments per cycle of line frequency input voltage, two segments per phase - one for its positive half cycle and one for its negative [63]. These six segments (ripple) in the output DC-volatage is depicted in graph 3.3b.

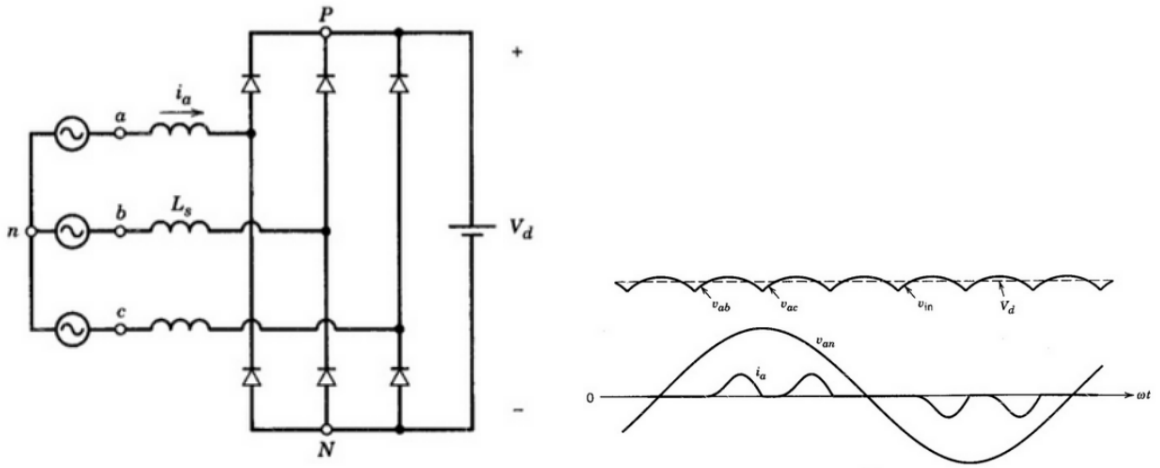

(a) **(b)**

Figure 3.3: (a) Three-phase diode-bridge rectifier with a constant DC voltage at the output terminal. (b) The corresponding circuit waveforms. The output voltage is depicted in the upper part while the input phase voltage (for a single phase) and its corresponding phase current is given in the lower part. [26]

The presence of a inductance, L_s, connected at the AC-side of the rectifier, makes the commutation from one diode to an other to not happen instantaneous. Some energy will be stored in the inductance causing an other diode to be forward biased before the current in the prior diode has reach zero. As a result, during commutation, three diodes will be turned on at the same time, causing 2-phase short-circuit and a drop in the voltage which further leads to a reduced average DC voltage. The resulting average DC voltage in the presence of a finite commutation interval is therefore given by:

$$V_d = V_{do} - \Delta V_{\text{commutation}} = 1.35 V_{\text{LL,RMS}} - \frac{3}{\pi}\omega L_s I_d \tag{3.19}$$

I_d and $V_{\text{LL,RMS}}$ represents the rectified DC current and line-to-line AC root mean square (RMS)

voltage, respectively. ω is given by $2\pi f$ where f represents the system frequency.

At light loads with low values of DC current I_d, the I_d waveform becomes discontinuous. This is because the ripple in the DC current is large enough to cause the polarity of the applied current to reverse. As a consequence, the dc current will remain at zero value until the next diode becomes forward biased. In the presence of a constant counter voltage, E_d connected at the DC side, a larger value of E_d will result in a smaller DC current. [26, p.134,148-149]

Power electronics introduces current or voltage distortion, in form of harmonics, into the power system and the diode rectifier is not an exception. Hansen [64, p.467] states that the diode rectifier is a highly nonlinear load and it is therefore considered to be the main source of harmonic currents in today's power system. Figure 3.4 shows a line current i_s drawn from the utility by a power electronic equipment that deviates significantly from a pure sinusoidal waveform. The current i_s in steady state is the sum of all its harmonic components. The fundamental component (1st order) has a pure sinusoidal waveform and is represented by i_{s1} while the higher order harmonics are presented by i_{dis} indicated in Figure 3.4. The distorted current can further lead to a distortion in the utility-supplied voltage [26].

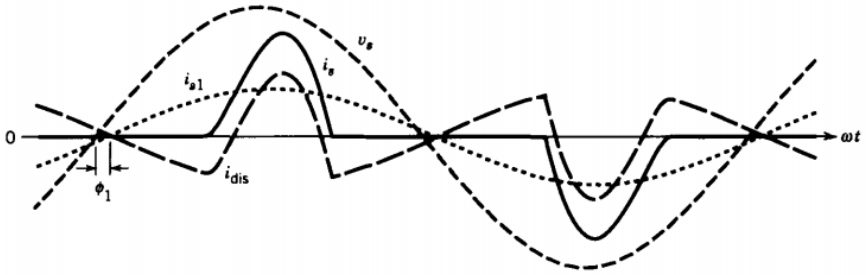

Figure 3.4: Line-current distortion [26, p.41].

The amount of distortion in the voltage or current waveform (here in the input current) is quantified by an index called total harmonic distortion (THD):

$$\begin{aligned} \%THD_{\mathrm{i}} &= 100 \cdot \frac{I_{\mathrm{dis}}}{I_{\mathrm{s1}}} \\ &= 100 \cdot \sqrt{\sum_{h \neq 1} \left(\frac{I_{\mathrm{sh}}}{I_{\mathrm{s1}}} \right)^2} \end{aligned} \tag{3.20}$$

where I_{sh} is the RMS value of the waveform corresponding to harmonic component h. Pure sinusoidal current has no harmonic distortion and hence a THD equal to zero.

An other consequence of non-sinusoidal currents and voltages is a reduced power factor (PF)

and an additional term is added to its expression:

$$\text{PF} = \frac{I_{s1}}{I_s} cos(\phi_1) \tag{3.21}$$

The power factor do not only depend on the displacement, ϕ_i, between the fundamental component of the input voltage and current, but also on the rms value of the fundamental current component with respect to the rms of the total waveform [26].

Increasing the relationship presented by Equation 3.22 reduces the THD.

$$\frac{I_d}{I_{\text{short-circuit}}}, \qquad I_{\text{short-circuit}} = \frac{V_{LL}/\sqrt{3}}{\omega_1 L_s} \tag{3.22}$$

As a result, for a given I_d, increasing the internal impedance, L_s connected at the AC-side of the rectifier, a smaller $I_{\text{short-circuit}}$ and thus a lower THD and an increased PF. On the other hand, an increased impedance leads to a larger decrease in the average output voltage due to an increased loss during commutation.

For a three-phase, six-pulse, full-bridge diode rectifier, the present harmonic components is given by:

$$h = \pm 6i$$

where i is an positive integer starting at $i = 1$. The even (2, 4, 6, 8 etc.) and triplen harmonics(odd multiples of the third) are zero, such as 8, 9, 10, 12, 14, 15 etc.. The number 6 comes from the fact that it is a six pulse bridge and as a result h = 5,7,11,13, and their magnitudes, I_{sh}, decreases with the ratio $\frac{1}{h}$ such that $I_{sh} = \frac{1}{h} I_{s1}$.
If i_{s1} is in phase with the input phase voltage, v_s, the three-phase, six-pulse, full-bridge diode rectifier obtains a PF equal to 0.955 [26].

Figure 3.5a shows a three-phase diode-bridge rectifier-loaded synchronous generator and 3.5b shows its corresponding AC line-to-line voltage and phase current waveforms. A resistive load is connected to the DC-terminals. The shape of these waveforms are quite distorted and is explained by the fact that the full-bridge diode-rectifier introduces a 60° commutation angle because of the large generator inductance (L_s) and its heavy load current [65],[66]. This is consistent with the relationship presented by 3.19.
As a result of 60° commutation angle, three diodes conduct at any time, resulting in 60° interval series of the operating generator, where one generator line to line voltage being zero, and the other two being equal to V_{DC} and $-V_{DC}$. Because the circuit shown in Figure 3.5a contains a large capacitor connected across the DC terminals, V_{DC} is close to constant and the result is a square-shaped voltage and a current with "humps". However, these waveforms are load-dependent and changes as the operating point changes. If the load decreases, both output current and frequency decrease, resulting in a smaller commutation angle which further leads

to a less square voltage waveform (more sinusoidal) where the ”humps” in the current shrinks [65].

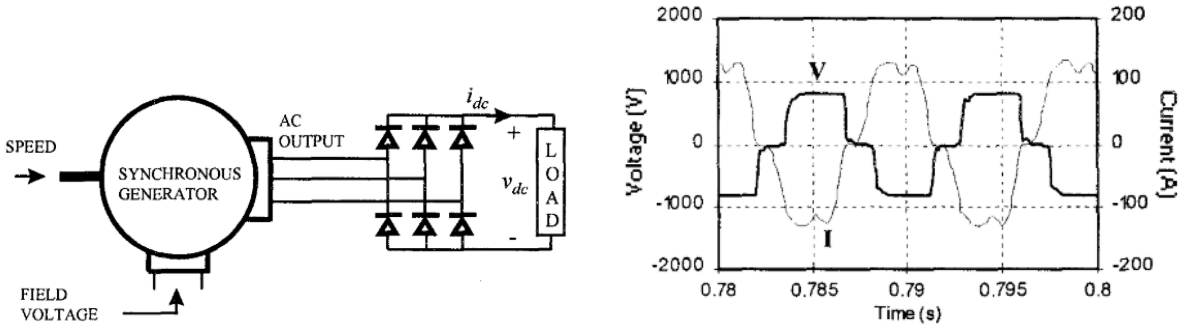

(a) **(b)**

Figure 3.5: (a) Three-phase diode-bridge rectifier-loaded synchronous generator. A resistive load as well as a large filter capacitor is connected to the DC-terminals. (b) The corresponding circuit waveforms. The input voltage presented by the bold line and the corresponding input current presented by the light line [65].

A circuit similar to the one shown in 3.5a is studied by [63]. They explain the ”humps” in the input current due to the fact that power only is drawn by the main supply when the DC bus voltage falls below that of AC main supply level.

Hansen [64] analyzes the power quality of power systems and states that predicting the harmonic current generated by the diode rectifier is quite difficult. However, a typical line-current waveform is proposed in Figure 3.6a. Hansen [64] further states that a three-phase diode rectifier connected to an unbalanced system may lead to uneven ”humps” in the input current, typically as shown in Figure 3.6b.

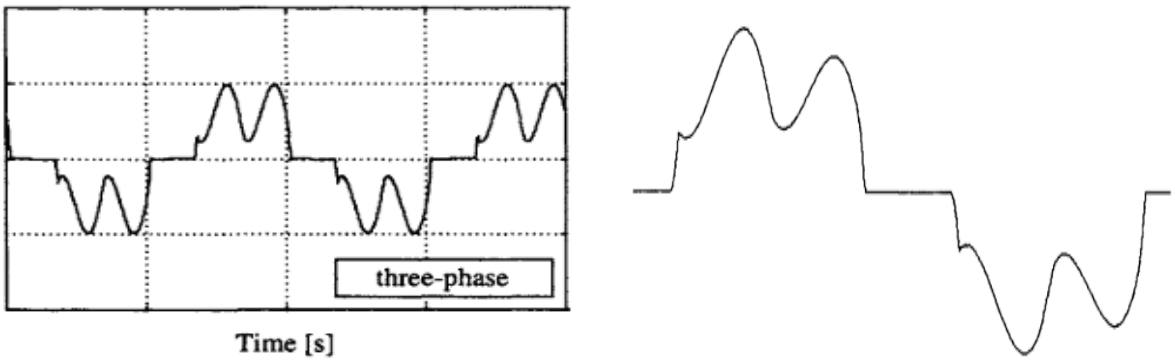

(a) **(b)**

Figure 3.6: (a) Typical input line current of three-phase diode rectifier [64, p.468]. (b) Current drawn by a three-phase diode rectifier connected to a unbalanced power system [64, p.465].

3.5 Synchronous Generator

There are two main structures of the synchronous machine, round rotor or salient pole rotor, depending on the operating speed. As speed is inverse proportional with the number of poles, low speed generators operates with a relatively large number of poles, and opposite for high speed generators [56]. Salient pole generators are better suited for low speed operation and are mostly used in hydro generator plants. On the other hand are round rotor generators better suited for high speed operation and are mostly used in nuclear, gas and thermal power plants.
Salient pole generator are laminated, contains concentrated field windings and is normally equipped with short-circuited damper windings designed to damp out speed oscillations. The round rotor generator do usually not have such damper windings but their solid-steel rotor body provides paths for eddy currents which have the same effect [25; 56].

The rotor of a synchronous generator may only have one physically identifiable field winding, additional concentrated windings are often used to represent the distributed damper windings and the effect of current flow in the rotor iron. Two such additional windings are usually used for salient-pole rotor machines: one in the d-axis and one in the q-axis. Ong [67] states that most synchronous generator can be adequatley represented by a model that is based on an equivalent idealized machine with one or two sets of damper windings, besides the field winding which are located in the d-axis. Damper windings can be used to represent physical armotisseur windings, or the damping effect provided by the eddy currents in the solid-steel rotor body [56; 67]. A circuit representation of an idealized synchronous generator, comprising three stator armature windings, one field winding and two damper windings are presented in Figure 3.7. Direct current flows through the field winding, producing a magnetic field which further induces AC voltages in the stator windings. The magnetic coupling between the windings is a function of the rotor position and the flux linkage of the windings is therefore a function of the rotor position [56; 68].

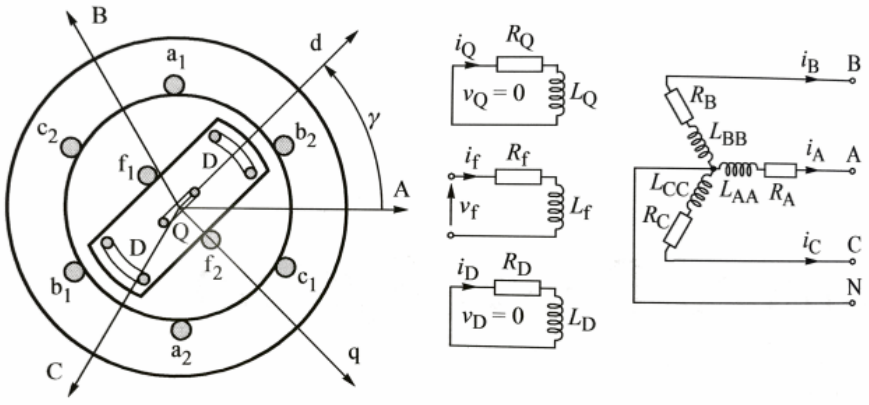

Figure 3.7: A schematic cross-section of a synchronous generator and its circuit representation. The machine is assumed to contain a three-phase stator armature winding (A, B, C), a rotor field winding (F) in the d-axis and two rotor damper windings - one in the d-axis (D) and one i the q-axis (Q). [25, p. 434]

3.5.1 Salient Pole Generator

A schematic of the cross-section of a two-pole salient pole synchronous generator is depicted below, Figure 3.8.

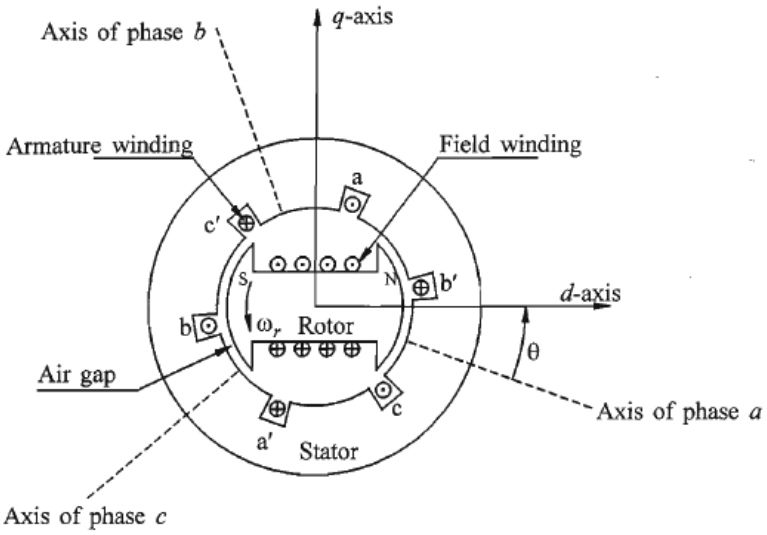

Figure 3.8: Cross section of a three-phase synchronous salient-pole machine with one pair of field poles [56].

The schematic shows, different from a round rotor which has a uniform distributed air gap, the air gap of a salient pole machine varies. The narrowest gap is along the d-axis and the widest is along the q-axis. As a result, the reluctance of the air gap varies between its minimum value, $\mathcal{R}_d$ and its maximum value $\mathcal{R}_q$. A consequence of non-uniform air gap, the mmf and flux vectors are not in phase and since the flux tends to take the path of least reluctance, the flux vector is aligned with the d-axis. Because of this, the two vectors are only aligned when the mmf vector is aligned with the d-axis or with the q-axis. A *two-reaction theory* which analyze the mmfs acting in the machine along the d- and q-axis and their corresponding emfs component are, as a result of non uniform air-gap, considered separately in each of the two axis. The armature mmf is analyzed by a q- and d- axis component while the excitation mmf is always aligned with the d-axis. This two-reaction theory is summarized in Figure 3.9, where the d-axis is defined to lead the q-axis by 90°.

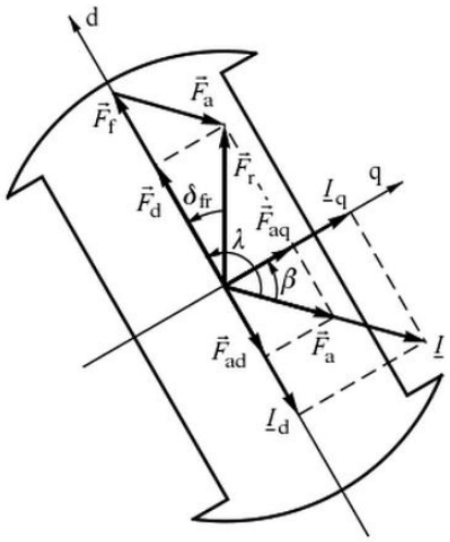

Figure 3.9: MMFs and currents modeled in the d- and q-axis components of a salient pole machine [25, p.85].

The resulting air-gap emf can as a result be written as:

$$\underline{E}_r = \underline{E}_f + \underline{E}_{aq} + \underline{E}_{ad} = \underline{E}_f - jX_{ad}\underline{I}_d - jX_{aq}\underline{I}_q \tag{3.23}$$

Where $\underline{E}_f$ is the excitation emf, set up by the excitation mmf, acting along the q-axis. $\underline{E}_{aq}$ and $\underline{E}_{ad}$ are the emf set up by the armature d- and q-axis mmf respectively. X_{aq} and X_{ad} are inversely proportional to the q- and d-axis reluctance and since $\mathcal{R}_d < \mathcal{R}_q$, $X_{ad} > X_{aq}$. By adding the armature leakage reactance, X_l, the terminal voltage can be determined:

$$\underline{V}_g = \underline{E}_r - jX_l\underline{I} - R\underline{I} = \underline{E}_f - jX_{ad}\underline{I}_d - jX_{aq}\underline{I}_q - jX_l(\underline{I}_d + \underline{I}_q) - R\underline{I}$$

which further can be written as

$$\underline{V}_g = \underline{E}_f - j(X_{ad} + X_l)\underline{I}_d - j(X_{aq} + X_l)\underline{I}_q - R\underline{I} \tag{3.24}$$

or

$$\underline{E}_f = \underline{V}_g + jX_d\underline{I}_d + jX_q\underline{I}_q + R\underline{I} \tag{3.25}$$

A schematic of the corresponding phasor diagram is shown in Figure 3.10.

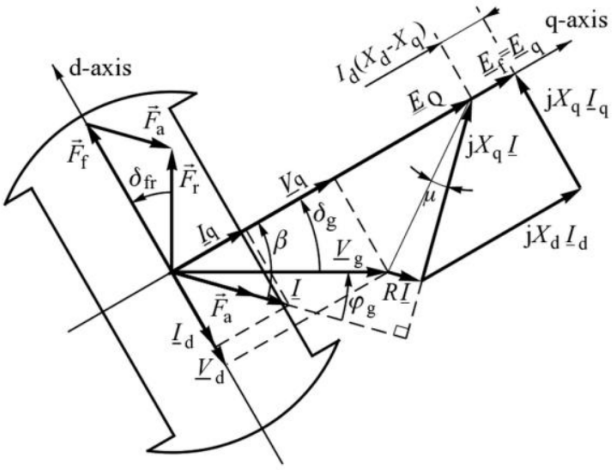

Figure 3.10: Phasor diagram for a salient-pole generator [25, p.86].

$\underline{E}_Q$ is given by the following:

$$\underline{E}_Q = \underline{V}_g + (R + jX_q)\underline{I}$$

Resolving Equation 3.25 into d- and q-axis components results in the two following relationships:

$$\begin{aligned} E_d &= V_d + RI_d + X_qI_q = 0 \\ E_q &= V_q + RI_q + X_dI_d = E_f \end{aligned} \tag{3.26}$$

Note that the components in the two latter equations are in phase with each other, hence, given as real number (not complex). E_d is equal to zero as there is no excitation in the q-axis. E_q is proportional to the excitation flux and since the excitation flux is proportional to the field current, it is also known as E_f.
The d- and q- components of the terminal voltage and current are:

$$\begin{aligned} V_d &= -V_g \sin\delta_g, & V_q &= V_g \cos\delta_g \\ I_d &= -I \sin\beta, & I_q &= I \cos\beta \end{aligned} \tag{3.27}$$

where $\beta = \phi_g + \delta_g$.

3.5.2 The dq0-Reference Frame

Different rotor reference frame are used when studying electrical machines. Some examples are the $abc-$ reference frame, the $\alpha\beta 0-$reference frame and the $dq0-$reference frame. abc and $\alpha\beta 0$ are stationary frames while $dq0-$ is a rotating frame. One can convert a given frame to another by the use of transformation matrices, such as Clarke and Park transformation [69]. Inductances that vary depending on position of the rotor relative to the stator, which would be the case if saliency had been introduced, become constant in the $dq0-$reference frame. Because of this, the $dq0-$reference frame is to prefer when studying salient-pole synchronous generator.

The $dq0-$reference frame is a two axis reference frame which is fixed to the rotor and thus rotates at the rotor electrical speed. The $dq0$-reference frame is centered in the rotor, with the d-axis aligned with the north pole of the rotor and the q-axis aligned orthogonal to the d-axis. The selection of d-axis leading the q-axis by 90° (Figure 3.7, 3.9 and 3.10) or q-axis leading d-axis by 90° (Figure 3.8) is purely arbitrary [25, p.87]. IEEE (1969) recommended d-axis to lead q-axis because the d-axis current usually causes demagnetization of the machine and should be negative in the generator reference frame [70]. Machowski [25] assumes the d-axis to lead q-axis while Kundur [56] and Ong [67] assume q-axis to lead d-axis. For the latter case, there is need to remove the minus sign from Equation 3.27 and change the sign of the reactive terms in Equation 3.26.
Different from the d and q components, the 0 sequence component does not have a physical representation in the machine, but is zero during balanced steady state conditions and represent the current circulating during imbalanced operation.

3.5.3 Synchronous Generator Dynamics

Power systems disturbances cause the armature flux to change, which further causes the rotor windings to initiate currents in order to prevent the armature flux from entering these windings; they have the effect of *screening the rotor* from these changes in armature flux [25, p.135].
Figure 3.11 indicates the characteristic states that correspond to three different stages of rotor screening. Immediately, the current induced both in the rotor field and damper winding prevents the armature reaction flux completely from entering the rotor and hence maintaining a constant rotor flux. Figure 3.11a illustrates this phenomena and the syncronous generator is said to operate in the subtransient state. As the current in the rotor flows, energy is dissipated in the rotor winding resistance, and the currents decays with time allowing the flux to enter the windings. Because the resistance in the rotor damper winding is the largest, the damper current is the first to decay and hence allowing the armature flux to enter the rotor pole face.

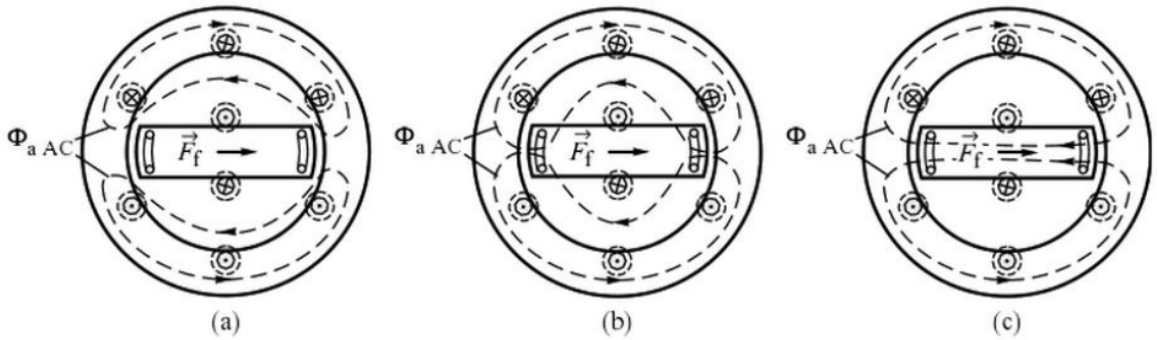

Figure 3.11: The path of the armature flux in: (a) the subtransient state (screening effect of the damper winding and the field winding); (b) the transient state (screening effect of the field winding only); (c) the steady state. In all three cases the rotor is shown to be in the same position but the actual rotor position corresponding to the three states will be separated by a number of rotations [25, p.135].

However, the field winding is still preventing the armature reaction flux from entering its winding, Figure 3.11b shows this, and the synchronous generator is said to operate in transient state. After some additional time, the field current decays, thus, allowing the armature flux to enter the whole rotor. This is illustrated in Figure 3.11c and the synchronous generator is said to operate in steady-state.

In order to study the dynamics of the generator in each of these states mentioned above, equivalent circuits for each of the states are established. The inductance of a winding is defined as the ratio of the flux linked to the current initiating the flux. Consequently, a low-reluctance path results in a large flux and a large inductance (or reactance) and opposite. Four common flux paths are represented by four different reactances:

- X_l, the armature leakage reactance represents the path taken by the armature leakage flux around the stator windings.
- X_a, the armature reaction reactance represents the path taken by the flux across the air gap.
- X_D, represents the path taken by the flux around the damper winding.
- X_f, represents the path taken by the flux around the field winding.

By combining these above armature reactances in each of the states, the following three equivalent reactances are obtained:

- X''_d, the direct-axis subtransient reactance.
- X'_d, the direct-axis transient reactance.
- X_d, the direct-axis synchronous reactance.

These equivalent circuits are illustrated in Figure 3.12. Because the flux path in air is longest in the subtransient state and shortest in the steady state, $X''_d < X'_d < X_d$.

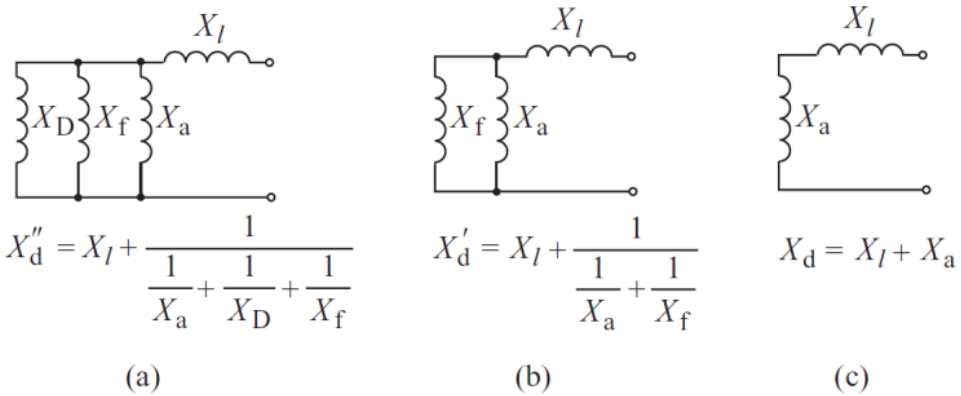

Figure 3.12: Equivalent circuits for each of the three states: (a) subtransient state; (b) transient state; (c) steady state [25, p.136].

Figure 3.11 shows the path taken by the AC armature flux assuming that the armature mmf is aligned with the d-axis, which is only true for generators operating at no-load prior to the disturbance. For a generator operating at a load prior to the disturbance, an armature flux q-axis component will also be present [25] and the following will yield:

- Subtransient state:
  - For armature mmf directed along the rotor d-axis:
    - X''_d represents the flux path when currents are induced in the field winding, the damper winding and the rotor core.
  - For armature mmf directed along the rotor q-axis:
    - X''_q represents the flux path when rotor eddy currents are induced as well as current in the q-axis damper winding.

  Generators with only d-axis damper winding have a much weaker q-axis screening effect compared to the d-axis screening effect which results in $X''_q > X''_d$. The difference between these two subtransient reactances is called *subtransient saliency* [25]. For generators with both d- and q-axis damper windings, $X''_q \approx X''_d$.

- Transient state:
  - For armature mmf directed along the rotor d-axis:
    - X'_d represents the flux path when currents are induced in the field winding.
  - For armature mmf directed along the rotor q-axis:
    - X'_q represents the flux path when rotor eddy currents are induced, which is only the case for round-rotor structure.

  For this state, because of no q-axis field winding, there will always be a weaker screening in the q-axis and as a result, $X'_q > X'_d$ and a *transient saliency* will always be present. X'_q is typically twice as large as X'_d. For salient pole generator, no eddy currents flows in the rotor due to the laminated rotor core construction and hence no screening is produced causing $X'_q = X_q$.

Circuit time constants are defined for the different states and they identifies at which rate the flux produced in the winding decays to zero and is given by the relationship $\frac{L_{winding}}{R_{winding}}$.

- T''_d, the d-axis subtransient short-circuit time constant represents the decay ratio a DC-current will experience by flowing in the damper winding.
- T'_d, the d-axis transient short-circuit time constant represents the decay ratio a DC-current will experience by flowing in the field winding.

Because the damper winding restistance usually is much greater than the field winding restistance, $T''_d << T'_d$ and the DC component of the damper winding current will decay much faster than the DC component of the field winding current. T''_q and T'_q are defined in the same way as for the d-axis time constants. The time constants above corresponds to the armature winding when short-circuited. However, time constants for the armature winding when open-circuited do also exist and by neglecting X_l and following the same procedure as in Figure 3.12, one obtain the following:

$$X'_d \cong \frac{X_a X_f}{X_a + X_f} \tag{3.28}$$

$$X''_d \cong \frac{1}{\frac{1}{X_D} + \frac{1}{X'_d}}, \qquad X_D \cong \frac{X'_d X''_d}{X'_d - X''_d} \tag{3.29}$$

$$T''_d = \frac{X_D}{\omega R_D} \cong \frac{X'_d X''_d}{\omega_s R_D (X'_d - X''_d)} \tag{3.30}$$

$$T''_{do} = \frac{X_D + \frac{X_a X_f}{X_a + X_f}}{\omega R_D} \cong \frac{X_D + X'_d}{\omega R_D} \tag{3.31}$$

Dividing Equation 3.30 by Equation 3.31, and substituting for X_D by the use of Equation 3.29, results in $\frac{T''_d}{T''_{do}} \approx \frac{X''_d}{X''_{do}}$. Following a similar procedure for the remaining time constants gives the following relationships:

$$T''_d \cong T''_{do}\frac{X''_d}{X'_d} \qquad T''_q \cong T''_{qo}\frac{X''_q}{X'_q} \qquad T'_d \cong T'_{do}\frac{X'_d}{X_d} \qquad T'_q \cong T'_{qo}\frac{X'_q}{X_q} \tag{3.32}$$

Finally, a generator circuit equation can be defined for each of the three characteristic states, where the generator may be represented by a constant internal emf E'', E' and E acting behind reactances X''_d and X''_q, X'_d and X'_q or X_d and X_q, respectively. These three are listed below:
Subtransient equation:

$$\underline{E}'' = \underline{E}''_q + \underline{E}''_d = \underline{V}_g + R\underline{I} + j\underline{I}_d X''_d + j\underline{I}_q X''_q \tag{3.33}$$

Transient equation:

$$\underline{E}' = \underline{E}'_q + \underline{E}'_d = \underline{V}_g + R\underline{I} + j\underline{I}_d X'_d + j\underline{I}_q X'_q \tag{3.34}$$

Steady state equation:

$$\underline{E} = \underline{E}_q + \underline{E}_d = \underline{V}_g + R\underline{I} + j\underline{I}_d X_d + j\underline{I}_q X_q \tag{3.35}$$

By rewriting the latter equation and inserting Equation 3.33 and Equation 3.34, the following two equations are obtained, respectively: [25, p.140-142].

$$\underline{E} = \underline{E}'' + j\underline{I}_d(X_d - X''_d) + j\underline{I}_q(X_q - X''_q) \tag{3.36}$$

$$\underline{E} = \underline{E}' + j\underline{I}_d(X_d - X'_d) + j\underline{I}_q(X_q - X'_q) \tag{3.37}$$

3.5.4 Sixth-Order-Mathematical-Model

Last subsection described the effect of a fault that cause the current in, and the flux linking, the different windings to change in such a way that three characteristic states can be identified; subtransient state, transient state and steady state. It further explained that during each of these states, a generator may be represented as a constant internal Electromotive Force (EMF) (E, E' and E'') acting behind a reactance with an appropriate value and that the transition from one state to another occurred instantaneously. In reality, the transition from one state to another happens smoothly and so does the values of the fictitious internal emfs [25]. This subsection presents a dynamic, sixth order mathematical model of a synchronous generator, which includes the effect of the fictitious internal emf to change smoothly with time.

The following six differential equations describes the synchronous generator, when neglecting the armature resistance, R:

$$\begin{aligned} M\Delta\dot{\omega} &= P_m - P_e \\ \dot{\delta} &= \Delta\omega \\ T'_{d0}\dot{E}'_q &= E_f - E'_q + I_d(X_d - X'_d) \\ T'_{q0}\dot{E}'_d &= -E'_d - I_q(X_q - X'_q) \\ T''_{d0}\dot{E}''_q &= E'_q - E''_q + I_d(X'_d - X''_d) \\ T''_{q0}\dot{E}''_d &= E'_d - E''_d - I_q(X'_q - X''_q) \end{aligned} \tag{3.38}$$

where the two first differential equations represent the mechanical system; the speed deviation and angle change of the rotor, and the four last differential equations represent the electrical system; they describe the change in emfs as the flux linking the rotor circuit decays and the armature flux gradually penetrates into the rotor [25]. The differential Equation describing the electrical system constitutes, on the left hand side, a time derivative of the emf multiplied by the relevant time constant. The right hand side constitutes the equivalent d- or q-axis armature circuit; a driving voltage and a voltage drop due to the relevant reactance. The resistance, R, in the armature circuit is neglected in these four differential equations.
Changes in the mechanical power, P_m, and the field voltage, E_f should be calculated based on the differential equation describing the turbine system and excitation system, respectively. Algebraic Equations describing the air gap power and the armature voltage equations are presented below:

$$P_e = V_d I_d + V_q I_q + (I_d^2 + I_q^2)R \tag{3.39}$$

$$\begin{bmatrix} V_d \\ V_q \end{bmatrix} = \begin{bmatrix} E''_d \\ E''_q \end{bmatrix} - \begin{bmatrix} R & X''_q \\ -X''_d & R \end{bmatrix} \begin{bmatrix} I_d \\ I_q \end{bmatrix} \tag{3.40}$$

Equation 3.40 corresponds to Equation 3.33 presented in last subsection, 3.5.3. All quantities are expressed in per-unit notation.

Chapter 4

Model Implementation and Validation

This chapter describes the process of modelling the studied system, both the detailed simulation model and the simplified numerical model. Furthermore, it describes the model validation process, the linearization of the simplified model, limitations and simplifications made, the cases to be studied, and the methods used.

The software used in this thesis were MATLAB® [71] and Simulink® by Matlab [72] for dynamic simulations.

4.1 Methodology

The detailed simulation model was implemented with the mindset of keeping it as simple as possible, only including the system components which are believed to be necessary in order to recreate the unstable phenomenon, described in Chapter 2. If the model turns out to be too simple one can rather make it more complex. This was done in order to facilitate a better understanding of the phenomenon behind, to investigate if the AVR or the Governor is the reason itself or to investigate whether it is an electromagnetic phenomenon or an electromechanical phenomenon. Furthermore, keeping the detailed model simple, makes the process of developing a simplified mathematical model easier, when based on the detailed model to be used for stability analysis. Therefore, the word *detailed* does not mean a detailed model of the topology shown in Figure 2.1b, but *detailed* because a numerical model will be established based on this model, and it will simplify the diode-rectifier as well as the synchronous generator. Thus, compared to this simplified numerical model, it is a *detailed* model.
Keeping this latter paragraph in mind, an attempt to reproduce the unstable behavior by implementing the system sketched in Figure 2.1b was made. Operating a rectifier synchronous generator set in parallel with a battery, instead of another synchronous generator set, eliminates the need for an AVR to perform voltage-droop-control, and thus contribute to keep the model simple. The detailed model was implemented by the use of Simulink/Matlab system blocks from the ”Simscape Electrical Specialized Power Systems” library. The implementation pro-

cess is described in Section 4.2.
It was chosen to implement a simplified average model of the detailed model capable of reproducing the unstable behavior and qualifying for linear analysis. The reason why linear analysis is chosen as a suitable tool is that the unstable behaviour reminds of a small signal problem, only a minor change or perturbation is enough to make the system unstable. In addition, linear analysis provides better insight to the unstable phenomenon.
First of all, when developing the simplified model, differential equations describing the system were derived. Next, these equations were implemented in the simulation tool Simulink/Matlab and several trial-and-error processes were pulled through before the model succeeded with reproducing the unstable behaviour. The synchronous generator equations are based on the six-order model presented in Section 3.5.4, the DC circuit containing the battery and a filter capacitor is described by a simple differential equation, while the equations used to describe the simplified diode switching are based on the technique used by Jatskevich [45], in which he develops an average-value model of a synchronous machine-rectifier system. The implementation process is described in Section 4.3

The unstable behaviour recreated in the detailed simulation model was compared against the instability detected by the simulation model developed during the project work in fall of 2020 [19]. This was done in order to ensure that the unstable behaviour corresponds to the same phenomenon detected by previous studies. The simplified numerical model was further validated and compared to the detailed model developed during this thesis and the corresponding process and validation results are presented in Section 4.4.

The simplified model equations were further implemented in the programming tool Matlab where the model was linearized, the state matrix **A** was formulated and linear stability analysis techniques were performed. The process is described in Section 4.5.

4.2 Implementation of Detailed Model

A circuit schematic of the implemented system is shown in Figure 4.1. This schematic is based on the system under study, which could be a part of a shipboard power system, presented in Figure 2.1b.

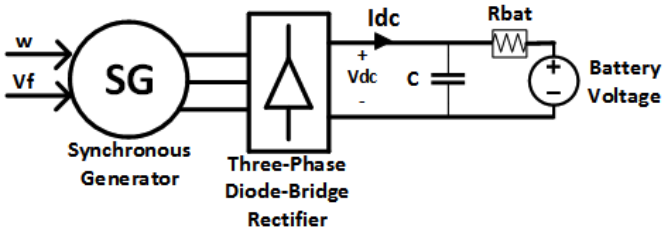

Figure 4.1: A circuit schematic of the system to implement.

4.2.1 Synchronous Generator

The synchronous generator is modeled by using the existing simulink modelling block "*Synchronous Machine pu Standard*" from the following library: Simscape / Electrical / Specialized Power Systems / Electrical Machines. The electrical part of the machine is represented by a sixth-order state-space model while the mechanical part is represented by a second-order model. A detailed description of these models are given in [73] and [74]. The model accounts for the dynamics of the stator, field and damper windings. The equivalent circuit of the electrical model as well as the equation describing the mechanical model can be found in Appendix B. Five different generator data sets have been used during the thesis and they are presented in Table 8.1 in Appendix A. It was chosen to model the synchronous generator with the absence of an AVR and a Governor, so that one can understand whether it is these components that create the instability.

4.2.2 Three-Phase Diode-Bridge Rectifier

The three-phase diode-bridge rectifier model is modeled by using the existing simulink modelling block "*Universal Bridge*" from the following library: Simscape / Electrical / Specialized Power Systems / Power Electronics. A technical description of this model is given in [75] and its electrical circuit is depicted in Appendix B. Because the studied system is characterized as a fairly high frequency system, the generator subtransient reactance can be considered as the commutation inductance, L_s, which is depicted in Figure 3.3a.

4.2.3 DC circuit

Across the DC terminal, a quite large filter capacitor is connected in order to reduce the ripple voltage. A capacitor size of 20 mF per MW is used. The battery is connected in parallel with the filter capacitor and it is modelled as an ideal DC voltage source connected in series with an internal resistance. The value of the internal resistance corresponds to about a 20 V voltage drop during full load operation.

4.2.4 Combined Model

The implemented simulink model is shown in Figure 4.2. The generator is fed with a constant 1 pu speed which is analogous to operating the generator with a very high moment of inertia; one does not allow changes in generator speed. The generator is also fed by field voltage which is set based on the power to be delivered. The generator inputs are utilizing per unit values while the output of the generator, the rectifier, as well as the DC circuit, are using real values. The generator data used for this model is given by the column "*SP1*" in Table 8.1 in Appendix A. It is a 60 Hz system having a nominal power of 3 MVA, a nominal line-to-line voltage of 690 V, and hence a nominal DC voltage of $690\ V \cdot 1.35 = 931.5$ V.

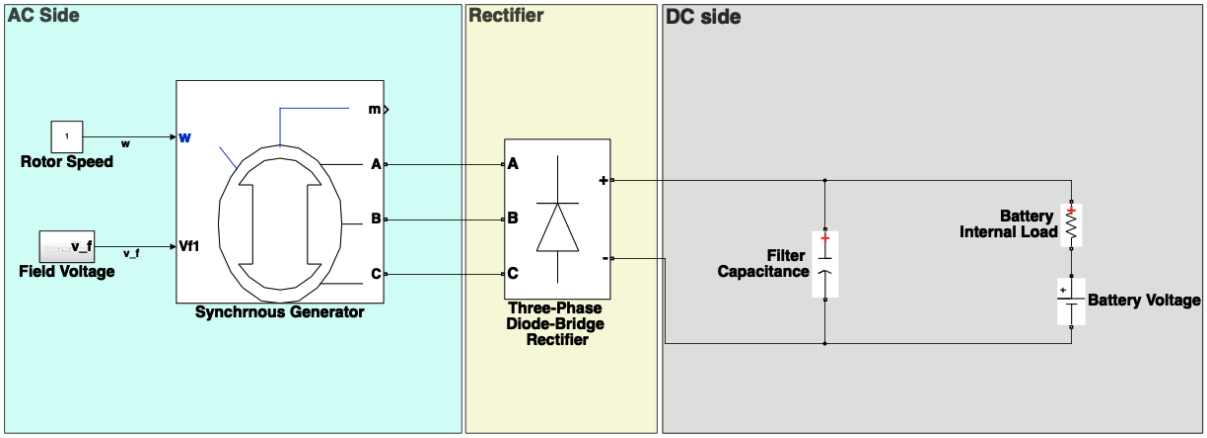

Figure 4.2: Simulink model of a three-phase diode-bridge rectifier connectd to a battery. The synchronous generator is fed by a constant 1 pu speed and a field voltage able to change manually. This is presented to the left (blue area). The synchronous generator are further connected to the three-phase diode-bridge rectifier (yellow) providing power to a battery (grey area).

A three-phase voltage and current measurement block was added to the output generator terminal in order to measure the line voltage and current. In addition there was need to install a small parasitic resistive load, at the generator terminals, to avoid numerical oscillations [73]. These two blocks are not shown in Figure 4.2. In order to calculate the AC line-to-line RMS voltage, an RMS block provided by the Simulink library was used. This block computes the true RMS value of the input signal calculated over a running average window of one cycle of the system fundamental frequency (60 Hz):

$$RMS\big(f(t)\big) = \sqrt{\frac{1}{T}\int_{t-T}^{t} f(t)^2} \tag{4.1}$$

where $f(t)$ is the input signal and T is 1/(fundamental frequency).

The system is modelled with the absence of a cable impedance (inductance) connected between the generator and rectifier. However, this impedance is small compared to the internal generator impedance and will not play a critical role.

With the intention of investigating whether the model is detailed enough (containing enough system components) being able to reproducing the unstable phenomenon, some simulation cases were performed. The field voltage is increased linearly from 0 pu to 2.8 pu where an additional square wave with small voltage steps are superimposed onto the ramp in order to excite possible oscillations in the system. This applied response is shown in Figure 4.3. X'_d was scaled by four different values such that, according to the stability criteria presented in Equation 2.2 and based on the results from the project work [19], an unfavourable generator data-set is present. The larger the ratio $\frac{X_q}{2X'_d}$ the more unpleasant behavior. The four different values used for K_{scale} are presented in Table 4.1. The corresponding stability ratio is also presented.

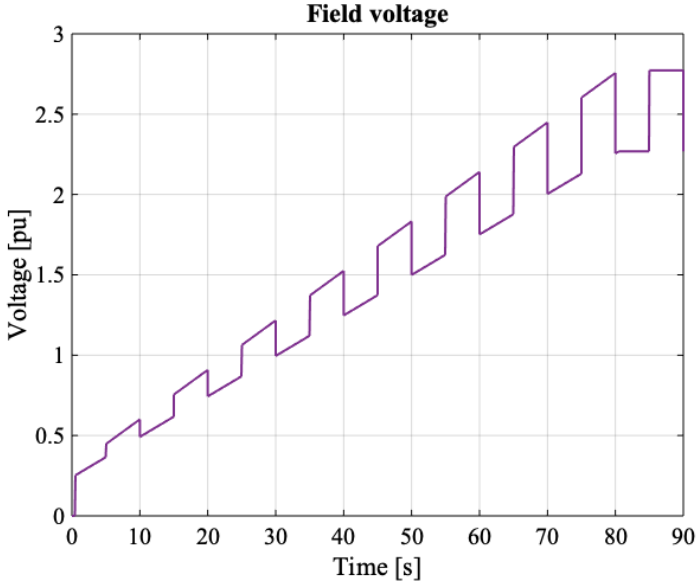

Figure 4.3: The applied field voltage response.

Table 4.1: Four cases of K_{scale} and hence for the stability scenario presented in Equation 2.2.

	K_{scale}	$\frac{X_q}{2\ K_{\text{scale}}\ X'_d}$
Case 1:	1.027778	2.25
Case 2:	1.000000	2.3125
Case 3:	0.963542	2.4
Case 4:	0.889423	2.6

The battery voltage was set to $931,5$ V (1 pu DC voltage), the filter capacitance to 60 mF (20 mF for each MW) and the internal resistance to $0.0062\ \Omega$. This corresponds to 20V voltage drop during nominal load operation:

$$\mathrm{R_{bat}} = \frac{\text{Voltage loss}}{\mathrm{I_{DC,n}}} = \frac{20V}{\frac{3MW}{931,5V}} = 0.0062\ \Omega \tag{4.2}$$

The filter capacitance and the internal battery resistance becomes in per-unit values equal to 0.021471 and 0.017354, respectively. The calculations are shown below.

$$r_{bat} = \frac{\mathrm{R_{bat}}}{Z_{base,DC}} = \frac{\mathrm{R_{bat}}}{(V_{base,DC})^2/P_{base}} = \frac{0.0062\ \Omega}{(931.5\ \mathrm{V})^2/3\ \mathrm{MW}} = 0.021471\ \text{pu} \tag{4.3}$$

$$c = C \cdot Z_{base,DC} = C \cdot \frac{V^2_{base,DC}}{P_{base}} = 60\ mF \cdot \frac{931.5^2\ \mathrm{V}}{3\ \mathrm{MW}} = 0.017354\ \text{pu} \tag{4.4}$$

Figure 4.4 shows the DC voltage, the battery voltage, the DC current and the DC power responses for the simulation case 4, were X'_d is scaled by 0.889423 and thus exacerbating the stability criterion presented in Equation 2.2. Figure 4.5 shows the same responses as in 4.4, but

is zoomed for t = 34s to t = 47s. The matlab code used for initializing the detailed model is attached in 8 in Appendix C.

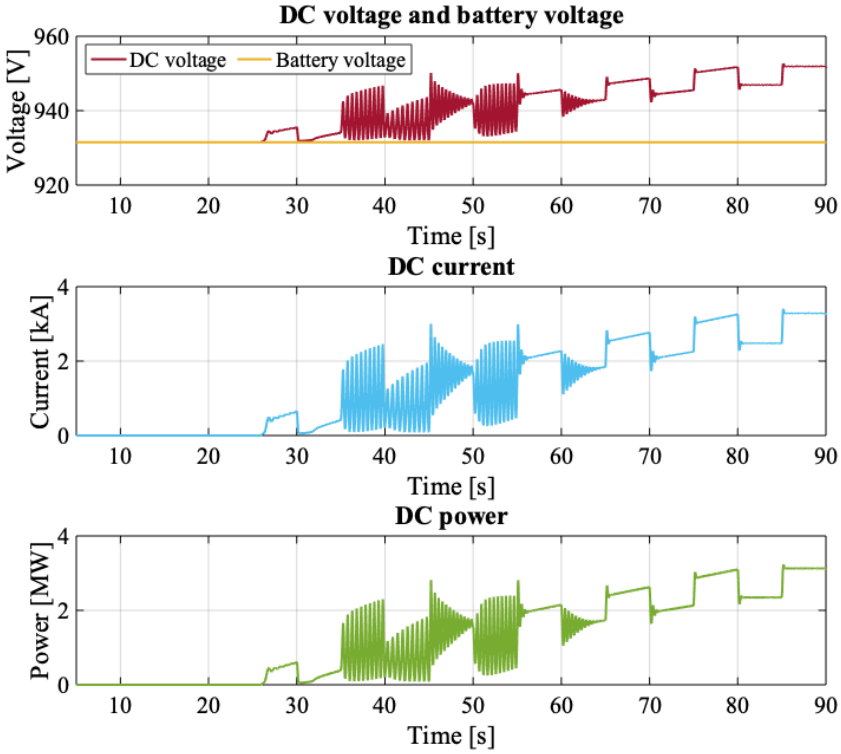

Figure 4.4: DC voltage, battery voltage, DC current and DC power responses corresponding to the simulation case 4. X'_d is scaled by 0.889423 such that the ratio $\frac{X_q}{2X'_d}$ equalize 2.60. The field voltage is increased linearly from 0 pu to 2.8 pu where an additional square wave with small voltage steps are superimposed onto the ramp (Figure 4.3).

Figure 4.4 shows that the DC current is zero, or a very small negative value, until the AC voltage has built up such that V_{ac} is greater than V_{DC}, and the diodes become forward biased and are able to deliver power from the generator. Until this, the DC voltage is given by the sum of the battery voltage and a negligible small voltage due to the drop in the internal battery resistance. Further, undamped oscillations are detected in the DC-output current and power between 20% load and 50% load and the system is considered unstable. The frequency of the oscillations are about 1.5 Hz $-$ 2.6 Hz. Disturbances are detected in the AC voltage and AC currents. Figure 8.3 in appendix C shows the corresponding responses to different variables, such as AC voltage, AC current, d-axis current, q-axis voltage etc..

The responses obtained from the other three cases are not included in this thesis, but they strengthen the fact that the unstable behaviour corresponds to the one detected by previous studies and one can conclude that this model is able to recreate the unstable phenomenon. The unstable phenomenon is characterized by small frequency oscillations, 1 Hz $-$ 3 Hz, between 20% and 50% load. The more load, the greater becomes the frequency of the oscillations.

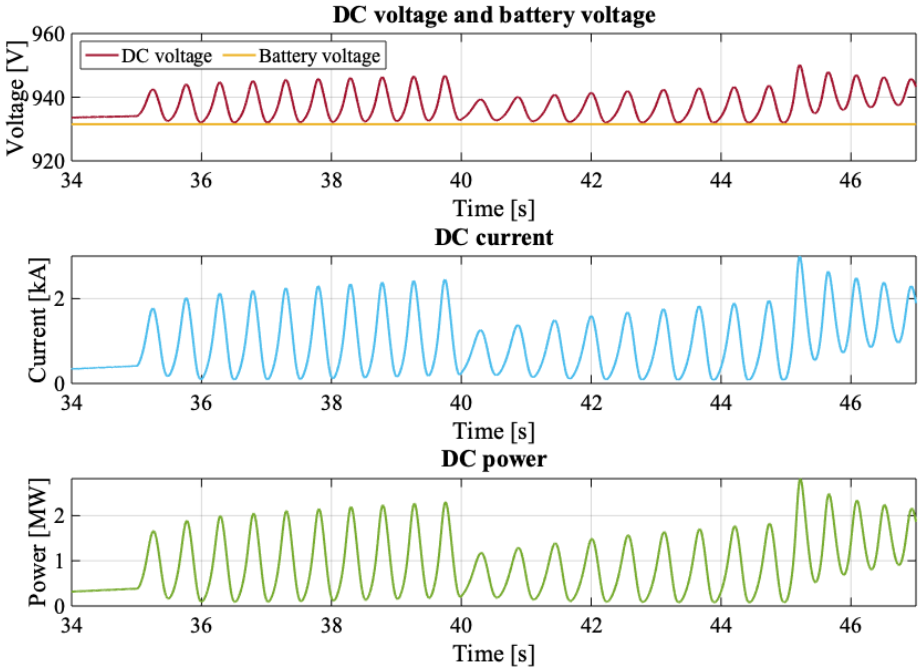

Figure 4.5: DC voltage, battery voltage, DC current and DC power responses, for t=34 s to t=47 s, corresponding to the simulation case 4. X'_d is scaled by 0.889423 such that the ratio $\frac{X_q}{2X'_d}$ equalize 2.60. The field voltage is increased linearly from 0 pu to 2.8 pu where an additional square wave with small voltage steps are superimposed onto the ramp (Figure 4.3).

The instability is a function of load and a worst-case load seems to occur when the generator is loaded about 33% load. The system operates well at higher loads, even for large values of $\frac{X_q}{X'_d}$. The smaller value of X'_d, the larger the ratio $\frac{X_q}{X'_d}$, and the worse the operation becomes. By increasing the ratio between X_q and X'_d so does the range of load that experiences unstable oscillations.
Further, one can conclude that the AVR and the Governor are not the reason causing these unstable oscillations.

4.3 Implementation of Simplified Numerical Model

The simplified model is implemented in three main steps. First, mathematical equations describing each part of the system, as well as equations describing the relationship between them were established. Next step was the main part of the process and contains a time consuming trial and error process. The second step includes the following parts:

- Perform numerical simulation of the mathematical equation derived for each of the parts in the system. This was done step-by-step. First the synchronous generator equations were simulated when feeding an AC load. Secondly, the AC load was replaced by a rectifier and a resistive DC-load. Finally, the resistive DC load was replaced with system

equation describing the filter capacitor operating in parallel with a battery. A trial and error process were performed until the combined model worked properly and yielded sensible results.

- The next step was to investigate whether the model was detailed enough, being able to recreate the unstable behaviour. This was done by scaling X'_d such that an unfavourable generator data set is present. According to the the detailed model should oscillating behaviour be present for all of the four cases listed in Table 4.1. $\mathrm{K_{scale}}$ was set to 1.4453125 during the process of establishing a functioning model. This was done in order to ensure that the unstable phenomenon is not causing any problem during the development process.
- Different values of $\mathrm{K_{scale}}$ was simulated, as well as different level of loads in order to ensure that the unstable behaviour detected by the model corresponds to the one addressed by the detailed model.

After finishing the second step there is need to validate the simplified model with the detailed one. This process is described in the next section, 4.4.
The method used when implementing the simplified model is summarized by the flow chart depicted in Figure 4.6.

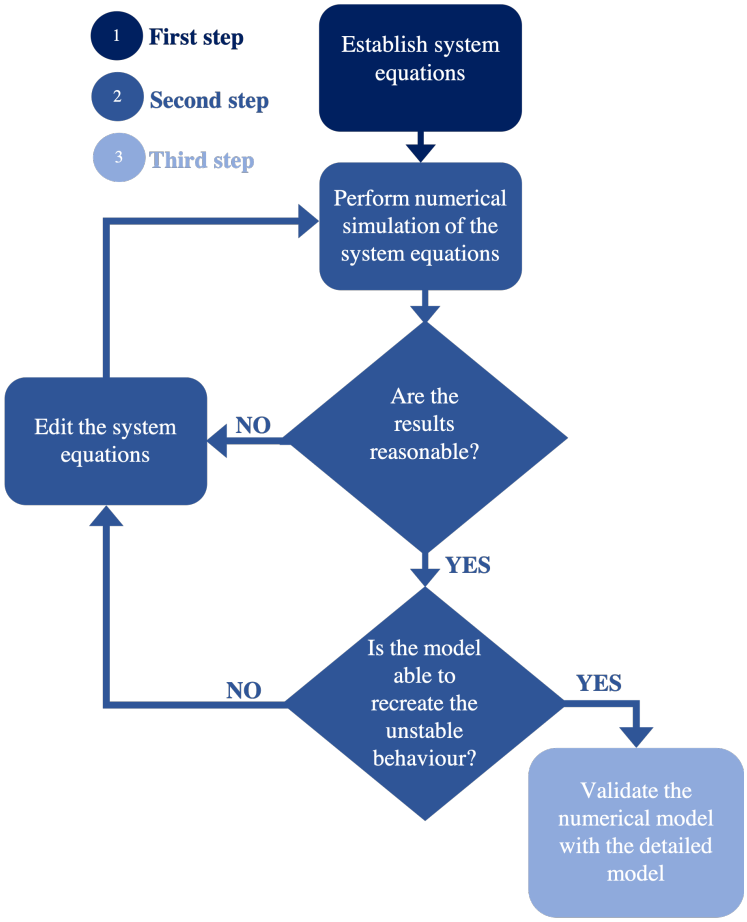

Figure 4.6: Flow chart summarizing the implementation process of the simplified model.

4.3.1 Synchronous Generator

Having the idea of keeping the model simple and to understand whether the unstable phenomenon is an electromagnetic of electromechanical phenomenon, it was chosen to try to exclude the mechanical part of the synchronous generator, only include the electrical part. Thus, the four last differential equation presented in Equation 3.38 in Chapter 3.5.4, as well as the two algebraic equation presented in Equation 3.40. The dq-reference frame is aligned according to the IEEE-standard [70] with the d-axis 90° ahead of the q-axis. A phasor diagram visualizing the dq-reference frame used for implementation of the simplified model is sketched in Figure 4.7. The load angle, δ, is for a synchronous generator defined as the angle between the rotor flux and the resultant air gap flux and it corresponds to the angle between the output AC voltage and the q-axis in the rotor [76]. The phase angle, ϕ, denotes the phase shift between the AC output voltage and the AC output current while the angle between the AC output current and the q-axis in the rotor is determined by the sum of δ and ϕ.

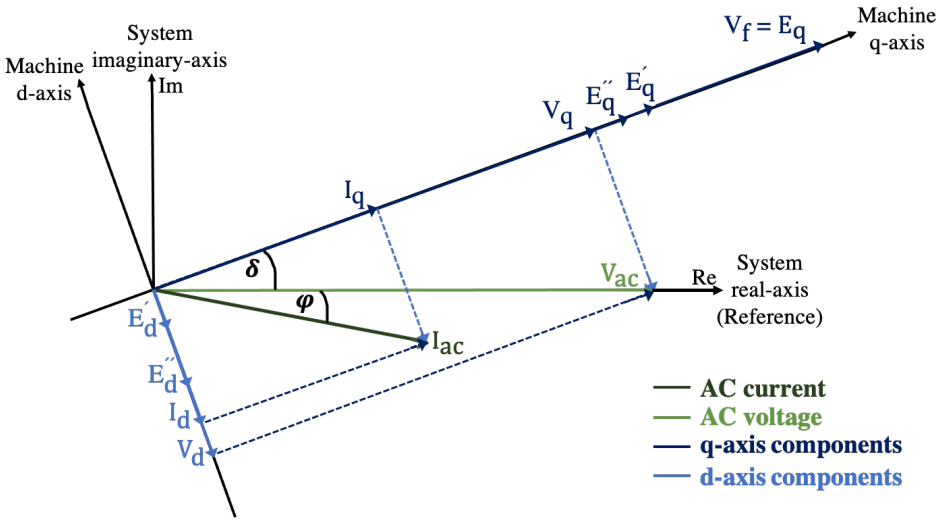

Figure 4.7: Phasor diagram visualizing the dq-reference frame used for implementation of the simplified numerical model.

The mathematical equation used to described the synchronous generator are summarized below:

$$\begin{aligned} T'_{d0}\dot{E}'_q &= E_f - E'_q + I_d(X_d - X'_d) \\ T'_{q0}\dot{E}'_d &= -E'_d - I_q(X_q - X'_q) \\ T''_{d0}\dot{E}''_q &= E'_q - E''_q + I_d(X'_d - X''_d) \\ T''_{q0}\dot{E}''_d &= E'_d - E''_d - I_q(X'_q - X''_q) \end{aligned} \tag{4.5}$$

$$\begin{bmatrix} I_d \\ I_q \end{bmatrix} = \frac{1}{R^2 + X''_d X''_q} \begin{bmatrix} -R & X''_q \\ -X''_d & -R \end{bmatrix} \begin{bmatrix} V_d - E''_d \\ V_q - E''_q \end{bmatrix} \tag{4.6}$$

The last expression 4.6 corresponds to the equations presented in 3.40 but with the currents expressed as a function of the voltages. Further, because $X_q \approx X'_q$ yields for all the generator data sets used during this thesis, one can eliminate the second equation in 4.5 and the remaining model corresponds to a fifth order synchronous machine model which neglects the screening effect of the rotor body eddy currents in the q-axis [25, p.455]. One of the synchronous generator set studied during this thesis is a round rotor synchronous generator. As explained in Chapter 3, such generators usually satisfy $X_q > X'_q$ due to the rotor body eddy currents flowing in its rotor core construction. However, why the round rotor synchronous generator data made available for this thesis satisfies $X_q = X'_q$ is unknown. E_f in the first equation corresponds to the field voltage which in the implemented models is referred to as V_f.

The five reminding equations are further implemented into simulink as shown in Figure 4.8. The model is implemented by the use of per-unit values. I_d and I_q are calculated based on E''_q, E''_d, V_d and V_q and are further fed into the three differential equations in order to update the state variables E'_q, E''_q and E''_d. The rectifier is also fed by I_d and I_q.

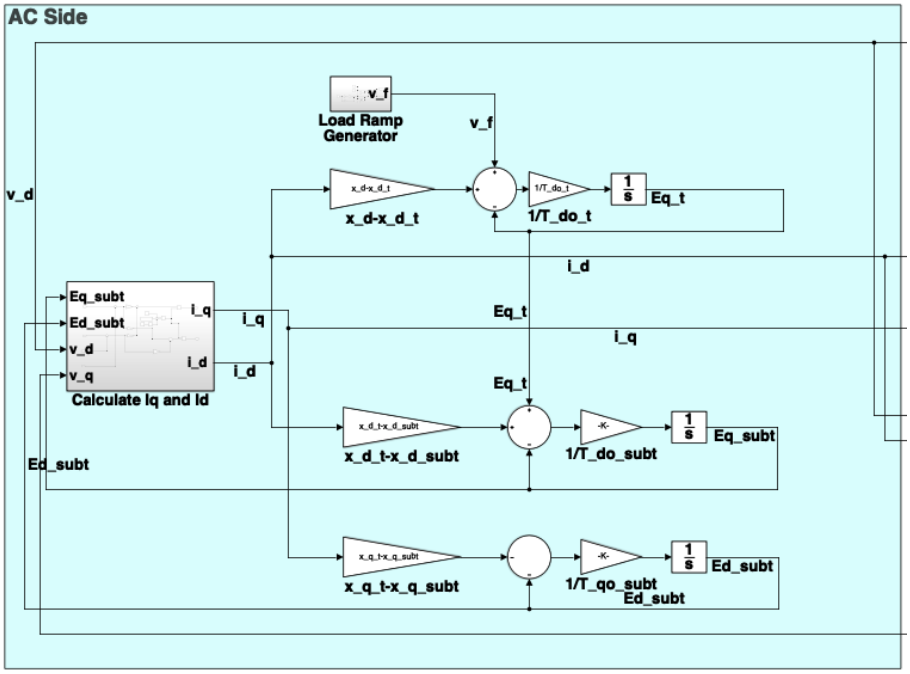

Figure 4.8: Synchronous generator mathematical equations implemented in Simulink.

4.3.2 Three-Phase Diode-Bridge Rectifier

The most time-demanding part of the implementation process was to find a appropriate way to simplify the switching in the diodes, as well as how to connect the generator to the rectifier. Section 2.3 presents some existing methods for eliminating the diode switching and the outcome was to follow the technique used by Jatskevich [45], which is an average-value model used for eliminating the switching action in the rectifier. The mathematical equations used to represent

the rectifier are derived based on the phasor diagram shown in Figure 4.7 and they are listed in 4.7.

$$\begin{aligned} i_{DC} &= \beta\sqrt{i_d^2 + i_q^2} \\ v_d &= -\alpha \sin(\delta) v_{DC} \\ v_q &= \alpha \cos(\delta) v_{DC} \\ \delta &= \arctan\left(\frac{-i_d}{i_q}\right) - \phi \end{aligned} \tag{4.7}$$

where α, β and ϕ are a obtained from simulation of the detailed model and are calculated as shown in 4.8.

$$\begin{aligned} \beta &= \frac{i_{DC}}{\sqrt{i_d^2 + i_q^2}} \\ \alpha &= \frac{\sqrt{v_d^2 + v_q^2}}{v_{DC}} \\ \phi &= \arctan\left(\frac{i_d}{i_q}\right) - \arctan\left(\frac{v_d}{v_q}\right) \end{aligned} \tag{4.8}$$

α and β can be interpreted as a transformer ratio between the AC and DC side, or as a measure of the efficiency in the rectifier. The minus sign used in front of i_d when calculating δ, as well as the one used when calculating v_d in 4.7 is due to the definition of the d-axis leading the q-axis in the simplified model. These minus signs, in front of i_d and v_d when calculating ϕ in 4.8, are not included because the detailed model uses a Simulink block model of a synchronous generator that has defined the q-axis to lead the d-axis [73].

Figure 4.10 shows the response of α, β and ϕ when v_f is increased linearly from 0 pu to 2.8 pu (Figure 4.9a), which corresponds to a linear increase in the power delivered from the generator to the battery, from 0 pu to 1.06 pu (Figure 4.9b). Figure 4.11 shows the same response as in Figure 4.10, but only for the time when the AC output voltage is large enough to cause the diodes to conduct and thus power is supplied from the AC side to the DC side. α, β and ϕ are all a function of load, however, as seen in Figure 4.11 the changes due to variation of load are small. The maximal deviations in each of the variables, ϕ, α, and β, for the period where power is delivered from the AC side to the DC side are 0.0534 rad, 0.146 and 0.0981, respectively. ϕ varies from 0.1806 to 0.2334 which corresponds to a power factor varying between 0.973 and 0.984. These obtained values for the power factor corresponds well to the theoretical value, 0.955, mentioned in Chapter 3.4.

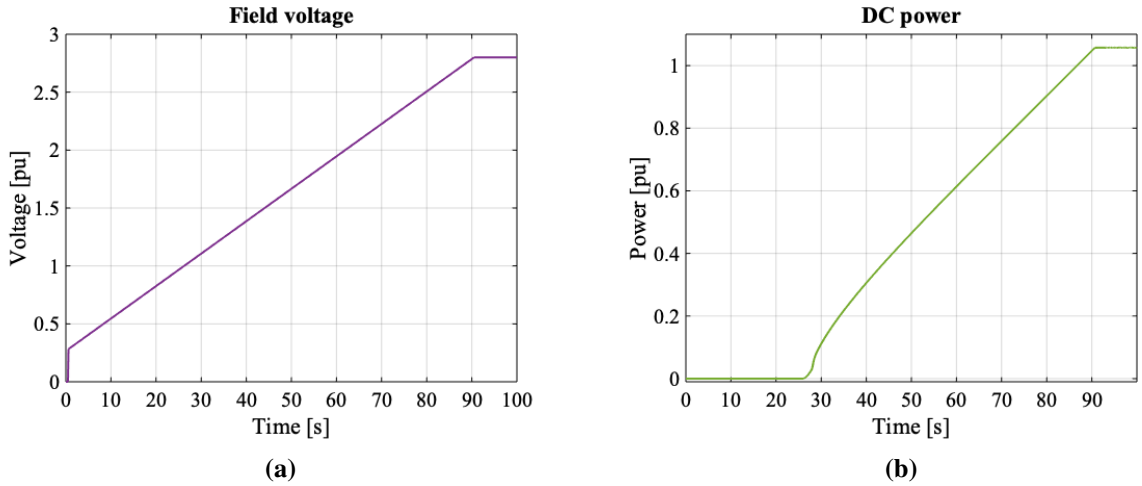

Figure 4.9: (a) The applied field voltage response and (b) the corresponding DC power response.

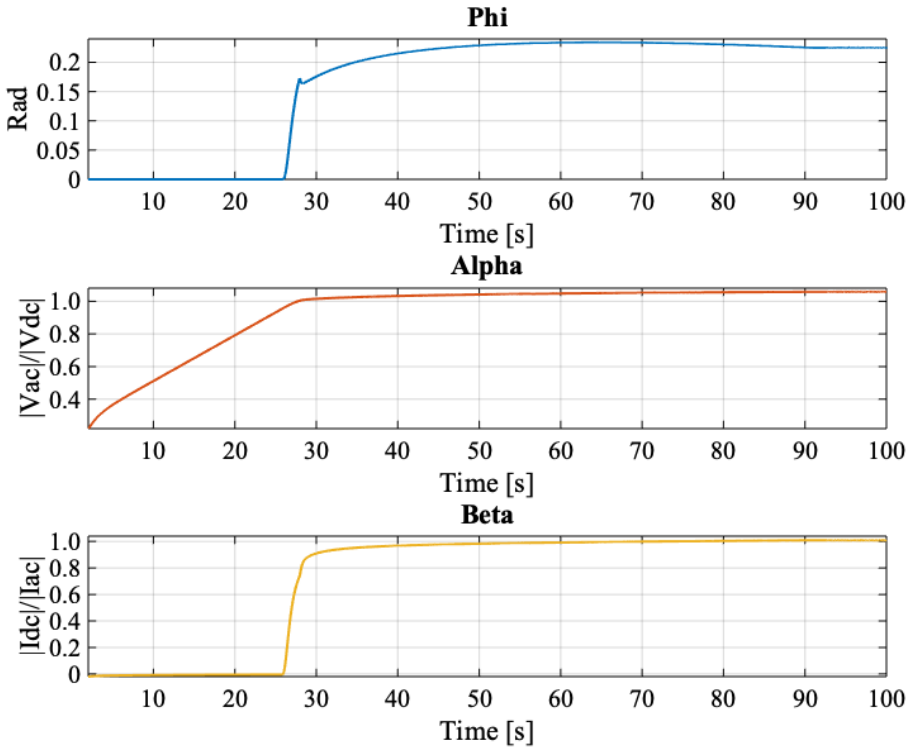

Figure 4.10: The ϕ, α and β responses when the field voltage is increased linearly from 0 pu to 2.8 pu.

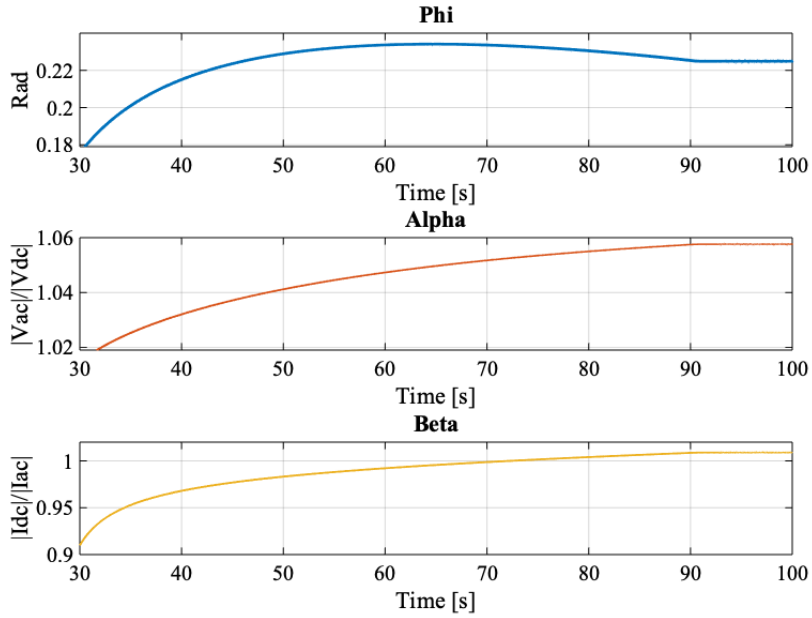

Figure 4.11: The ϕ, α and β responses when the field voltage is increased linearly from 0 pu to 2.8 pu, for the time where the diodes are forward biased and able to deliver power from the AC side to the DC side.

The first equation in 4.7 is implemented into Simulink as shown in Figure 4.12. The currents i_q and i_d are fed from the synchronous generator into the rectifier and appears on the DC side as i_{DC}. The DC current direction is calculated based on the calculated AC power polarity. A negative AC power means that the AC output voltage is smaller than the DC voltage (mainly the battery voltage) and the current is flowing from the battery towards the DC side. On the other hand, a positive AC power means that the AC output voltage is greater than the DC voltage and the current is flowing from the generator towards the battery. To be more exact, one should not allow the AC power to be negative because the diodes become reversed bias as soon as the current through it goes to zero, and it blocks for a current trying to flow from the DC side towards the AC side.

The three last equations in 4.7 are further implemented into Simulink as shown in Figure 4.13. i_q and i_d are fed from the AC side and v_{DC} from the DC side. Because $arctan(x)$ goes to $\frac{\pi}{2}$ as x goes to infinity, a switch is inserted right after the inverse-tangent is applied to the ratio $\frac{-i_d}{i_q}$. The switch takes action as soon as i_q approaching zero. This problem with division by zero can be avoided by replacing $\arctan\left(\frac{-i_d}{i_q}\right)$ with $\arcsin\left(\frac{-i_d}{\sqrt{i_d^2+i_q^2}}\right)$. Further, subtracting the angle ϕ, gives the power angle δ which has to be delayed by $10-100$ms in order to prevent an algebraic loop to occur. It is not enough to just initialize δ, then the problem is just delayed to a later instance of time. In order to stabilize the simulation model upon start, δ is kept constant and equal a suitable initiating value during the first 0.5s. Finally, v_d and v_q are calculated and fed to the synchronous generator. The model is implemented by the use of per-unit values.

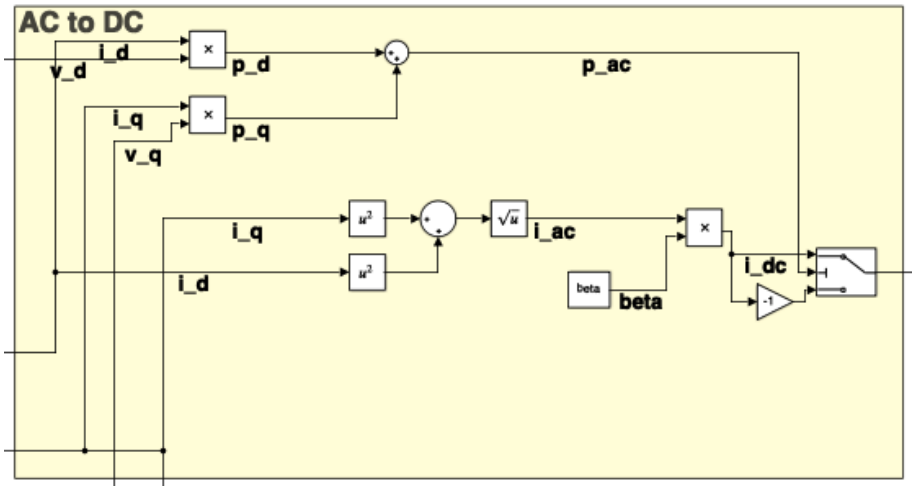

Figure 4.12: AC to DC mathematical equations implemented in Simulink.

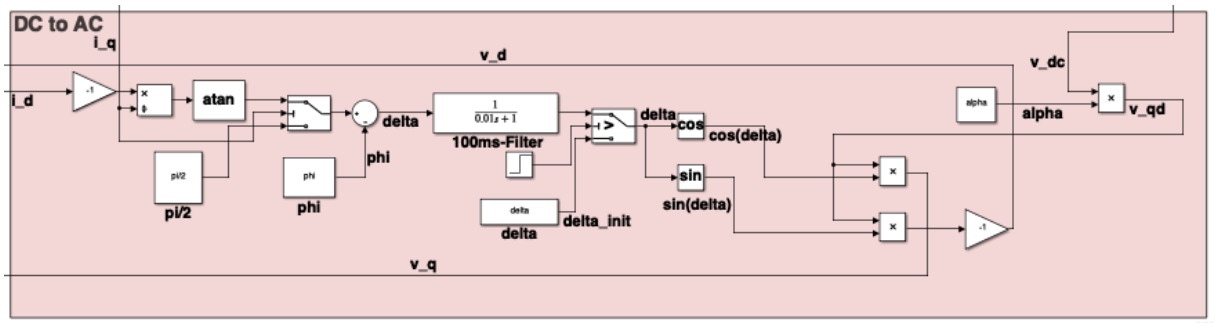

Figure 4.13: DC to AC mathematical equations implemented in Simulink.

The installation of a 10 - 100 ms filter gives rise to a new additional differential equation:

$$\dot{\delta} = \frac{1}{T_\delta}\left(-\delta + \arctan\left(\frac{-i_d}{i_q}\right) - \phi\right) = \frac{1}{T_\delta}\left(-\delta + \arcsin\left(\frac{-i_d}{\sqrt{i_d^2 + i_q^2}}\right) - \phi\right) \tag{4.9}$$

where T_δ is the filter time constant. As already mentioned, the benefit of using the expression containing $arcsin()$ is to avoid the problem with division by zero.

4.3.3 DC-model

A circuit schematic of the DC circuit is depicted in Figure 4.14.

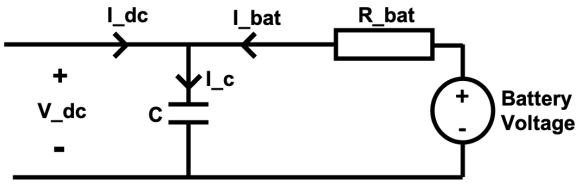

Figure 4.14: A circuit schematic of the DC circuit to model.

The following three equations yields for the DC circuit:

$$\begin{aligned} I_c &= I_{DC} + I_{bat} \\ I_{bat} &= \frac{V_{bat} - V_{DC}}{R_{bat}} \\ I_c &= C\frac{\partial V_c}{\partial t} = C\frac{\partial V_{DC}}{\partial t} \end{aligned} \tag{4.10}$$

Inserting the second equation into the first and further inserting the first into the third gives the following:

$$I_{DC} + \frac{V_{bat}}{R_{bat}} - \frac{V_{DC}}{R_{bat}} = C\frac{\partial V_{DC}}{\partial t} \tag{4.11}$$

Rewriting equation 4.11 yields:

$$\dot{V}_{DC} = \frac{1}{C}\left(I_{DC} + \frac{V_{bat}}{R_{bat}} - \frac{V_{DC}}{R_{bat}}\right) \tag{4.12}$$

which is further implemented in Simulink as shown in Figure 4.15. Per-unit values are used.

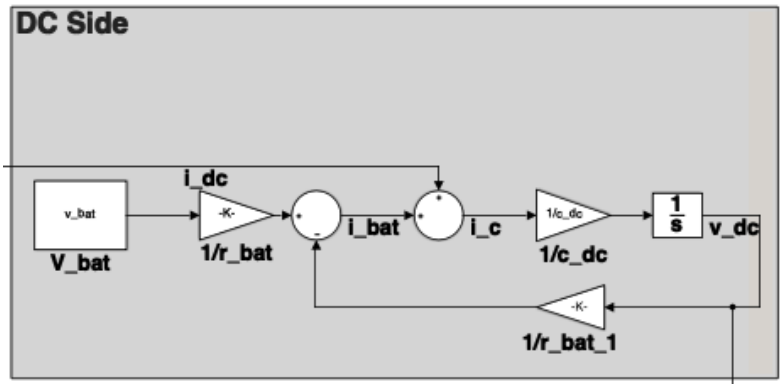

Figure 4.15: DC circuit mathematical equation implemented in Simulink.

4.3.4 Combined Model

The so far discussed mathematical equations used to implement the simplified average model consists of five differential equations and five other algebraic equations. They constitutes a non-linear model and are all summarized in 4.13.
The five differential equation give rise to the five state variables E'_q, E''_q, E''_d, δ and V_{DC}. If $X_q \not\approx X'_q$ one should include the second equation listed in 4.5 to the total combined model. However, this equation is excluded from the total combined model because $X_q \approx X'_q$ yields for all the generator data sets used during this thesis. E_f in the first equation corresponds to the field voltage which in the implemented models is referred to as V_f.

$$
\begin{aligned}
&\text{Synchronous Generator} \begin{cases}
\dot{E}'_q = \frac{1}{T'_{d0}} \left[E_f - E'_q + I_d(X_d - X'_d) \right] \\
\dot{E}''_q = \frac{1}{T''_{d0}} \left[E'_q - E''_q + I_d(X'_d - X''_d) \right] \\
\dot{E}''_d = \frac{1}{T''_{q0}} \left[E'_d - E''_d - I_q(X'_q - X''_q) \right] \\
\begin{bmatrix} I_d \\ I_q \end{bmatrix} = \frac{1}{R^2 + X''_d X''_q} \begin{bmatrix} -R & X''_q \\ -X''_d & -R \end{bmatrix} \begin{bmatrix} V_d - E''_d \\ V_q - E''_q \end{bmatrix}
\end{cases} \\
&\text{Diode Bridge Rectifier} \begin{cases}
I_{DC} = \beta \sqrt{I_d^2 + I_q^2} \\
\begin{bmatrix} V_d \\ V_q \end{bmatrix} = \alpha V_{DC} \begin{bmatrix} -\sin\delta \\ \cos\delta \end{bmatrix} \\
\dot{\delta} = \frac{1}{T_\delta} \left[-\delta + \arctan\left(\frac{-I_d}{I_q} \right) - \phi \right]
\end{cases} \\
&\text{DC Circuit} \begin{cases}
\dot{V}_{DC} = \frac{1}{C} \left[I_{DC} + \frac{V_{bat}}{R_{bat}} - \frac{V_{DC}}{R_{bat}} \right]
\end{cases}
\end{aligned}
\tag{4.13}
$$

Combining the above equations listed in 4.13 results in a simplified average model. Figure 4.16 shows this simplified combined model implemented in Simulink. Merging the models shown in Figure 4.8, 4.12, 4.13 and 4.15 results in the combined implemented Simulink model shown in Figure 4.16. Per-unit values are utilized.

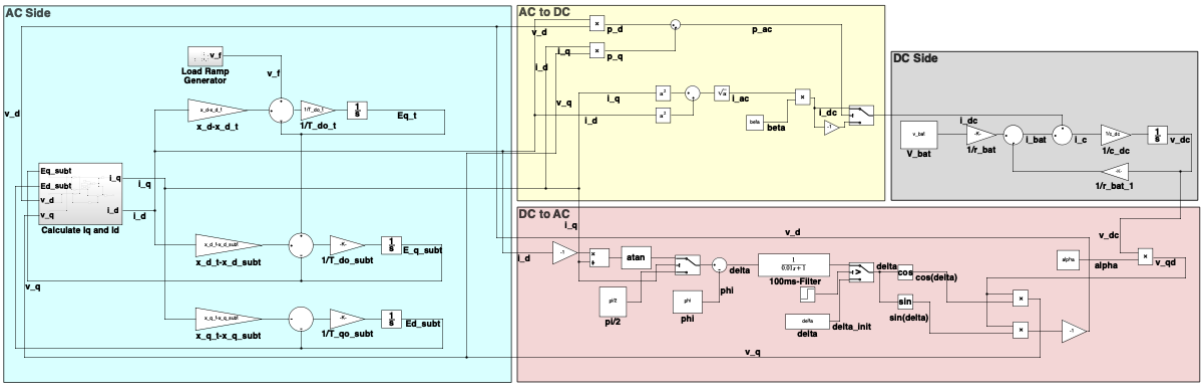

Figure 4.16: The simplified combined model implemented in Simulink. It combines the models shown in Figure 4.8, 4.12, 4.13 and 4.15. The model operates with per-unit values.

V_d and V_q are calculated based on V_{DC}, α and δ and are then fed to the synchronous generator equations. V_d and V_q are used to calculate I_d and I_q which further are used to update E'_q, E''_q and E''_d, as well as I_{DC} and δ. I_{DC} is finally used to update V_{DC} and so it continues, on and on. Figure 4.17 illustrates this process where arrows are used to visualize the flow between the different equations.

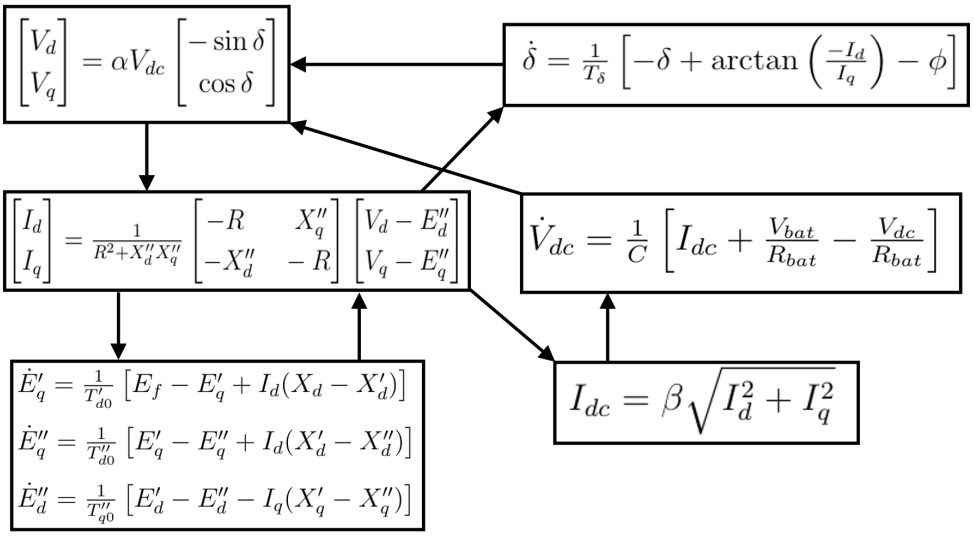

Figure 4.17: Visualization of the flow between the different algebraic equations in the simplified model.

In order to run the simplified model one must choose a operating point (a level of load) and hence a field voltage, V_f. There is also need to set the generator data parameters, the filter capacitance as well as the battery parameters. Based on this information simulations in the detailed model can be performed in order to obtain suitable values for α, β and ϕ. Steady state values for V_{DC} and I_{DC} are also obtained from the detailed simulation model in order to initialize the state variables E'_q, E''_q, E''_d, δ and V_{DC}. It is important that detailed model operates at steady state when obtaining these values and a stable generator data set must therefore be present. The Matlab script used to initialize these state variables and the other necessary parameters needed in order to run the simplified model in Simulink, are attached in 8 in Appendix D. This procedure on how to operate the model is summarized by Figure 4.18.

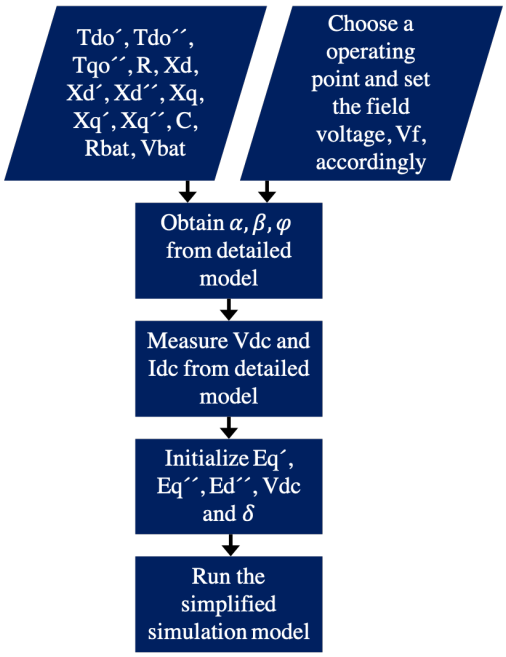

Figure 4.18: Flow chart summarizing how to operate the model.

In order to examine whether the model is able to reproducing the unstable phenomenon, some simulation cases were performed. The battery voltage was set to 1 pu and the field voltage to 1.8 pu, which corresponds to 56% AC load, where an additional square wave with 2% voltage steps are superimposed onto the field voltage in order to excite possible oscillations in the system. This applied response is shown in Figure 4.19. Because the simplified model operates with constant values for α, β and ϕ, which corresponds to a field voltage of 1.8 pu, large changes in the field voltage should be avoided. However, Section 4.3.2 shows that changes in load only results in minor changes in α, β and ϕ. X'_d was scaled by three different values such that, according to the stability criteria presented in Equation 2.2 and based on the results from the project work [19], unfavourable generator data-sets are present. The larger the ratio $\frac{X_q}{2X'_d}$ the more unpleasant behavior. The three different values used for K_{scale} are presented in Table 4.3. The corresponding stability ratio is also presented.

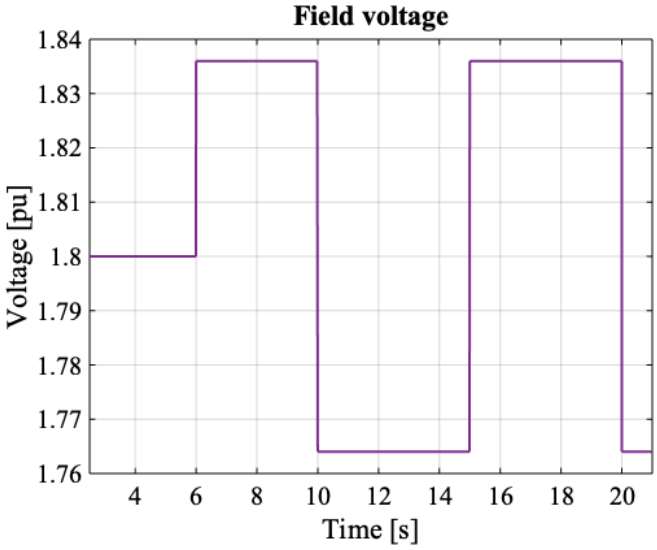

Figure 4.19: The applied field voltage response.

Table 4.2: Three cases of K_{scale} and hence for the stability scenario presented in Equation 2.2.

	K_{scale}	$\frac{X_q}{2\ K_{\text{scale}}\ X'_d}$
Case 1:	1.000000	2.3125
Case 2:	1.027778	2.25
Case 3:	1.217105	1.90

Initializing the detailed simulation model with the Matlab script attached in Appendix C resulted in the values shown in Table 4.3, which was used when initializing the simplified simulation model. The Matlab script used to initialize the simplified model is attached in Appendix D.

Table 4.3: Values obtained from simulation of the detailed model when the field voltage and battery voltage are set to 1.8 pu 1 pu, respectively.

Parameter	Value obtained
α	1.0444
β	0.9880
$\phi\ [rad]$	0.2321
v_{DC}	1.0114
i_{DC}	0.5325

Figure 4.20 shows the DC voltage, DC current and DC power responses obtained by running case 1, which corresponds to the original value of X'_d. The corresponding output responses obtained for other system variables are shown in Figure 8.4 in Appendix D. Figure 4.20 shows undamped oscillations between 10 s and 15 s. Comparing the obtained responses with the graph of the applied field voltage shown in Figure 4.19 indicates that the oscillatory behaviour gets worse for lower values of the v_f = 1.8 pu and hence for lower values of 56% load. The frequency of the oscillations is about 2.5 Hz. Corresponding graphs are obtained for case 2 and 3 and they are shown in Figure 8.6, 8.5, 8.8 and in 8.7 in Appendix D. 4.21 contains the DC voltages for each of the three cases and it shows that the smaller X'_d and hence the larger ratio $\frac{X_q}{2X'_d}$, the more unstable the system becomes.

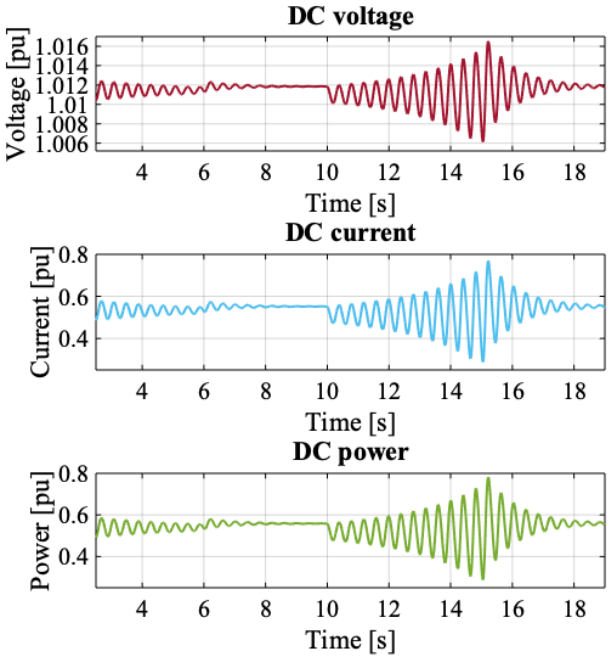

Figure 4.20: DC voltage, DC current and DC power responses for $t = 2.5$ s to $t = 19$ s. The simplified model is operated at about 56% load where small steps in the field voltage are applied (Figure 4.19). The battery voltage is set to 1 pu. The responses corresponds to the simulation case 1 presented in Table 4.3, X'_d corresponds to its original value and hence the ratio $\frac{X_q}{2X'_d}$.

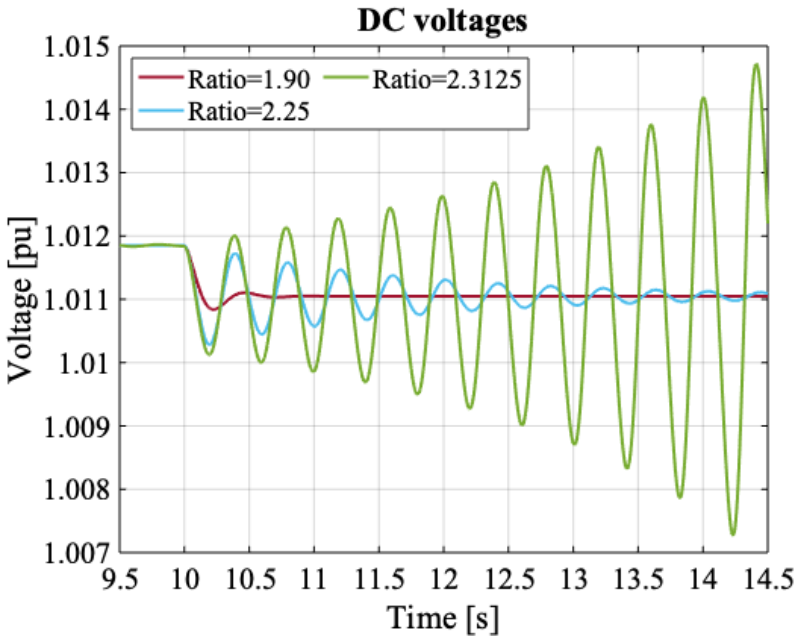

Figure 4.21: DC voltages responses for varying values of X'_d and thus for the ratio $\frac{X_q}{2X'_d}$. The green curve, the blue curve and the red curve coresponds to simulation of case 1, 2 and 3, respectively.

These observed characteristics reminds of the unstable phenomenon presented in Chapter 2. To strengthen this hypothesis, similar simulations were run for different values of field voltage and thus for different values of load. Also this indicated the presence of the same phenomenon. It is a function of load, having a worst case load about 33%, the frequencies of the oscillations are about 1.5Hz - 2.6Hz and the instabilities gets worse as X'_d decreases and hence the ratio between X_q and X'_d.

At this point, because the simplified model is operating the generator with the absence of a mechanical system, the conclusion is that well-known rotor oscillations is not a part of the underlying problem and the instability is considered an electromagnetic phenomenon, not an electromechanical phenomenon.

In addition, based on the fact that the simplified model became unstable, despite that the dynamics associated with diode switching were removed, this indicates that the diode commutation as such is not part of the underlying problem.

4.4 Model Validation

At this point, two simulation models with different degrees of detail are able to reproducing the unstable phenomenon detected by previous literature. A next step was to validate the simplified model against the detailed model. To do so, both of the models was operated with the same conditions, with the same battery voltage of 1 pu and the same level of field voltage. The simplified model operates with values for α, β and ϕ that corresponds to the operation point

and are obtained from simulation of the detailed model as described in the previous section. Further, small voltage step was injected to the field voltage such that the field voltage was decreased and increased by 2% from the initialized operation point. The shape of the applied field voltage is shown in Figure 4.22. The simplified model was validated for several different level of load, and four of them are presented in Table 4.4.

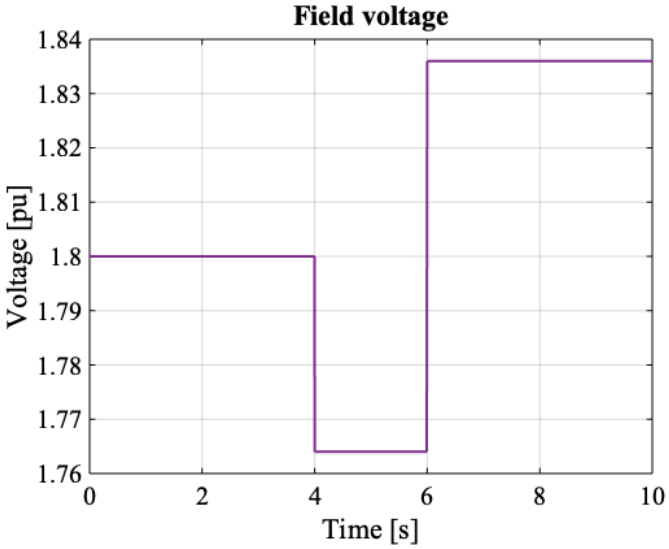

Figure 4.22: The field voltage applied when validating the simplified model against the detailed model. This Figure represents the case were the models are validated around a field voltage of 1.8 pu.

Table 4.4: Four of the operation point used when validating the simplified model against the detailed model.

	v_f [pu]	p_{ac} [%]
Case 1:	2.5	92.9
Case 2:	1.8	55.6
Case 3:	1.4	33.0
Case 4	1.1	12.2

The field voltage graph shown in Figure 4.22 corresponds to validation case 2, but similar shapes are applied for the other cases where instead of operating around 1.8 pu, one operates around 2.5 pu 1.4 pu and 1.1 pu for case 1, case 3 and case 4, respectively. In order to prevent the simplified model from collapsing, due to large undamped oscillations, it was chosen to increase X'_d from its original value such that the ratio $\frac{X_q}{2X'_d}$ equalizes 1.60.

Figure 4.23 shows the DC voltage, DC current, DC power and AC power responses for validation case 1, for both simplified and detailed model, where the field voltage is initialized at 2.5 pu. The simplified model seems to follow the detailed model very well.

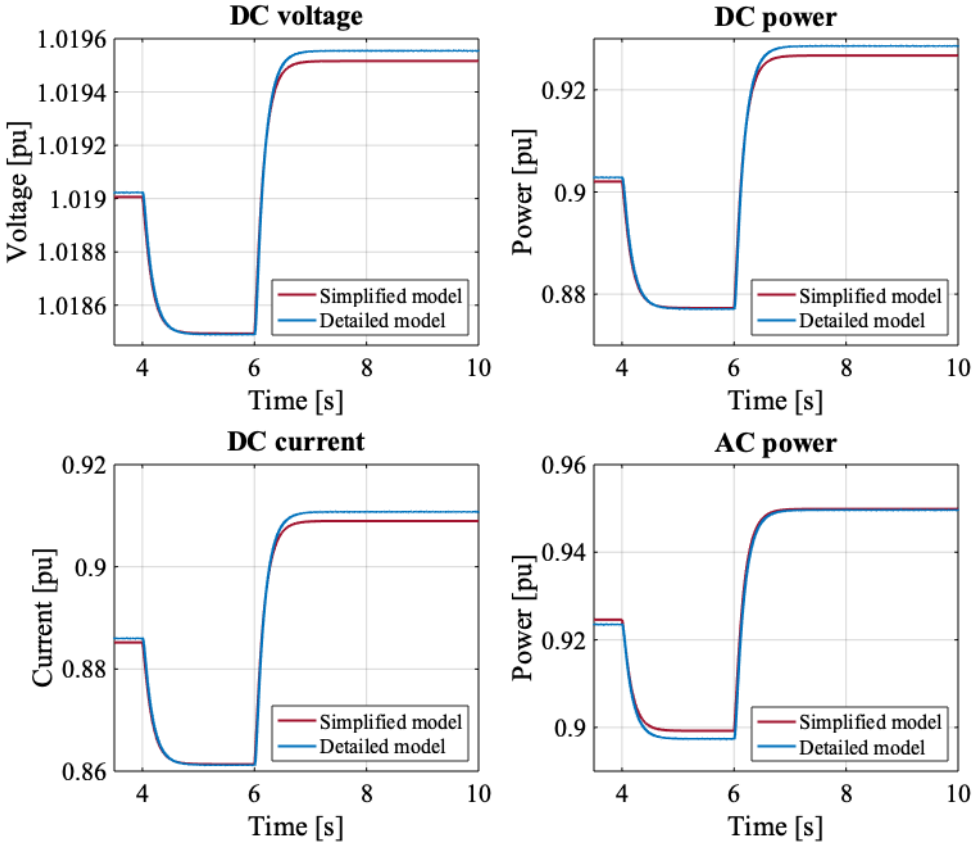

Figure 4.23: The DC Current, DC voltage, DC power and AC power responses corresponding to validation case 1, where the field voltage is stepped by $\pm 2\%$ from 2.5 pu. The applied field voltage follows the same shape as the graph shown in Figure 4.22.

The corresponding responses obtained for the q-axis and d-axis voltages and currents are depicted in Figure 4.24. Because the Simulink synchronous machine model defines the q-axis to lead the d-axis while the simplified model does the opposite, there was need to change the polarity of the data obtained for the d-axis components to more easier compare their responses. 4.24 shows that the shape of the d- and q-axis responses obtained for the models corresponds well, however, they are shifted with some small an constant value from each other. The same yields for the responses obtained for the load angle δ, that are depicted in Figure 4.25.

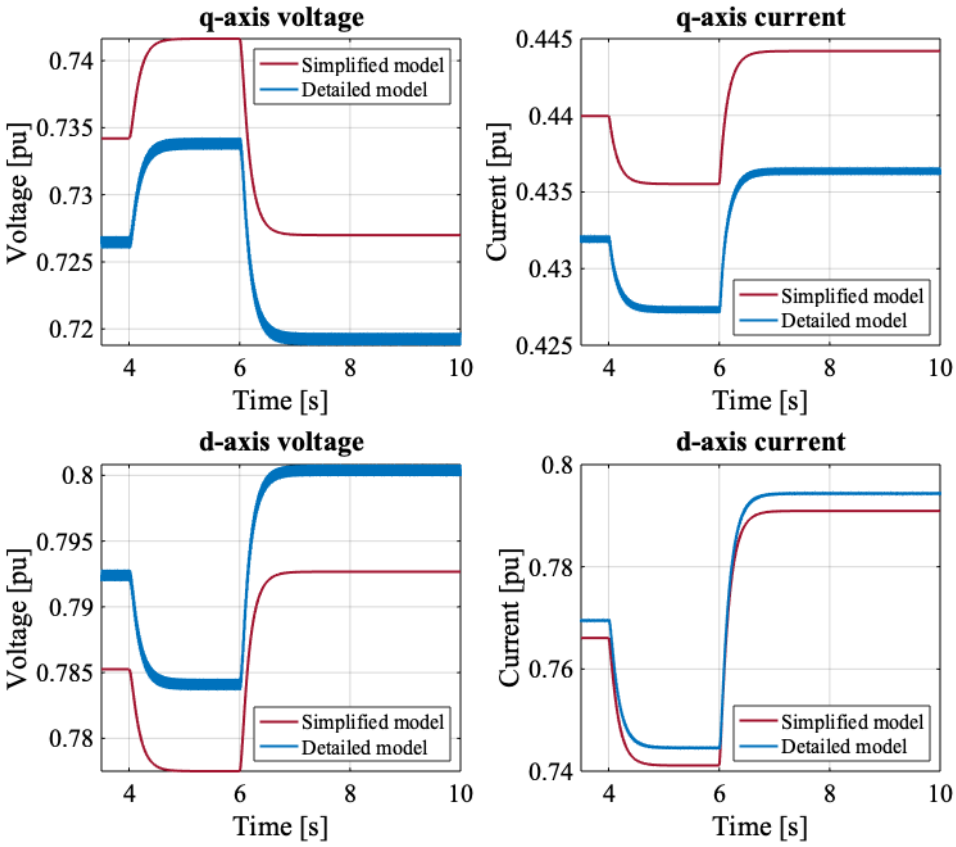

Figure 4.24: The d- and q-axis voltage and current responses corresponding to validation case 1, where the field voltage is stepped by $\pm 2\%$ from 2.5 pu. The applied field voltage follows the same shape as the graph shown in Figure 4.22.

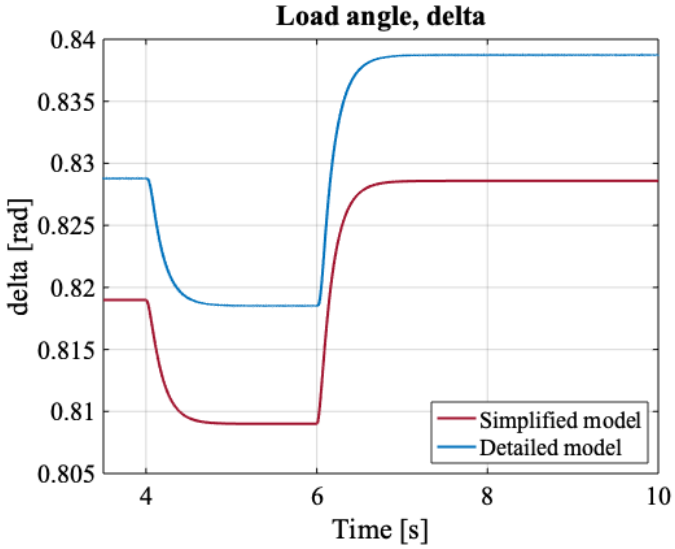

Figure 4.25: The Load angle, δ, responses corresponding to validation case 1, where the field voltage is stepped by $\pm 2\%$ from 2.5 pu. The applied field voltage follows the same shape as the graph shown in Figure 4.22.

The corresponding responses obtained for validation case 4, which corresponds to an operation around 12% load, are shown in Figure 4.26, 4.27 and 4.28. Previous simulations have shown that these level of load is more prone for the unstable phenomenon. However, X'_d was, as already mentioned, increased from its original value in order to make the operation more pleasant.

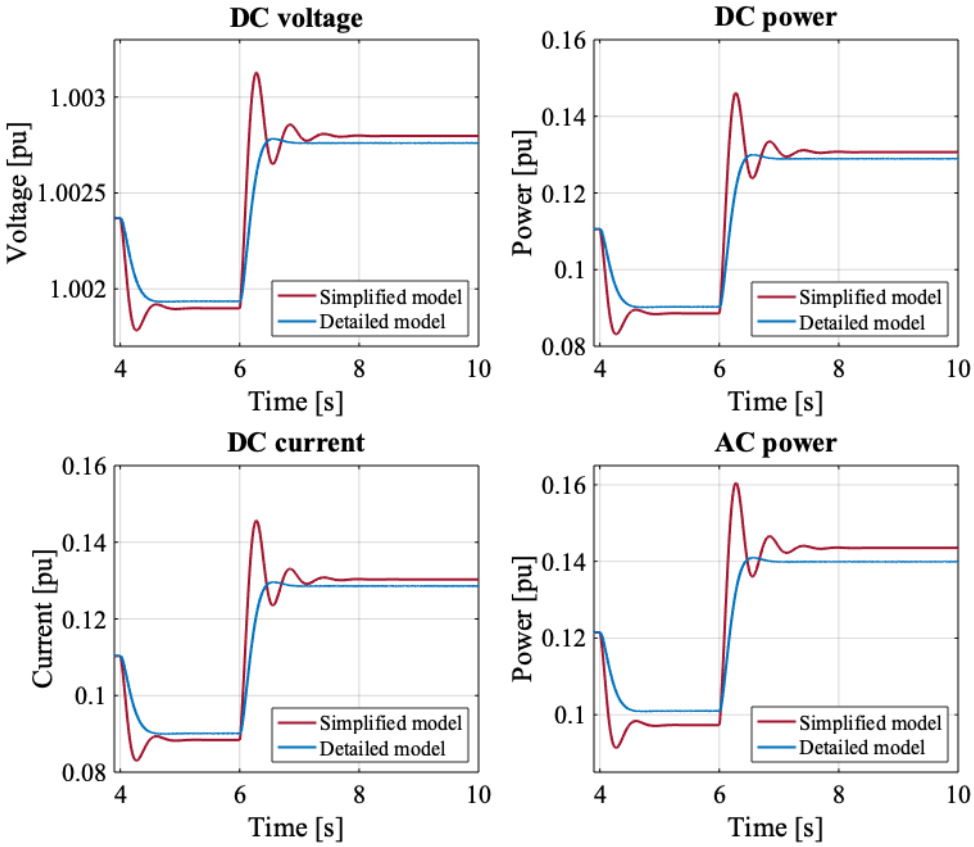

Figure 4.26: The DC Current, DC voltage, DC power and AC power responses corresponding to validation case 4, where the field voltage is stepped by $\pm 2\%$ from 1.1 pu. The applied field voltage follows the same shape as the graph shown in Figure 4.22.

The nine different responses obtained for this validation case shows that the simplified model follows the detailed model well, however, the shape of the graphs differ. The responses obtained for the simplified model are model oscillatory and and weaker damped. Some of the modes corresponding to the simplified mode, for this level of load, seems to be located more to the right in the complex plane, compared to the modes of the detailed model. Studying Figure 4.28 shows that the simplified model follows the detailed model better after $t = 6$, which corresponds to a 2% increase in the field voltage. As seen from the last equation in 4.7, δ depends on ϕ, which might indicate that ϕ has been mismeasured from the detailed model and that the value used better suits the field voltage with a 2% increase.

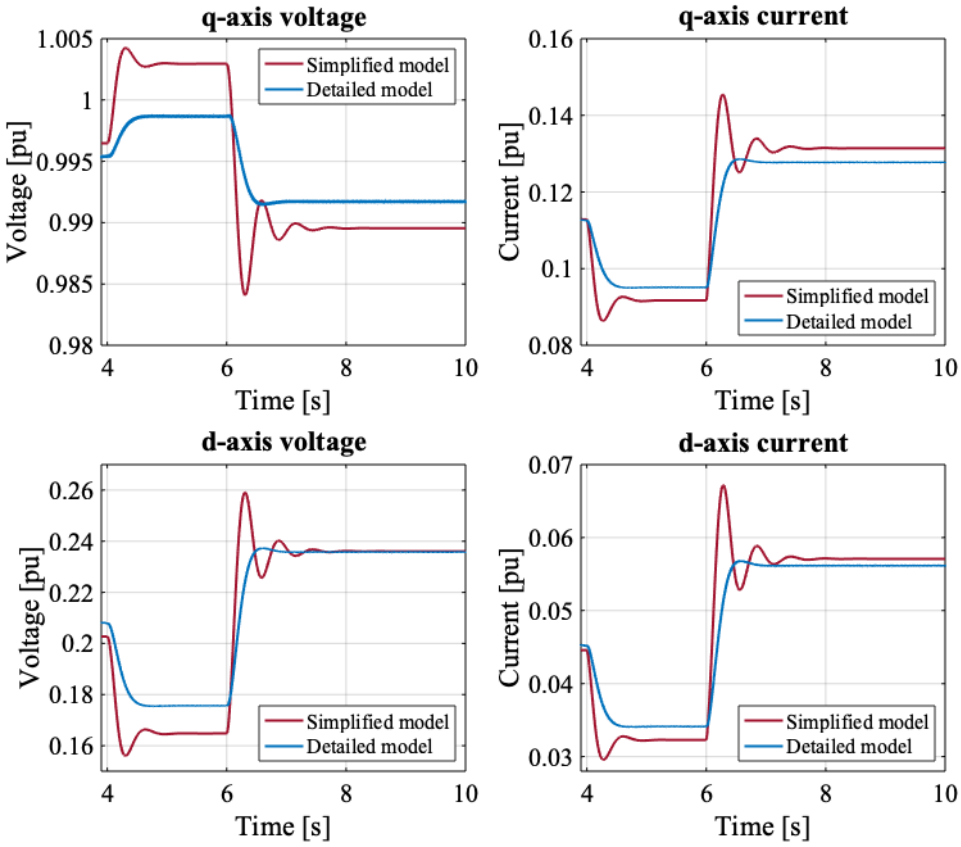

Figure 4.27: The d- and q-axis voltage and current responses corresponding to validation case 4, where the field voltage is stepped by $\pm 2\%$ from 1.1 pu. The applied field voltage follows the same shape as the graph shown in figure 4.22.

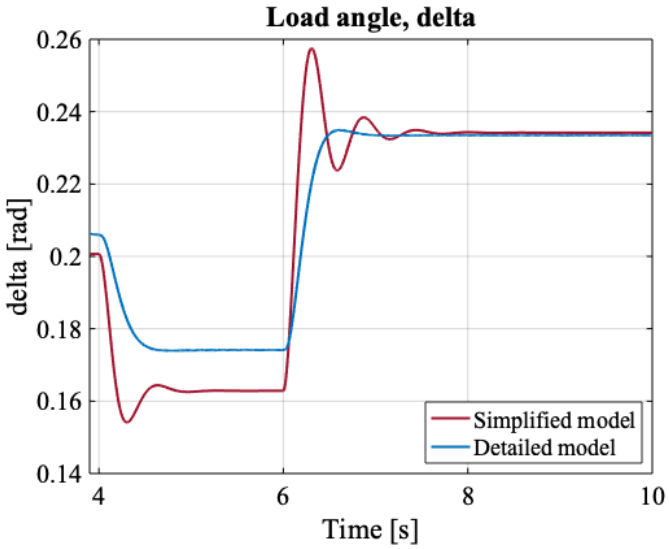

Figure 4.28: The Load angle, δ, responses corresponding to validation case 4, where the field voltage is stepped by $\pm 2\%$ from 1.1 pu. The applied field voltage follows the same shape as the graph shown in Figure 4.22.

Equivalent variable responses corresponding to validation case 2 and validation case 3 are depicted in Figure 8.9, 8.10, 8.11 and 8.12, 8.13, 8.14 in 8 in Appendix E respectively. The same trend are observed in these responses: The simplified model responses follows the detailed model responses quite well, but the responses corresponding to the simplified model are more oscillatory and weaker damped. These differences in response could be caused by the following:

- The detailed model contains a mechanical system while the simplified model operates with the absence of a mechanical system.
- The simulink diode-bridge rectifier model present in the detailed model contains a large (but not infinite) resistance connected in parallel with each of the diodes (snubber resistance), as well as a small internal resistance connected in series with each of the diodes [75]. The snubber capacitnce is set to inf such that a pure resistive snubber is obtained. The simplified model do not contain any such elements when representing the rectifier.
- The switching action of the diodes is neglected in the simplified model. Consequently, the simplified model does not include the discontinuous current conduction mode operation of the rectifier, mentioned in Section 3.4, and might be invalid at light loads.
- The detailed model contains a small parasitic resistive load at the output terminals of the generator in order to avoid numerical issues.
- The differential equation describing the electrical system in the synchronous machine neglects the effect of the synchronous reactance.
- The user might have been inaccurate when measuring the values representing α, β and ϕ. In addition are α, β and ϕ kept constant during $\pm 2\%$ steps in field voltage.

However, the aim when developing the simplified model was not to obtain a model that fits perfectly with the detailed one, but a numerical model containing less system components which are still capable of reproducing the unstable behaviour. The less components, the less equations needed and the easier it will be to better understand the phenomenon behind. Hence approaching a final explanation of the physics behind the instability. For this reason, it was chosen to proceed with the simplified model without further changes.

4.5 Linearization of the Simplified Model

As the simplified non-linear model represented by the equations in 4.13 are capable of reproducing the unstable phenomenon, further analysis of this mathematical model is of high importance. The model was therefore represented in a state-space form and further implemented in Matlab for linear analysis purposes. A brief description of the process is given in this section.

First, the five differential equations result in the five state variables: E'_q, E''_q, E''_d, V_{DC} and δ. These five constitutes the vector $\mathbf{x}$ shown in Equation 3.3, while $\dot{E}'_q$, $\dot{E}''_q$, $\dot{E}''_d$, $\dot{V}_{DC}$ and $\dot{\delta}$ constitutes the vector $\dot{\mathbf{x}}$ shown in Equation 3.4. This leads to the following representation:

$$\mathbf{x} = \begin{bmatrix} E'_q \\ E''_q \\ E''_d \\ V_{DC} \\ \delta \end{bmatrix} \qquad \mathbf{f} = \begin{bmatrix} f_1 \\ f_2 \\ f_3 \\ f_4 \\ f_5 \end{bmatrix} = \begin{bmatrix} \dot{E}'_q \\ \dot{E}''_q \\ \dot{E}''_d \\ \dot{V}_{DC} \\ \dot{\delta} \end{bmatrix} = \begin{bmatrix} \frac{1}{T'_{d0}} \left[E_f - E'_q + I_d(X_d - X'_d)\right] \\ \frac{1}{T''_{d0}} \left[E'_q - E''_q + I_d(X'_d - X''_d)\right] \\ \frac{1}{T''_{q0}} \left[E'_d - E''_d - I_q(X'_q - X''_q)\right] \\ \frac{1}{C} \left[I_{DC} + \frac{V_{bat}}{R_{bat}} - \frac{V_{DC}}{R_{bat}}\right] \\ \frac{1}{T_\delta} \left[-\delta + \arctan\left(\frac{-I_d}{I_q}\right) - \phi\right] \end{bmatrix} \tag{4.14}$$

where the differential equation, represented by $\mathbf{f}$ depends on the following algebraic equations:

$$\begin{aligned} V_d &= -\alpha\, V_{DC} \sin\delta \\ V_q &= \alpha\, V_{DC} \cos\delta \\ I_d &= \frac{1}{R^2 + X''_d X''_q} \left[R\,(E''_d - V_d) - X''_q\,(E''_q - V_q)\right] \\ I_q &= \frac{1}{R^2 + X''_d X''_q} \left[X''_d\,(E''_d - V_d) + R\,(E''_q - V_q)\right] \\ I_{DC} &= \beta \sqrt{I_d^2 + I_q^2} \end{aligned} \tag{4.15}$$

Because of the non-linear characteristic of this model, it is necessary to linearize it in order to apply the linear analysis techniques presented in Section 3.3. The state matrix $\mathbf{A}$, defined in Equation 3.9, was calculated in Matlab, and so were the corresponding eigenvalues and participation factors. The implemented Matlab code is presented in 8 in Appendix F. The existing Matlab functions "*diff(f,x)*" and "*eig(A)*" were used. The first equation differentiate the differential equation *f* with respect to the state variable *x* while the second function computes the eigenvalues of the state matrix A. The obtained state matrix A is quite complex, and it is represented by symbolic values and attached in 8 in Appendix F.

To ensure that the existing Matlab function computed the state matrix correctly, an other method was used for validation. This method calculates each of the state matrix elements, one by one. First, when calculating the elements in the first column of $\mathbf{A}$, a small deviation *dx* is applied to the first state variable element, E'_q. Next, it is measured how this change in the variable E'_q impacts each of the differential equation in $\mathbf{f}$. The change in $\dot{E}''_d$ caused by a small change in E'_q constitutes the element $\mathbf{A}(3,1)$, while the change in $\dot{\delta}$ caused by a small change in E''_q constitutes the element $\mathbf{A}(5,2)$. The implemented Matlab code is attached in 8 in Appendix F. This code requires the Matlab code attached in 8 in Appendix D to be executed in advanced.

Eigenvalues were calculated for varying values of X'_d in order to understand whether linear analysis techniques are an appropriate tool to study the unstable phenomenon further. The

eigenvalues were evaluated based on whether it was possible to detect a complex pair of unstable eigenvalues that corresponded to the time-domain responses, achieved by executing the simplified mathematical model for the corresponding cases of X'_d. Since this applied to these cases, a decision was made to go ahead, studying the simplified mathematical model further by using linear analysis techniques. A modal analysis is carried out in section 5.1.

4.6 Limitations and Simplifications

During this thesis, when modelling the system under study, only the main components are included. In real-life systems, these components are usually further connected to an AVR, a governor system, to other generator units, to different kinds of load, including motor drives, etc.. The remaining components will affect the system stability. The system under study can be interpreted only as a part of a shipboard power system. However, by reducing the number of components in the system, the easier it is to reach the core of the problem causing unpleasant behaviour.

Furthermore, the components modelled are assumed ideal, hence no losses are taken into account. The system is modeled in the absence of a cable impedance (inductance) connected between the generator and the rectifier. However, this impedance is small compared to the internal generator impedance and will not play a critical role. Moreover, the battery is modelled as an ideal DC voltage source connected to a small internal resistance. In the detailed model, the synchronous generator is operated at constant rotor speed, thus at constant frequency. In real-life system, the generator has the opportunity to operate with varying speed and hence frequency.

The simplified model, which is a simplified mathematical model describing the system under study, contains several simplifications. However, this is a part of the approach used in order to develop a model that facilitates studying and aiding the understanding of the unstable phenomenon. The simplifications include the absence of a mechanical system and an average-value rectifier model, which does not take the dynamic characteristics of the diodes into account. Consequently, the model does not include the discontinuous-current conduction mode operation of the rectifier. Further, a kind of fictitious time constant, T_δ, is included in the simplified model in order to avoid the model from containing an algebraic loop. This numerical reason is why the power angle, δ, resulted as a state variable. These simplifications made are presented during the thesis, where applicable.

4.7 Cases to be Studied

With the aim to better understand why a synchronous generator connected to a battery through a diode-bridge rectifier, or multiple synchronous generator-rectifier system connected in parallel at the dc side becomes unstable becomes unstable, different cases are studied:

1. A sensitivity analysis of the system variables presented in Table 4.5. Each of the parameters, one by one, are adjusted by $\pm 5\%$ and $\pm 10\%$ from its original value, while keeping the other parameters unchanged. The corresponding change in the real part of the complex pair of unstable eigenvalues are measured. This analysis will facilitate the understanding of which variables that contribute for making the system unpleasant.

   Table 4.5: The parameters to be studied during sensitivity analysis.

Parameter	Symbol
Armature resistance	r_a
Direct axis synchronous reactance	x_d
Direct axis transient reactance	x'_d
Direct axis subtransient reactance	x''_d
Quadrature axis synchronous reactance	x_q
Quadrature axis transient reactance	x'_q
Quadrature axis subtransient reactance	x''_q
Direct axis open-circuit transient time constant	T'_{do}
Direct axis open-circuit subtransient time constant	T''_{do}
Quadrature axis open-circuit subtransient time constant	T''_{qo}
Internal battery resistance	r_{bat}
Filter capacitor	c
Load angle time constant	T_δ

   This analysis is done for the five synchronous generator sets presented in Table 8.1 in Appendix A. It is four salient pole machines and one round rotor machine. However, for the analysis purpose, the nominal power and frequency of the generators were set equal to the values of generator set *SP1*. Each of the synchronous generators are operated at about 55% load. The detailed simulation model needs to be executed in advance to obtain suitable values for V_f, α, β, ϕ, V_{DC} and I_{DC}, to be used as input in the linearized model.

2. Simulations of both the simplified model and the detailed model are examined by replacing the battery model with an equivalent restive load. A circuit schematic of this system is depicted in Figure 4.29a. Figure 4.29b shows a schematic of the system which the detailed and simplified model is based on and is attached for comparable reasons. α, β and ϕ are retrieved from the detailed model when connected as shown in Figure 4.29a.
   The field voltage is set to 1.4 pu and the DC resistance to 3 pu, such that the generator is

loaded at about 33% load, which has been experienced as a worst-case load seen in context with the unstable phenomenon. The d-axis transient reactances are scaled such that the relationship $\frac{X_q}{2X'_d}$ equalizes 2.60 and thus, an unfavourable parameter set is present. Further on, small voltage step was injected to the field voltage such that the field voltage was decreased and increased by 2% from the initialized operation point. The shape of the applied field voltage is shown in Figure 4.30. Afterwards, the field voltage was kept constant and small steps were applied to the resistive load by connecting and disconnecting parallel-connected resistive loads, such that the load was decreased and increased by 2% from the initialized operation point.

These variations in field voltage and DC load was done in order to excite possible oscillations in the system.

For the sake of comparison, an analogous simulation case is examined for the system shown in Figure 4.29b, containing the battery model. By doing so, more information is gained about how the instability is related to the type of load connected at the DC side.

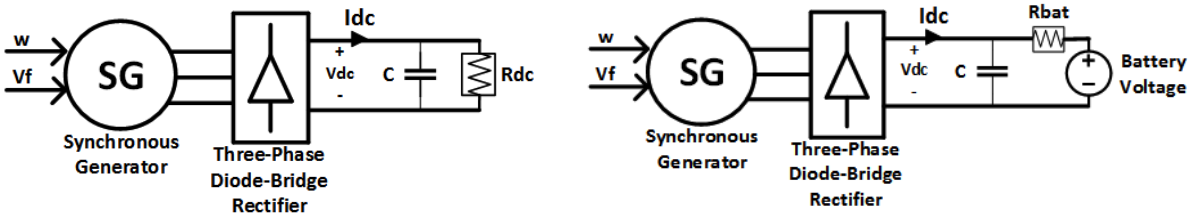

(a) **(b)**

Figure 4.29: Circuit schematics of the systems, to be compared from case study 2. (a) The DC load is a pure resistive while the DC load in (b) is a battery modelled as counter voltage connected to a tiny resistance.

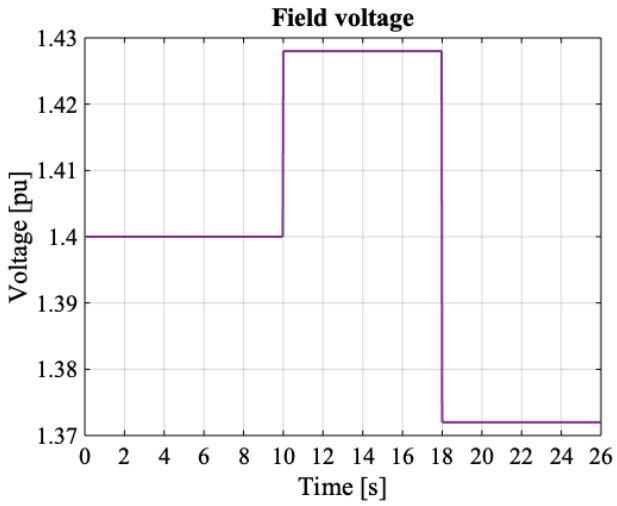

Figure 4.30: The field voltage applied when examining the impact of a counter voltage. This level of field voltage corresponds to operation of about 33% load.

3. The detailed model is modified, the diode-bridge rectifier is removed, and an additional synchronous generator is connected in parallel with the existing synchronous generator. The generators are feeding a common equivalent three-phase star-connected resistive AC load. A circuit schematic of this system is depicted in Figure 4.31a. The generators are fed by constant field voltage and constant rotor speed. The two synchronous generators are identical except that the second generator has its field voltage set-point at 0.5% below the first one. Consequently, the system is capable of delivering twice as much power. The generator data is presented below *SP1* in Table 8.1 in Appendix A. The resistive AC load is set such that each of the generators is operated at about the worst-case load, 33% load. A trial-and-error process is performed in order to find suitable values for the field voltages and rotor speeds. Also here the d-axis transient reactances are scaled such that the relationship $\frac{X_q}{2X'_d}$ equalizes 2.60 and thus, unfavourable parameter sets are present. A negative 2% step in load is applied in order to excite possible oscillations in the system. This was done by installing an additional three-phase star-connected resistive AC load in parallel with the first AC load. The second load is set to 2% below the first one. After some time, the first load is disconnected while the second one is connected. The field voltages and rotor speeds used are summarized in Table 4.6. The power consumed by a three-phase star-connected load are given by Equation 4.16. As a consequence, the first and second resistive loads are calculated by Equations 4.17 and 4.18, respectively.

   Next, a second simulation with the detailed model is examined, where each of the generators is connected to a three-phase diode-bridge rectifier, and the resistive AC load is replaced by an equivalent resistive DC load. The generators are fed by the same field voltages and rotor speeds as in the first simulation, and the generator data is identical to the data used in the first simulation. Figure 4.29b shows a circuit schematic of this described system.
   This analysis is carried out to confirm if the diode-bridge rectifier needs to be present in order to make the system unstable.

Table 4.6: The final value to be used during simulation of two synchronous generator feeding a common AC load.

Parameter	Symbol	Value
Field voltage generator 1	$v_{f,1}$	1.2682
Rotor speed generator 1	ω_1	0.98575
Field voltage generator 2	$v_{f,2}$	1.2619
Rotor speed generator 2	ω_2	0.98575

$$P_{3,\phi} = 3 \cdot \frac{(V_{phase})^2}{R} = 3 \cdot \frac{(V_{line}/\sqrt{3})^2}{R} = \frac{(V_{line})^2}{R} \tag{4.16}$$

$$R_{load,1} = \frac{(V_{line})^2}{P_{33\%}} = \frac{(690\ \text{V})^2}{(1/3) \cdot 6\ \text{MW}} = 0.23805\ \Omega \tag{4.17}$$

$$R_{load,2} = 1.02 \cdot R_{load,1} = 0.24281\ \Omega \tag{4.18}$$

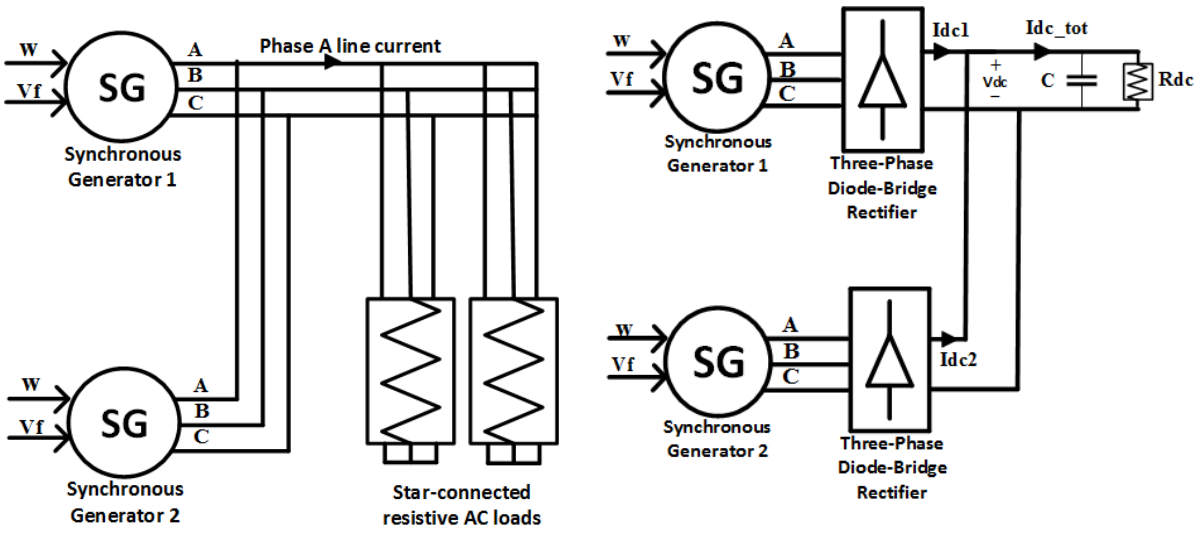

(a) **(b)**

Figure 4.31: Circuit schematics of the systems to compare in case study 3. (a) Does not contain three-phase diode-bridge rectifiers while (b) does.

Chapter 5

Analysis and Results

This chapter contains the results obtained when the cases presented in Section 4.7 are conducted. First, eigenvalues and participation factors corresponding to generator SP1 are studied. Second, the sensitivity analysis results for the five different synchronous generator are presented. Third and fourth, the impact of a counter voltage and a three-phase diode bridge rectifier is presented, respectively. A brief discussion of the sensitivity analysis results are presented in the end of Section 5.1. A complete discussion regarding to all the results appears in Chapter 6.

5.1 Modal Analysis

Eigenvalues and Participation Factors

The salient pole synchronous generator SP1 is operated at different operation points and the corresponding eigenvalues are calculated. Table 5.1 shows the eigenvalues obtained when loading the generator at 33.0% and 55.6%. Because the state vector defined in 4.14 contains five state variables, five eigenvalues are obtained. Two of them are complex and three of them are pure real. As mentioned in Section 3.3.1, a system containing at least one eigenvalue with a positive real part is considered unstable. The two operation scenarios presented in Table 5.1 are thus considered unstable. λ_3, λ_4 and λ_5 contains a high negative real value and these modes are therefore well damped and do not contribute making the system unstable.
Eigenvalues were calculated for different level of loads as well as for different variations of the d-axis transient reactance, x'_d. The simplified mathematical model was simulated for the corresponding cases and the results were compared against the calculated eigenvalues. In the presence of an eigenvalue containing a positive real part, oscillation with increasing magnitude should be observed by time-domain simulations. Further, the frequency of the oscillations should correspond to the frequency obtained in the imaginary part of the unstable modes. This theory was confirmed in these cases. As an example, time-domain simulation of the salient pole synchronous generator SP1, with original generator parameters at 55.6% load, resulted in oscillations with a frequency of 2.503 Hz. This corresponds well to the imaginary part of modes

λ_1 and λ_2 presented in the right column in Table 5.1. Dividing the imaginary part with 2π results in a damped frequency equal 2.516 Hz. The small difference may be due to inaccurate measurement of the frequency obtained from time-domain simulation.

Table 5.1: Eigenvalues, $\lambda = \sigma + j\omega$, corresponding to operation at 33.0% and 55.6% load of salient pole generator SP1. The system parameters are set to its original values shown in Table 8.1 in Appendix A.

33.0% Load	55.6% Load
$\lambda_1 = \ 9.3274 + j12.0094$	$\lambda_1 = \ 1.3763 + j15.8088$
$\lambda_2 = \ 9.3274 - j12.0094$	$\lambda_2 = \ 1.3763 - j15.8088$
$\lambda_3 = -123.5023 + j0.0000$	$\lambda_3 = -123.8281 + j0.0000$
$\lambda_4 = -501.6571 + j0.0000$	$\lambda_4 = -402.9405 + j0.0000$
$\lambda_5 = -2656.7236 + j0.0000$	$\lambda_5 = -2693.9752 + j0.0000$

Next, the participation factors corresponding to the 33% operation case are calculated and presented in the following matrix:

$$\begin{bmatrix} -0.4685 - j0.6171 & -0.4685 + j0.6171 & -0.0324 + j0.0000 & 0.0011 + j0.00000 & 0.0000 + j0.0000 \\ -0.1919 - j0.0795 & -0.1919 + j0.0795 & 1.2383 + j0.0000 & -0.0465 + j0.00000 & 0.0000 + j0.0000 \\ 0.4845 + j0.5086 & 0.4845 - j0.5086 & -0.2035 + j0.0000 & 0.3968 + j0.00000 & -0.0028 + j0.0000 \\ -0.0009 - j0.0009 & -0.0009 + j0.0009 & 0.0012 + j0.0000 & -0.0353 + j0.00000 & 1.0364 + j0.0000 \\ 0.1768 + j0.1889 & 0.1768 - 0.1889 & -0.0035 + j0.0000 & 0.6839 + j0.00000 & -0.0339 + j0.0000 \end{bmatrix}$$

As mentioned in Section 3.3.3, the participation factor p_{ki} measures the relative participation of the kth state variable in the ith mode. The state vector, $\mathbf{x}$, is defined in the following way:

$$\mathbf{x^T} = \begin{bmatrix} E'_q & E''_q & E''_d & V_{DC} & \delta \end{bmatrix}$$

Consequently, each of the five columns presented in the participation matrix corresponds to each of the five state variables, $E'_q, E''_q, E''_d, V_{DC}$ and δ, respectively. Studying each of the five columns, one by one, results in the following observations:

- The two first columns corresponds to the unstable modes, λ_1 and $\lambda_2 = 9.3274 \pm j12.0094$. The first and the third element of these two columns are of greater absolute value than the reminding elements. This indicates that the first and third state variables, E'_q and E''_d have the most dominating participation in these unstable unstable modes.

- The third column corresponds to the third eigenvalue, $\lambda_3 = -123.5023$. The second element in the column is with clarity the greatest, which further indicates that the second state variable E''_q has the most dominating participation in this specific mode, λ_3.

- The fourth column corresponds to the fourth eigenvalue, $\lambda_4 = -501.6571$. The fifth element in the column is the greatest, which further means that the fifth state variable δ has the most dominating participation in this specific mode, λ_4.

- Studying the fifth column in the same way results in the fourth state variable to dominate the fifth state variable, $\lambda_5 = -2656.7236$. The equation corresponding to the state variable, V_{DC}, is based on the DC-circuit sketched in Figure 4.14 in Section 4.3.3. This circuit has a time constant equal to:

$$\frac{1}{c \times r_{bat}} = \frac{1}{0.017354 \times 0.021471} = 2684$$

  This explains the high value achieved for eigenvalue λ_5.

Studying Equation 3.17 in Chapter 3, the participation factors can be interpreted as the sensitivity of the eigenvalue λ_i with respect to element a_{kk} in state matrix **A**. As an example, eigenvalue λ_5 is sensitive for changes in element a_{44}. The state matrix **A** is as already mentioned presented with symbolic values in Appendix F.
The Matlab code used to linearize the system equation and to calculate the corresponding eigenvalues and participation factors are, as previously mentioned, attached in Appendix F.

Figure 5.1 shows the modes obtained when the salient pole synchronous generator SP1 is operated at four different levels of load. λ_1 and λ_2 corresponds to the unstable modes observed to the right in the complex plane while λ_5 is the real mode observed to the left, between -2490 and -2710. Small variations are observed for the real mode λ_3, and the four associated modes are located on top of each other, at about -123. As the load varies, the real mode λ_4 is the mode that experiences the most changes. When the load is increased, λ_4 moves towards the right in the complex plane, from -850 to -330. However, independent of the level of load, the three modes, λ_3, λ_4 and λ_5 are all well damped and thus considered stable.

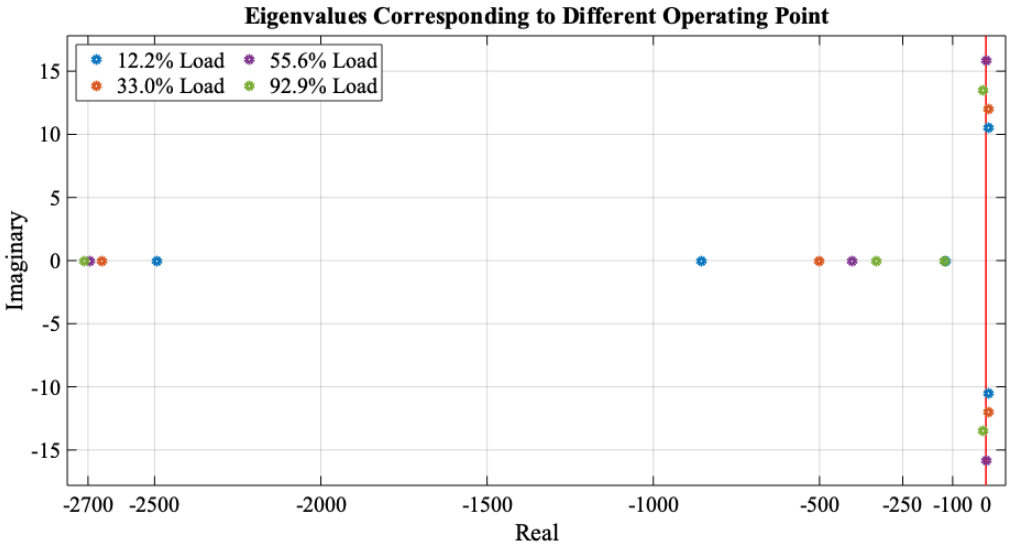

Figure 5.1: The five eigenvalues associated with four different levels of load. The eigenvalues corresponding to λ_1 and λ_2 are the complex eigenvalues observed most to the right. The four eigenvalues corresponding to λ_3 experiencing small changes and are therefore located on top of each other at about -123. λ_4 is spread from -850 to -330 while the four eigenvalues corresponding to λ_5 are the ones located most to the left.

Figure 5.2 zooms into the unstable complex modes associated with λ_1, located to the upper right in Figure 5.1. In addition, the unstable complex mode corresponding to a operation of 3.1% load is included.
λ_1 is considered to explain the unstable behaviour that is observed by time-domain simulations of both the detailed and the simplified model.
The curve attached is meant to visualize possible locations for the unstable mode when increasing the load of operation. The curve represents an approximated root locus.
The figure shows that increasing the load of operation causes λ_1 to move in a curve: from the lower-left half-plane towards the right, and further up and then back to the left half-plane. In the right half-plane, the frequency increases as the load increases, and the worst-case load seems to be about 33% load. Further on, the mode is moving back towards the left half-plane. The figure indicates that the higher the load, the higher is the imaginary part, thus the frequency of the mode. However, this is not true for the 3.1% load and the 92.9% load, which are located above the 12.2% load and below the 55.6% load on the imaginary axis, respectively. Anyway, the modes associated with the 3.1% load and the 92.9% load contain a negative real part and are consequently well-damped during operation. In addition, because the switching action of the diodes is neglected, the simplified model does not account for the discontinuous current conduction mode operation of the rectifier, mentioned in Section 3.4, and might be invalid at light loads.

Nevertheless, the overall observations made from Figure 5.2 seems to match with the so far experienced characteristics associated with the unstable phenomenon.

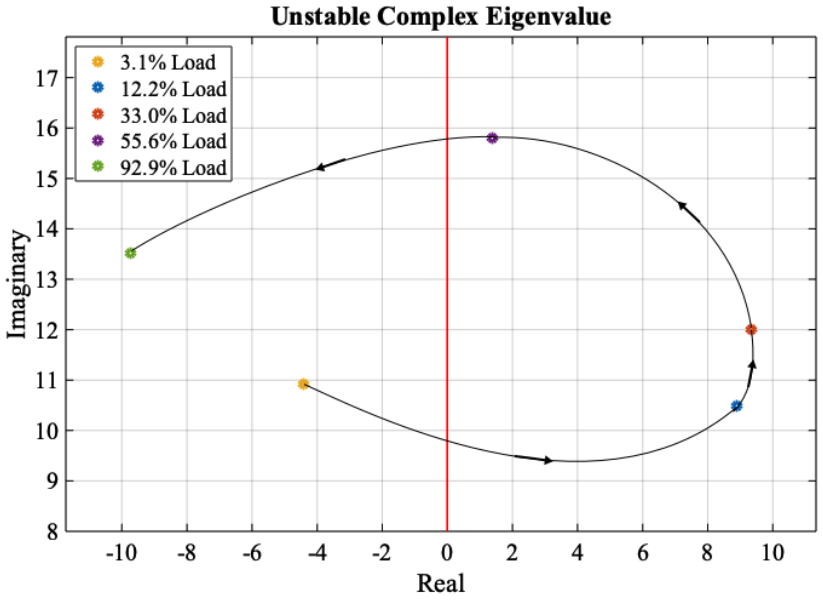

Figure 5.2: The unstable complex eigenvalue, λ_1, associated with five different levels of load. It zooms into the complex poles located most to the right in Figure 5.1, but an additional operation point, corresponding to 3.1% load, is also added. The curve represents an approximated root locus.

The calculation of the participating factors presents valuable information of which parts of the system that might participate in the unstable modes, thus contribute making the system unstable. However, the different state variables depend on several parameters and some of the modes turns out to be dominated by several state variables which further complicates the analysis. Carrying out a sensitivity analysis will hereby be of importance.

Sensitivity Analysis

The unstable unstable modes addressed in the previous section are further studied. These eigenvalues, λ_1, λ_2 are during this analysis referred to as *unstable modes*, regardless of whether they are located in the left or in the right side in the complex plane. The sensitivity analysis case described in case 1 in Section 4.7 are performed. Each of the twelve system parameters listed in Table 4.5 are, one at a time, changed by ± 5 and ± 10 from its original value, while keeping the other parameters unchanged. The corresponding change in the real part, $\Delta\sigma$, of the unstable modes are measured. The five synchronous generator sets presented in Table 8.1 in Appendix A, have been examined through this sensitivity analysis. It yields four salient pole structures and one round rotor structure. As mentioned in Section 3.5.3, salient pole generators are characterized with $x'_q = x_q$. Because of this, when studying the influence of x_q and x'_q for salient pole generators, x_q and x'_q are changed with the same value simultaneously, and hence analyzed as a common scenario. However, this is not the case when studying the round rotor synchronous generator, where x_q and x'_q are analyzed separately due to its solid-steel rotor core construction. The synchronous generators are operated at about 55% load and the values obtained from the detailed simulation model, which are used as input in the linearized model is presented in Table 5.2.

Table 5.2: Values used to initialize the linearized model, obtained from simulation of the detailed model, for each of the five generator sets. These values correspond to operation at about 55% load.

Synchronous generator	v_f [pu]	v_{bat} [pu]	α	β	ϕ [rad]	v_{DC} [pu]	i_{DC} [pu]	p_{ac} [%]
SP1	1.80	1.00	1.0444	0.9880	0.2321	1.0114	0.5325	55.6
RR	3.37	1.00	1.0473	0.9912	0.2084	1.0113	0.5264	55.2
SP2	1.80	1.00	1.0335	0.9820	0.2197	1.0114	0.5322	55.4
SP3	1.53	1.00	1.0234	0.9780	0.1890	1.0113	0.5291	54.0
SP4	1.74	1.00	1.0386	0.9840	0.2316	1.0114	0.5303	55.4

The bar plots shown in Figures 5.3, 5.4, 5.5, 5.6 and 5.7 present the results for each of the five mentioned synchronous generator sets. The figures contain one bar for each of the system parameters. The height of the bar represents the measured change in the real value, $\Delta\sigma$, of the unstable modes when the corresponding parameter is changed from 0.9 to 1.1 of its original base case value. The higher the bar is, the more sensitive is the unstable modes for change in the corresponding parameter. In other words, the higher the bar is, the more the corresponding parameter influences the instability. Furthermore, a red coloured bar indicates that an increase

in that specific system parameter causes the unstable modes to move towards the left in the complex plane, thus improving the system stability. On the other hand, a decrease in that specific parameter causes the unstable modes to move towards the right in the complex plane, thus worsen the system stability. The opposite yields for a blue coloured bar, which indicates that a decrease in that specific system parameter has a positive influence on the system stability, moving the unstable modes towards the left in the complex plane.

Sensitivity analysis examined for the filter capacitance turned out to not affect the unstable modes. This was expected, based on the participation factor calculation performed in the previous section. The filter capacitance is not presented in any of the diagonal elements a_{kk} that turned out to be related to the unstable modes. Therefore, the results obtained for the filter capacitance is neglected and excluded from the bar plots.

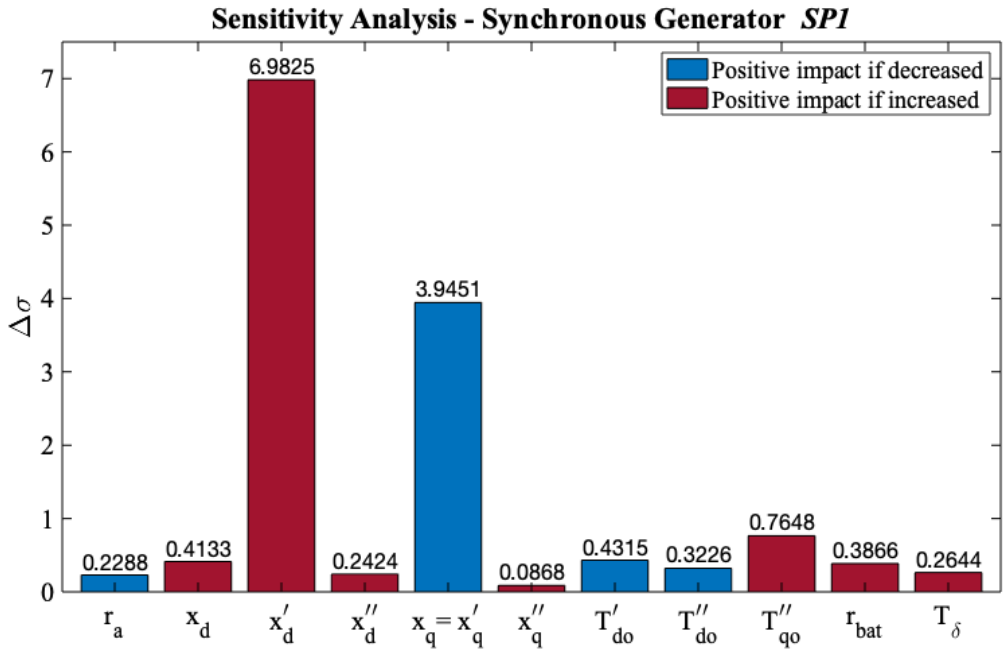

Figure 5.3: Sensitivity analysis results when studying the system parameters corresponding to the salient pole synchronous generator SP1. The height of the bar represents the measured change in the real value, $\Delta\sigma$, of the complex pair of unstable eigenvalues when the corresponding parameter is changed from 0.9 to 1.1 of its original base case value. A red coloured bar and a blue coloured bar indicate that an increase and a decrease in the specific system parameter have a positive impact on the system stability, respectively. As an example, an increase in a system parameter corresponding to a red coloured bar will make the unstable modes moving towards the left in the complex plane.

Figure 5.3 shows the results when studying the system parameters corresponding to the salient pole synchronous generator SP1. x'_d and $x_q = x'_q$ turned out to be the system parameters influencing the real part of the unstable modes the most, followed by T''_{qo}, T'_{do} and x_d. Several of these system parameters do also occur in the differential equation associated with the state variable E'_q and E''_d presented in 4.14. More correctly, the parameters included in the state matrix elements a_{11} and a_{33}. E'_q and E''_d were during the participation factor analysis found to be the

state variables dominating the unstable modes the most. This means that this unstable modes are sensitive for changes in state matrix element a_{11} and a_{33}. As previous mentioned, the state matrix, **A**, containing symbolic expressions is attached in Appendix F.

Furthermore, the results show that an increase in x'_d and x_d moves the poles toward the left in the complex plane, thus positively influencing system stability. The opposite yields for the parameters $x_q = x'_q$, where an increase in these parameters causes the poles to move towards the right in the complex plane. This opposite effect is observed between the subtransient open circuit time constants T''_{do} and T''_{qo}. An increase in T''_{qo} enhance the system stability, while an increase in T''_{do} weakens the system stability, moving the unstable poles towards the right in the complex plane.

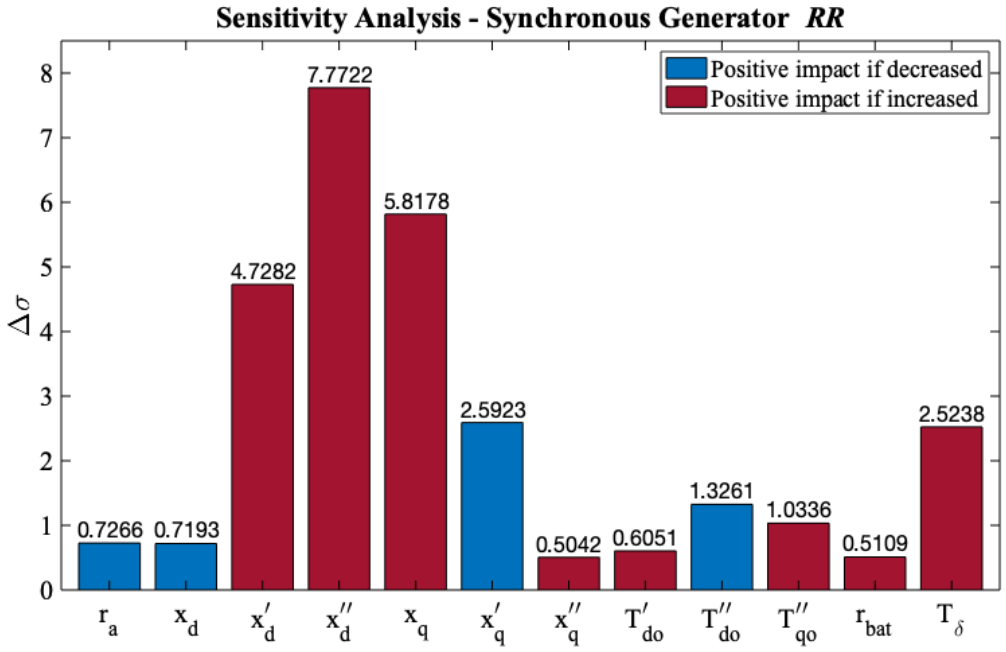

Figure 5.4: Sensitivity analysis results when studying the system parameters corresponding to the round rotor synchronous generator RR. The height of the bar represents the measured change in the real value, $\Delta\sigma$, of the complex pair of unstable eigenvalues when the corresponding parameter is changed from 0.9 to 1.1 of its original base case value. A red coloured bar and a blue coloured bar indicate that an increase and a decrease in the specific system parameter have a positive impact on the system stability, respectively. As an example, an increase in a system parameter corresponding to a red coloured bar will make the unstable modes moving towards the left in the complex plane.

Figure 5.4 shows the results when studying the system parameters corresponding to the round rotor synchronous generator RR. Also here, x'_d, x_q and x'_q turned out to be among the system parameters influencing the real part of the unstable modes the most. However, x''_d turned out to be the most notable parameter. Also, T_δ, T''_{do} and T''_{qo} are discovered to be of great importance. Increasing x'_d, x''_d, x_q, x''_q, T'_{do} and T''_{qo} enhance the system stability while increasing x'_q, x_d and T''_{do} weakens the system stability. They have the opposite effect.

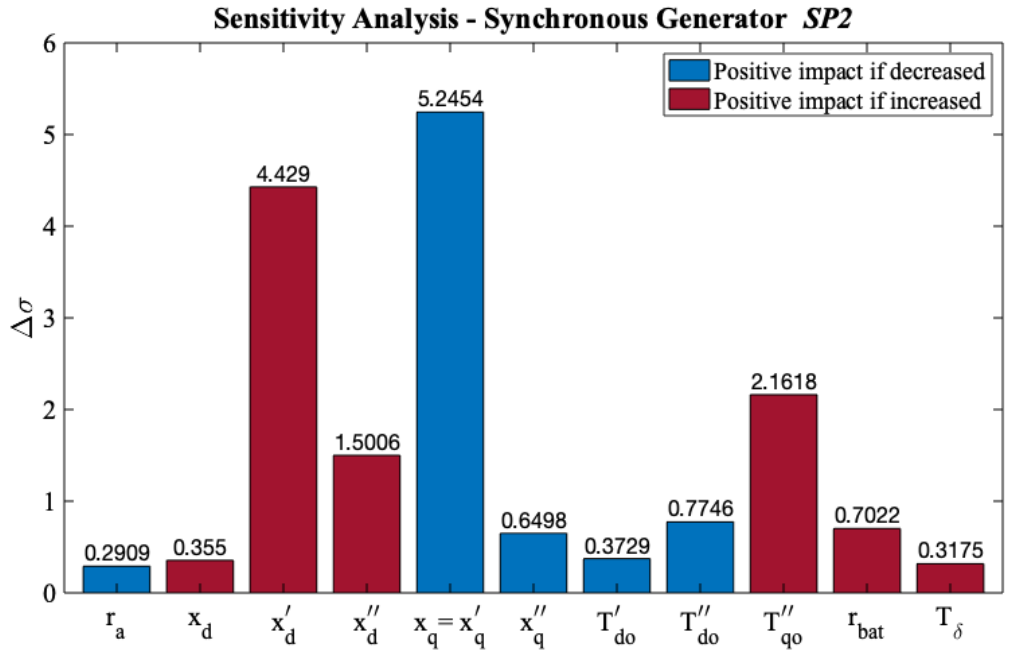

Figure 5.5: Sensitivity analysis results when studying the system parameters corresponding to the salient pole synchronous generator SP2. The height of the bar represents the measured change in the real value, $\Delta\sigma$, of the complex pair of unstable eigenvalues when the corresponding parameter is changed from 0.9 to 1.1 of its original base case value. A red coloured bar and a blue coloured bar indicate that an increase and a decrease in the specific system parameter have a positive impact on the system stability, respectively. As an example, an increase in a system parameter corresponding to a red coloured bar will make the unstable modes moving towards the left in the complex plane.

Figure 5.5 shows the results when studying the system parameters corresponding to the salient pole synchronous generator SP2. Once more, x_q = x'_d and x'_q turns out to be the system parameters of most importance, followed by T''_{qo} and x''_d. Decreasing the parameters x_q = x'_q, x''_q, T'_{do} and T''_{do} enhance the system stability, while decreasing x_d, x'_d, x''_d and T''_{qo} weakens the system stability by moving the unstable poles towards the right in the complex plane.

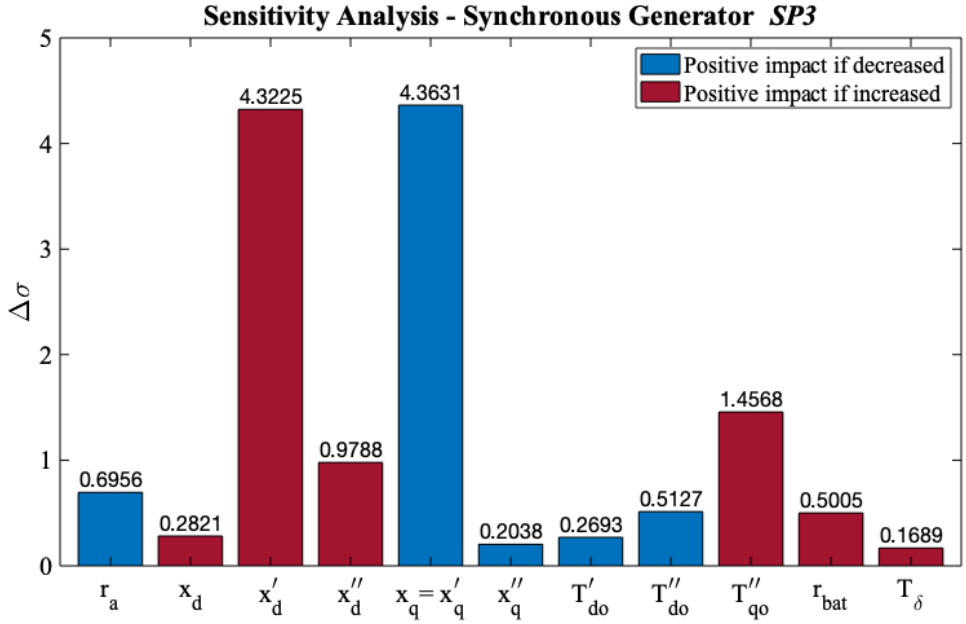

Figure 5.6: Sensitivity analysis results when studying the system parameters corresponding to the salient pole synchronous generator SP3. The height of the bar represents the measured change in the real value, $\Delta\sigma$, of the complex pair of unstable eigenvalues when the corresponding parameter is changed from 0.9 to 1.1 of its original base case value. A red coloured bar and a blue coloured bar indicate that an increase and a decrease in the specific system parameter have a positive impact on the system stability, respectively. As an example, an increase in a system parameter corresponding to a red coloured bar will make the unstable modes moving towards the left in the complex plane.

Figure 5.6 shows the results when studying the system parameters corresponding to the salient pole synchronous generator SP3. In order to achieve suitable values for v_f, α, β etc. to use as inputs in the linarized model, there was need to increase the d-axis transient reactance, x'_d from its original value, 0.09 pu, to 0.279 pu. Otherwise, the detailed simulation model collapsed. After achieving suitable input values, the system was linearized and eigenvalues were studied in order to understand why this collapse took place. The use of the original generator data set resulted in only real eiegenvalues, where two of them were located in the right half plane at 1.46 and at 91.49. A quite unstable system is thus present. Increasing x'_d slowly reduces the difference between these two unstable real modes: The one at 91.49 reduces while the one at 1.46 increases. Making x'_d sufficiently large transform these two unstable real modes into an unstable complex pair of eigenvalues, having a real value at about 6.5. Reducing x'_d in the other four synchronous generator sets, from their original value, the same effect was observed. This phenomenon might be explained in the following way: Too unstable complex pair of eigenvalues lead to time-domain oscillations with severe amplitude increase and parts of the system might reach their stability limits and voltage collapse might occur.
Figure 5.6 shows, not unexpected, that x_q = x'_d and x'_q are the system parameters influencing the unstable poles the most. x''_d and T''_{qo} are also among the most influencing parameters. x_d, x'_d, x''_d, T''_{qo} and x_q = x'_q, x''_q, T'_{do}, T''_{do} influence the system stability in a positive manner by being increased and decreased, respectively.

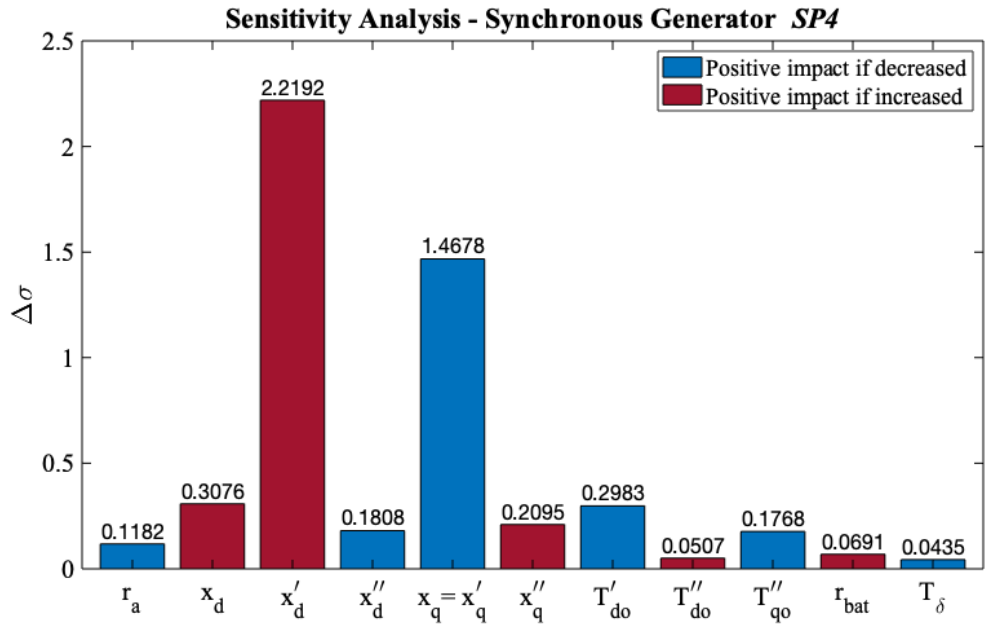

Figure 5.7: Sensitivity analysis results when studying the system parameters corresponding to the salient pole synchronous generator SP4. The height of the bar represents the measured change in the real value, $\Delta\sigma$, of the complex pair of unstable eigenvalues when the corresponding parameter is changed from 0.9 to 1.1 of its original base case value. A red coloured bar and a blue coloured bar indicate that an increase and a decrease in the specific system parameter have a positive impact on the system stability, respectively. As an example, an increase in a system parameter corresponding to a red coloured bar will make the unstable modes moving towards the left in the complex plane.

Figure 5.7 shows the results when studying the system parameters corresponding to the salient pole synchronous generator SP4. $x_q = x'_d$ and x'_q are also here the most notable results. x_d, x'_d, x''_q, T''_{do} and x''_d, $x_q = x'_q$, T'_{do}, T''_{qo} influence the system stability in a positive manner by being increased and decreased, respectively.

Discussion

Studying the sensitivity analysis results presented by the five preceding figures, the most striking findings are:

- For all the salient pole synchronous generators, x'_d and $x_q = x'_q$ turned out being the system parameters influencing the unstable pair of complex eigenvalues the most. Increasing x'_d or decreasing $x_q = x'_q$ enhance the system stability. This is in accordance with the stability criteria highlighted by previous literature, $\frac{x_q}{2x'_d} \leq 1$, which yields for synchronous generators satisfying $x'_q = x_q$ [16; 17]. Each of the five synchronous generators studied during this thesis satisfies $x'_q \approx x_q$. However, as previous mentioned, the reason why the round rotor synchronous generator data made available for this thesis satisfies $x_q = x'_q$ is unknown. Round rotor generators usually satisfy $x_q > x'_q$ due to the rotor body eddy currents flowing in its rotor core construction.

- These parameters, x_d, x_q and x'_q, in addition to x''_d, turned out being the most remarkable parameters for the round rotor synchronous generator.

- It is worth nothing that almost all of the results obtained indicate that the system wants to move towards the same direction, either by increasing the q-axis component and decreasing the d-axis component, or opposite. This is observed by studying the d- and q-axis component in each of the five preceding figures. If the d-axis component correspond to a blue coloured bar or to a red coloured bar, the associated q-axis component correspond to a red coloured bar or to a blue coloured bar, respectively. As an example, studying figure 5.5 or 5.6, x_d, x'_d, x''_d and T''_{qo} are associated with a red coloured bar, while x_q = x'_q, x''_q and T''_{do} are associated with a blue coloured bar. The only exceptions are x''_q and x''_d for the salient pole generator SP1 and for the round rotor generator RR. However, x''_q is in both cases associated with a much lower bar, which means the influence of x''_q is rather small, and a conclusion can not be drawn based on these two results. When it comes to the most remarkable parameters, x_d, x_q and x'_q, studying the generator parameters attached in Table 8.1 in Appendix A, the system wants to reduce the difference between x'_q and x'_d in order to enhance the system stability. This theory agrees with Auinger [16] which states that unfavourable relationship between the d- and q- axis components might be a reason to the unstable phenomenon. Further, Auinger asserts the d-axis open-circuit transient time constant being too slow, compared to the q-axis open-circuit transient time constant, as a part of the problem. The sensitivity analysis conducted for the salient pole synchronous generator supports this theory about reducing the system parameter, T'_{do}, in order to enhance the system stability.

- T_δ, which presents the filter time constant needed in order to avoid the simplified numerical model to result in an algebraic loop, turns out to enhance the system stability by being increased. The only exception is the results obtained for the synchronous generator SP4. However, for this case, the bar associated with T_δ is negligible compared to the other bars seen in Figure 5.7. The larger T_δ, the more time the system has to update the load angle δ. Thus, the result obtained for T_δ sounds reasonable.

- For all of the five synchronous generator sets, r_{bat}, turned out to enhance the system stability if being increased. This was expected because a pure resistive load is associated with a positive incremental impedance[31]. A positive incremental impedance tries to restore the steady-state operation point and thus acts like negative feedback and influence the system stability in a positive manner. The larger the resistance, the more damping it provides.
  On the other hand, connecting a resistance between the generator and the rectifier turns out to destabilize the system. The larger the armature resistance r_a, the more unstable the modes become. r_a is actually a parameter inside the generator, but in this model it can be interpreted as being connected between the generator and the rectifier. This is in analogy with the fact that an increase in the resistance connected to the generator's output

terminal, along the transmission line to the remaining network, results in a weaker system by introducing negative damping torque [55, p.467][77].

5.2 The Impact of a Counter Voltage

Figure 5.8a shows the DC voltage, DC current and DC Power output responses when studying the system shown in Figure 4.29a, described in Section 4.7. The case studies the impact of a battery, modelled as a counter voltage connected to a tiny resistance, connected at the DC side. The output responses shown correspond to the case where the simplified model is operated, and small steps are applied in the field voltage. Figure 4.30 shows the field voltage applied to the generator. The corresponding output responses obtained for generator d- and q-axis components, rotor speed, load angle δ etc. are shown in Figure 8.15 in Appendix G. The simplified model is modified and a 33% pure resistive DC load has replaced the battery, such that the model operates with the absence of a counter voltage. α, β and ϕ are retrieved from the detailed model when connected as shown in Figure 4.29a. The d-axis transient reactance is decreased such that the relationship $\frac{x_q}{2x'_d}$ equalizes 2.60. Thus, seen in context with the unstable phenomenon, an unfavorable condition are present. However, no unstable behaviour are present in the measured output variables and the system is considered stable.
The same simulation case was performed in the detailed model, both by applying steps in the field voltage and in the resistive load connected to the DC side. Similar results were obtained in the detailed model: Replacing the battery, modelled as a counter voltage connected to a tiny resistance, by a 33% pure resisitve load makes the system stable.

As mentioned in Section 4.7, an analogous simulation case is examined for the system shown i figure 4.29b, which contains the battery model. However, it was necessary to increase the transient d-axis reactance, x'_d such that the relationship $\frac{x_q}{2x'_d}$ equalizes 1.90. Simulations of $\frac{x'_d}{x_q} = 2.60$ resulted in huge oscillations and the simulation model was not able to solve the entire simulation case. This is because the instability worsens as the relationship $\frac{x_q}{2x'_d}$ increases and operating at about 33% load has in addition turned out to be a worst-case load. Figure 4.29b shows the corresponding output DC voltage, DC current and DC power responses when the simplified model is operated, and small steps are applied in the field voltage. Significant undamped oscillations are present in the measured output variable responses. The frequency of the oscillations are about 2.15 Hz. The corresponding output responses obtained for d- and q-axis components, rotor speed, load angle δ etc. are depicted in Figure 8.16 in Appendix G.

Based on the results obtained during this analysis, the type of load connected to the DC side is of crucial importance in relation to the unstable behavior. The battery, which can be interpreted as a counter voltage connected to a tiny resistance, causes the unstable modes to be moved towards the right in the complex plane. The movement of the unstable modes is relative to the case where only a relatively large pure resistive load is connected at the DC side.

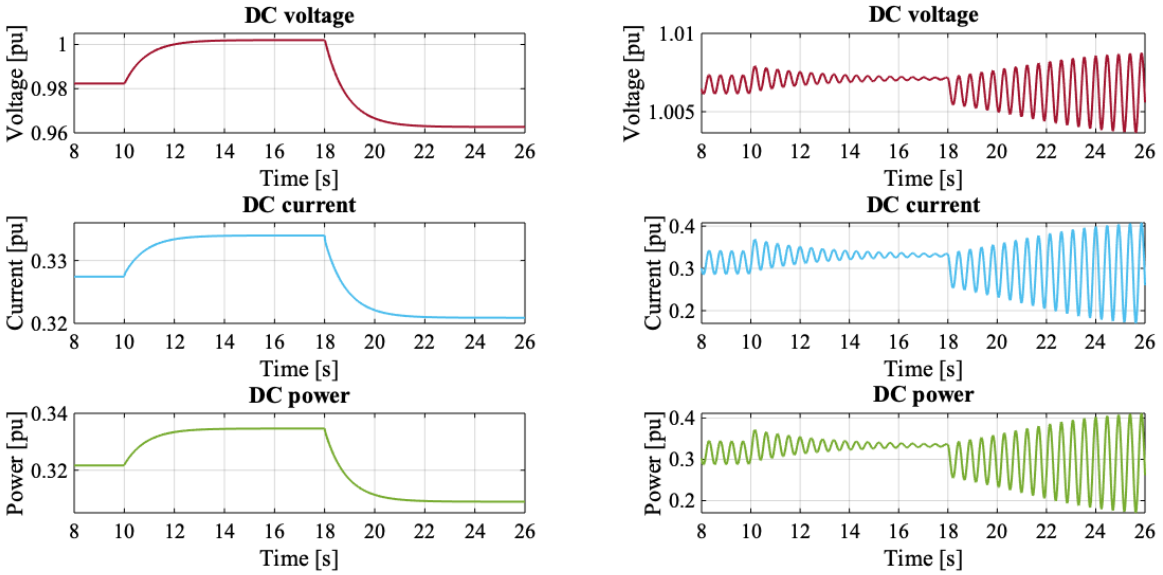

(a) **(b)**

Figure 5.8: DC voltage, DC current and DC power output responses corresponding to examination of case 2 presented in Section 4.7, studying the impact of a counter voltage. (a) Represents the measured output responses when the simplified model operates with the absence of a counter voltage. (b) Represents the corresponding measured output responses when the simplified model operates with the presence of a counter voltage.

5.3 The Impact of the Three-Phase Diode-Bridge Rectifier

The left column in Figure 5.9 shows the generators output voltage, current and active power responses when the first part of case 3 described in Section 4.7 is simulated. The synchronous generators operate with the absence of three-phase diode-bridge rectifiers, as shown by the schematic in Figure 4.31a. A few seconds are required for the machines in order to reach the desired operation point at about 33% load. Further, the column in the middle shows a zoomed-in version of the responses depicted in the left column. Because the two generators are fed by a 0.5% difference in the field voltage, the load is shared differently between them. The right column in Figure 5.9 shows the AC RMS line voltage, the RMS line current and the total active power delivered to the AC load. The spike present in all the responses at $t = 9$ s is caused by the disconnection and connection of the resistive AC loads. Figure 5.10 zooms into the spike that occurs in the output active power of the two generators. The corresponding output responses obtained for d- and q-axis components, field voltages, rotor speed etc. are depicted in Figure 8.17 and 8.18 for the first and second generator, respectively.

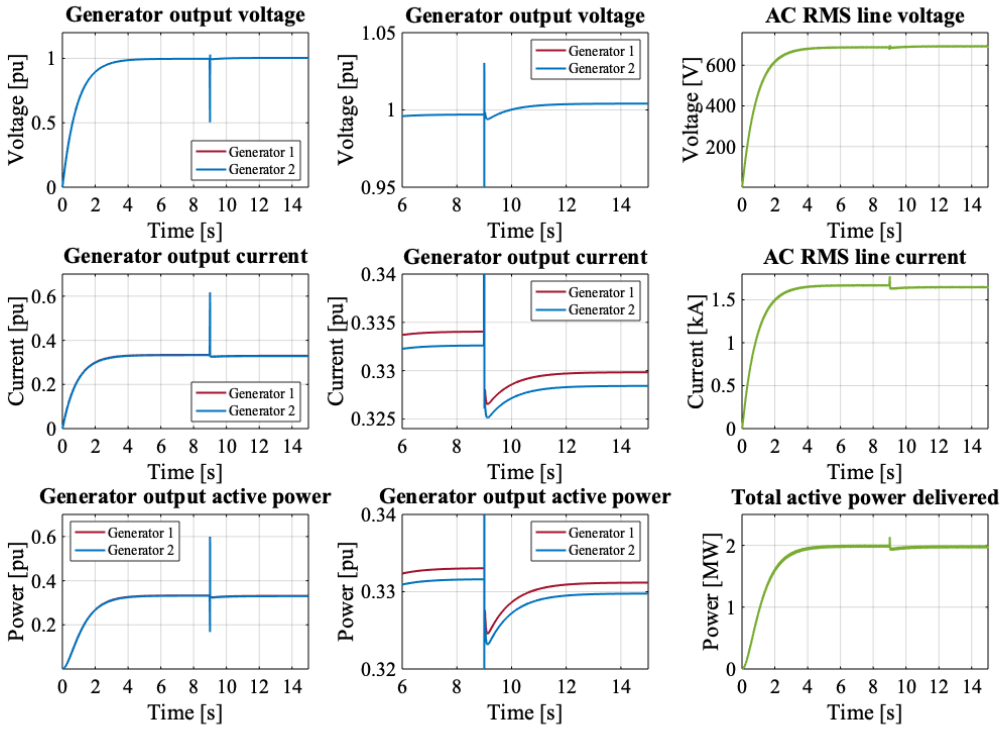

Figure 5.9: The left column shows the generators voltage, current and active power responses corresponding to the first part of simulation case 3. The column in the middle shows a zoomed-in version of the left column while the right column shows the AC RMS line voltage, AC RMS line current and the delivered active power responses. The generators power a common resistive three-phase AC load and the system operates with the absence of three-phase diode bridge rectifiers. A negative 2% step in load is applied at $t = 9$ s. The simulation is performed in a modified version of the detailed model.

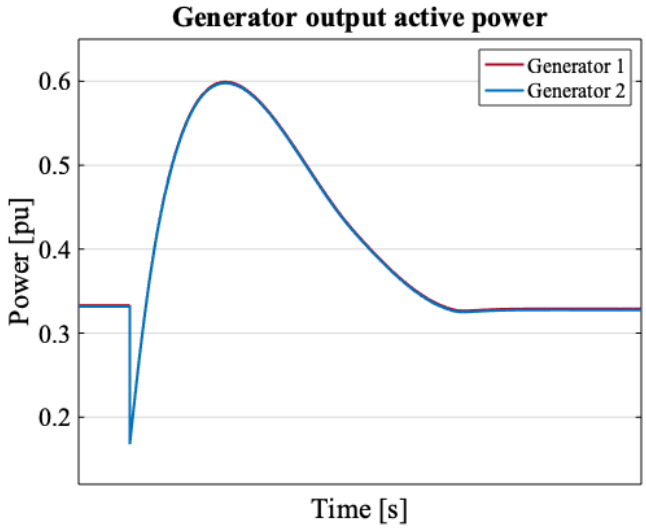

Figure 5.10: A zoomed-in version of the spike visible in the generator output active power response due to the negative 2% step in load.

As described in Section 4.7, both of the generators are operated at about the worst-case load, 33% load, where a 2% decrease in the AC load is applied at $t = 9$ s. The d-axis transient reactance, x'_d is decreased such that the ratio $\frac{x_q}{2x'_d}$ equalize 2.60. No oscillations are present in the measured responses and the system is considered stable.

Next, the second simulation described in case 3 in Section 4.7, where the three-phase diode-bridge rectifiers are connected (Figure 4.31b), is examined. Figure 5.11 shows the DC current, DC power and DC voltage responses. Significant undamped oscillations in the generator current and power are observed from the very beginning of the simulation. The frequency of the oscillations are about 1.94 Hz. The corresponding output responses obtained for d- and q-axis components, field voltages, rotor speed etc. are depicted in Figure 8.19 and 8.20, in Appendix H, for the first and second generator, respectively.
This result confirms the fact that a three-phase diode-bridge rectifier needs to be present in order to make the system unstable. Two synchronous generators connected in parallel, with the absence of rectifiers feeding a common AC load, are considered stable regarding to the unstable phenomenon.

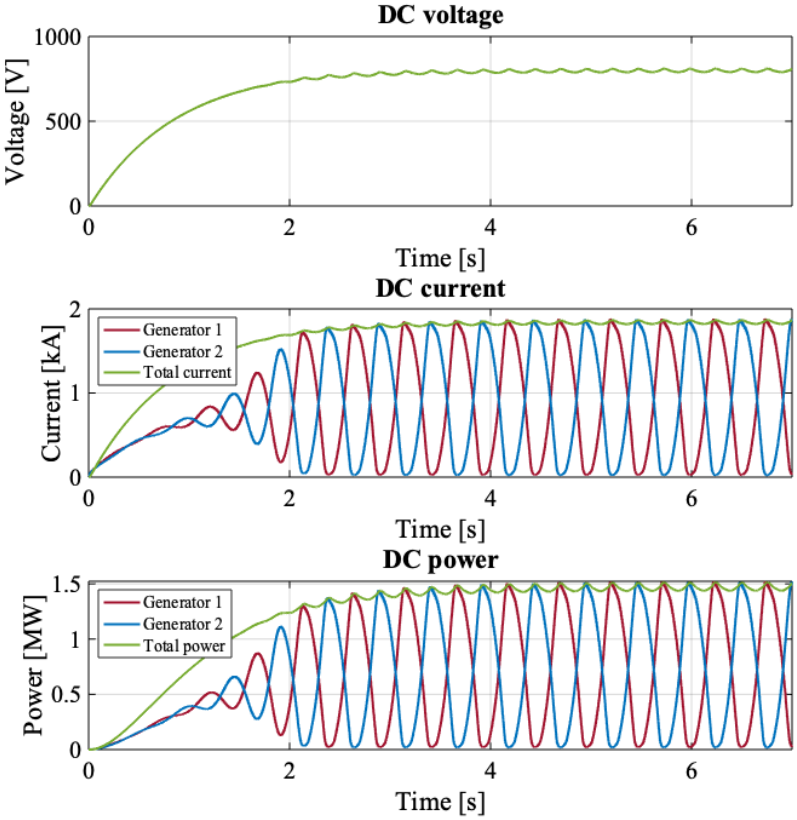

Figure 5.11: DC voltage, DC current and DC power responses corresponding to the second part of simulation case 3. Each of the generators are connected to a three-phase diode-bridge rectifier which further powers a common resistive DC load. The simulation is performed in a modified version of the detailed model.

Chapter 6

Discussion

This chapter aims to discuss the results obtained during this thesis. Some of the points presented here have already been discussed in Chapter 4 and 5, but are brought up again to unify all the remarks.

The present study was designed to improve insight into the unstable oscillations that may arise when a synchronous generator is connected to a battery through a diode-bridge rectifier, or multiple synchronous generator-rectifier systems are connected in parallel at the DC side.
The detailed simulation model and the simplified numerical model were developed based on this principle. Therefore, system components not believed to be a part of the unstable behaviour were excluded. Consequently, the simplified model is not able to follow the detailed model perfectly. However, this was not the aim. Using the idea of removing redundant components made it possible to discover that the unstable behaviour arise independently of the presence of an AVR and a governor system. In addition it was found, by removing the mechanical part of the synchronous generator, that the unstable behaviour is not an electromechanical phenomenon. Therefore, the instability is considered an electromagnetic phenomenon and the unstable behaviour is not related to well-known rotor angle oscillations, which Auinger believed in [15].

An essential disadvantage with the simplified model is the need of executing the detailed model in advance, to retrieve α, β and ϕ. In addition, the detailed model needs to be operated with the absence of unstable oscillations. Otherwise it complicates the process of extracting the correct values for α, β and ϕ. As a result, when operating the generator approximately at the worst-case load, 33%, the generator data needs to be adjusted such that a favourable relationship between x_q and x'_d is used. This may cause incorrect values for α, β and ϕ to be used in the simplified model, because they might be used for another relationship between x_q and x'_d. However, it was shown that α, β and ϕ did only experience slight changes, even when varying the load. Anyway, if the amplitude of the unstable oscillations becomes too large, the simplified model will become inaccurate. In addition, because the switching action of the diodes is neglected, the simplified model does not account for the discontinuous current conduction mode operation of the rectifier, mentioned in Section 3.4, and might be invalid at light loads.

A method of solving this problem, of operating the simplified model independent of the detailed model, could be to utilize lookup tables in the simplified model. The power or current drawn from the generator can be used as input values for the lookup tables where α, β and ϕ are the resulting output values. Then the value of the power or current drawn from the generator maps corresponding values for α, β and ϕ, for that specific operation point. The detailed model is executed once to retrieve the values needed in order to map a given power or current to a corresponding α, β and ϕ. However, only a certain number of data points are extracted, and interpolation techniques can be utilized in order to calculate the remaining values.

Also the present process of initializing the state variables, for a chosen field voltage, is complicated. The current process execute the detailed model in advance and measures the I_{DC} and V_{DC} at a given field voltage. Also in this case the detailed model needs to be operated with the absence of unstable oscillations. This is especially important during the process of validating the simplified model against the detailed model, such that the models actually are operated at the same operating point.
This initialization process can be simplified by changing the method used in the initialization code in Matlab. The field voltage is set based on the desired load to be delivered to the circuit and the DC voltage value is set by doing a reasonable guess.
Based on the fact that the simplified model became unstable, despite that the dynamics associated with diode switching were removed, this indicates that the diode commutation as such is not part of the underlying problem.

The simplified model was linearized and eigenvalues were calculated for all five synchronous generators. An unstable pair of complex eigenvalues were discovered in each of the five generators. However, the system using the round rotor generator RR and the system using the salient pole generators SP2 and SP3 resulted to contain the complex eigenvalues with the most positive real part and are thus considered as the most unstable generators. The system using the salient pole generator SP4 did only contain eigenvalues with negative real parts, and it is hence considered stable. SP4 is the generator with the smallest difference between x_q = x'_q and x'_d. In addition, SP4 is the generator with the largest q-axis open-circuit subtransient time constant, T''_{qo}. Time domain simulations were executed and the responses were compared with the obtained eigenvalues. When using an unfavourable relationship between x_q = x'_q and x'_d, it was possible to observe the excitation of the unstable pair of complex modes. This by confirming that the measured frequency of the time domain responses correspond to the frequency extracted from the imaginary part of the pair of complex modes.

Further, calculation of participation factors corresponding to the use of salient pole generator SP1 indicated that E'_q and E''_d are the state variables that have the most dominating participation in the unstable pair of complex eigenvalues. This means that this pair of unstable eigenvalues are sensitive for changes in state matrix elements a_{11} and a_{33}, which contains the following system parameters: T'_{do}, T''_{qo}, x''_d, x''_q, x'_q and r_a. Several of these system parameters were also

through the sensitivity analysis marked as important parameters, but x'_d was also found among the most influencing parameters during the sensitivity analysis.
However, the participation factor analysis conducted is too weak in order to draw any conclusions:
First, the participation factor matrix contains not only non-zero values for the elements that relates E'_q and E''_d to the unstable complex pair of eigenvalues, but also for E''_q and δ. The participation factors did not clearly show that only E'_q and E''_d were the participating factors; they only indicated these state variables to be among the most participating variables.
Second, in order to be able to draw any conclusions, a more comprehensive analysis is required, where several generator sets, as well as different level of loads are studied.
Third, T_δ is a kind of fictitious parameter needed in order to avoid the simplified model from containing an algebraic loop. This numerical issue explains why the power angle, δ, ended as a state variable, which is important to keep in mind when evaluating the results.
Therefore, a critically view is of importance when studying the results retrieved from the participation factor analysis.

Anyway, based on the sensitivity analysis results, there is no doubt that x_q, x'_q and x'_d are the three system parameters that attract most attention, followed by T''_{qo} and x''_d. The sensitivity analysis results agree about that increasing x'_d and decreasing x'_q influence the system stability in a positive manner.
The particular result agrees with previous literature that have reported a strong relationship between $x'_q = x_q$ and x'_d. [15; 16; 17] proposes $\frac{x'_q}{2x'_d} \leq 1$ as a stability criteria for synchronous generators that satisfy $x'_q = x_q$. Each of the five synchronous generators studied during this thesis satisfy $x'_q \approx x_q$. In addition, as mentioned in Section 2.2, [15; 16; 17; 18] do all argue for installing a suitable short-circuit q-axis winding such that also this axis can contribute with damping. [18] concludes that decreasing the q-axis damper winding resistance is of the utmost importance for system behaviour being stable. Decreasing the q-axis damper winding resistance results in an increased q-axis time constant which has also been recommended by Auinger in [15; 16]. Auinger namely claims the installation of short-circuited rotor winding in the q-axis, with sufficiently large time constant, capable of resisting changes in the induced q-axis magnetic field, to be the solution, getting rid of these low-frequency current oscillations. Weiming concludes in [17] that installing a short-circuited q-axis winding on the machine rotor has shown, both theoretically and experimentally, to effectively enhance the system stability. The installation of such additional q-axis damper winding was also performed in [22] and resulted in a stable system. A special design of the exciter winding is also believed to solve the problem, according to Auinger [16, p.86].

Moreover, the system analysis results illustrate that the system wants to move in a specific direction with respect to the d- and q-axis components. Figures 5.3 - 5.7 show that the d- and q-axis parameters representing the corresponding parameter, contains different colours on their respective bars. If the d-axis parameter corresponds to a blue coloured bar or to a red coloured

bar, the associated q-axis parameter correspond to a red coloured bar or to a blue coloured bar, respectively. As an example, studying Figure 5.5 or Figure 5.6, x_d, x'_d, x''_d and T''_{qo} are associated a red coloured bar, while $x_q = x'_q$, x''_q and T''_{do} are associated with a blue coloured bar. The only exceptions are x''_q and x''_d for the salient pole generator SP1 and for the round rotor generator RR. However, x''_q is in both cases associated with a significantly lower bar, which means the influence of x''_q is rather small and these results needs to be treated critically.
Anyway, this result, where the system wants to move the relationship between the respective d- and q-axis components towards a certain direction, might agree with Auinger and Hoeijmakers hypotheses in [16] and [18], respectively. Auinger states that the d-axis open-circuit transient time constant being too slow, compared to the q-axis open-circuit transient time constant, to be a part of the underlying problem. Hoeijmakers attempt to explain that a sudden loading of the machine will cause a rapid increase in the q-axis current which further causes the q-axis flux to rapidly increase, due to the small q-axis damper time constant. Further, the resulting decrease in the d-axis flux happens slowly due to the relatively large excitation winding time constant, which is located in the d-axis. Hoeijmakers proposes this to be a part of the problem, creating unpleasant behaviour.
The sensitivity analysis conducted for the synchronous generators do further support this theory about reducing the system parameter T'_{do} in order to enhance the stability.
In addition, the results show that reducing T''_{do}, and increasing the system parameter, T''_{qo}, influence the system stability in a positive manner. The only exceptions are the results obtained for RR and SP4. SP4 associates a decrease in T''_{qo} and an increase in T''_{do} to enhance the system stability, while RR associates an increase in T'_{do} to increase the system stability. However, the corresponding bars are quite small compared to the other results. In addition, SP4 is the only generator which resulted in eigenvalues with only negative real parts and is thus considered stable. Further on, SP4 is already the generator with the largest value for T''_{qo}, and may not be beneficial to increase. Additionally, 3.32 in Section 3.5.3 shows that increasing x'_d and reducing x_q results in a reduced T''_d and to an increased T''_q. However, this further leads to an increased T'_d and to a reduced T'_q, but these latter parameters do also depend on T'_{do}, x_d and T'_{qo} and x_q, respectively. Consequently, changing one system parameter might affects several machine parameters.

When the sensitivity analysis was carried out, each of the system parameters where changed one at a time, keeping the other parameters unchanged. However, as shown by the Equations 3.29 - 3.32 presented in Section 3.5.3 changing one system parameter might affects several machine parameters. As an example, changing the system parameter x'_d actually leads to a physical change in the system parameters T''_{do} and x''_d. To achieve a more accurate sensitivity analysis it is recommended to transform the present system parameters into machine parameters, such as field winding resistance r_{fd}, field leakage reactance x_{lfd}, leakage reactance of the d-axis damper winding x_{l1d} etc.. Pavella presents in [78, p.353-356] a method of doing this type of generator-parameter-transformation, which also is easy to follow. Unfortunately, due to time restrictions, this analysis was not conducted during this thesis work. Therefore, examining this analysis will be of high importance in further work.

Additionally, based on the experiences so far, it would be interesting to further explore the relationship between the corresponding system parameters in each of the generator d- and q-axis. As an example, it would be interesting to study how the relationship between x''_d and x''_q influences the system stability; Does a large or small difference between the d- and q-axis component enhance the system stability? Will the system stability improve if the ratio between the corresponding d- and q-axis becomes equal to 1? However, this is considered as future work.

Based on the sensitivity analysis results as well as the participation factor analysis, the filter capacitance is found to not influence the unstable complex pair of eigenvalues. Therefore, it is from the stability perspective seen as a redundant component and can be removed from the model such that an even simpler system is obtained. Consequently, V_{DC} is not longer treated as a state variable and the last differential equation presented in 4.13 is instead replaced by the algebraic Equation 6.1.

$$V_{DC} = R_{bat} I_{DC} + V_{bat} \tag{6.1}$$

The sensitivity analysis results obtained for the system parameters T_δ, r_{bat} and r_a are discussed in the two last bullet points on page 85.

After all, the sensitivity analysis results obtained during this thesis, present interesting indications about which system parameters that influence the instability the most. They also contain information about in which direction the parameters should be adjusted, in order to enhance the system stability. Concerning the parameters associated with a low bar, one should rather be more sceptic because changing one of the parameters might affect several system parameters at the same time.

The second case study investigated the impact of replacing the battery, modelled as a counter voltage connected to a tiny resistance, with a pure resistive DC load. Based on the achieved results, presented in Section 5.2, it seems that the unstable behaviour is strongly related to the type of load connected to the DC side. The only difference between the two systems is that an ideal DC voltage source, which is connected to a tiny resistance, is replaced with a large resistance. The internal resistance is only equal 0.022 pu while the new inserted resistance is equal to 3.00 pu, in order to achieve a 33% load operation. As a result, the new resistance is more than 100 times larger. As shown during the sensitivity analysis, a resistance connected to the DC side will enhance the system stability. The larger resistance, the more damping it provides. This might explain the reason why a stable system is achieved when replacing the counter voltage and the tiny resistance with a large resistance. A counter voltage connected to a tiny resistance will not provide sufficient damping to the system, and instability occurs. Based on this, it seems that an unfavourable type of DC load, not contributing with sufficient damping, needs to be present for the unstable phenomenon to occur. This further indicates that the

characteristics associated with what is connected to the DC side, is of main importance related to the unstable behaviour.

As mentioned in Section 2.4, during the specialisation project work, the unstable behaviour was detected, when two diode-bridge rectifier-loaded synchronous generator sets were operated in parallel, feeding a common constant current load. The fact that the parallel operation of multiple rectifier-synchronous generators turns out to be unstable, might be explained by the same reason as for the counter voltage: The load seen from the output of the rectifier is unfavourable in a way so that it does not contribute with sufficient damping, and the unstable eigenvalues are still located in the right half-plane in the complex plane.
It would be interesting to further study how different types of load influence the instability and if it is possible to recreate the unstable behaviour with the absence of a counter voltage, with only a small resistance connected to the DC side. This study can include an apparent impedance analysis, where the generator impedance seen from the output of the rectifier is extracted and compared against the impedance connected to the DC side. If the extracted apparent generator resistance is more negative than the DC resistance is positive, a net negative internal resistance is present, thus an unstable system [31]. On the other hand, if the sum of the extracted generator resistance and the DC load resistance is positive, a stable system is present. A system associated with a positive internal resistance act as a negative feedback, thus providing the system with damping.
This analysis might contribute to gain a better understanding of which combinations of generator data and type of DC load that can be used without causing the unstable phenomenon to occur.

The third case study investigated the impact of a three-phase diode-bridge rectifier when operating synchronous generators in parallel, feeding a common DC load. The result, presented in Section 5.3, confirms the fact that a three-phase diode-bridge rectifier needs to be present in order to make the unstable phenomenon to occur.

Further, based on the remarks experienced so far, an unfavourable relationship between the d- and q-axis components needs to be present in order to make the system unstable, and the utmost important system parameters seems to be x_q, x'_q and x'_d. Also, T''_{qo} and x''_d have shown to be among the more important system parameters. The studies conducted shows that reducing the difference between x'_q and x'_d enhance the system stability. Increasing x'_d such that x'_d is sufficient close to the value of x'_q, solves the problem of low-frequency system oscillations. Therefore, the conclusion is that the following two factors must be present simultaneously for the instability to occur:

1. An unfavourable relationship between the d- and q-axis generator parameters
2. An unfavourable type of DC load, not contributing with sufficient damping

So far, none of the cases conducted during this thesis have dealt with the case concerning rectifier-synchronous generators are connected in parallel at the AC side of the rectifier, and

further feeding a common DC load. However, it would be interesting to investigate the affect of connecting the generators in parallel at the AC side, rather than the DC side. This case can be studied by modelling the system sketched in 4.31b, where the rectifier connected to the second generator is removed, and the output terminal of the second generator are connected to the output terminals of the first generator. This analysis will indicate whether the location of the parallel connection affects the instability.

However, regardless of the underlying reason causing the instability, the phenomenon can be considered as a transient electromagnetic phenomenon, that primarily depends on the transient reactances and time constants.
Further work is needed in order to gain a fundamental understanding of the unstable phenomenon associated with diode-bridge rectifier-synchronous generator systems.

The instabilities have shown to be a function of load, where a worst-case load occurs about 33% load. Why this is the case is hard to say, but the stability criteria proposed in Equation 2.6 in Section 2.2 contains the load angle δ. The presence of δ, in the stability criteria proposed, indicates that the level of load is an influencing factor. The value of δ and the level of the current drawn from the generator, might be unfavourable for the machine when operated at about 33% load. Another explanation could regard the correspondingly distributed level of the d- and q-axis current at 33% load current, which might trigger an undesirable reaction in the machine due to an unfavourable relationship between the d- and q-axis parameters. It could be interesting to study how load-dependent variables in the machine, such as power angle δ, currents and induced voltages change with respect to each other. In other words, their derivatives with respect to each other. Perhaps some variables are experiencing a significant change with respect to some other variables at about 33% load, which might affect the unstable pair of complex eigenvalues in a negative manner. However, this is not prioritized during this thesis work.

Furthermore, the unstable phenomenon excites oscillations in the system with frequencies in the range of 1-5 Hz. In order to understand if this frequency origins from any of the system time constants, the influence of changing the available time constants used in the linearized model, T'_{do}, T''_{do}, T''_{qo} and T_δ were studied. How a $\pm 10\%$ change in the time constants affected the imaginary part of the unstable pair of complex modes, i.e. the frequency of the oscillations, were measured during the sensitivity analysis. T'_{do} was found to be among the time constants contributing the most, followed by T''_{qo} and T_δ. The affect of changing T''_{do} was rather small. These observations match the results obtained during participation factor analysis, where T'_{do} and T''_{qo} were found to be among the parameters which the unstable complex modes are believed to be sensitive to. However, it was not possible to directly correlate the value of the time constant to the frequency of the mode in any of the cases. Based on this, and the fact that the frequency of the oscillations increases as the load increases, the conclusion is that the frequency of the unstable behaviour is composed by several parameters and variables. In addition, some of these variables included need to reflect the level of load, for example through the load angle δ.

The sensitivity analysis results show that increasing the internal battery resistance moves the unstable poles toward the left in the complex plane and improves system stability. Anyway, getting rid of the unstable behaviour, increasing the internal resistance is not considered as a part of the solution. Increasing the resistance located at the DC side leads to increased power losses, which is an undesirable situation.
The key is to understand the combination of machine parameters that most effectively achieves a stable operation when connected to a diode-bridge rectifier and a battery. Thereafter, it would be valuable to develop a detailed model that accounts for other system components connected to the generator, such as AVR, governor system, internal resistances, loads connected etc.. Such a detailed model reduce the need of being too conservative when designing the generator. This because, other components connected to the generator influence the unstable pair of complex eigenvalues, and these components might contribute with damping. Further on, this model could act as an optimization model where factors such as stability margins, costs, weight and space are considered. However, the data sheet contains high uncertainties in the actual values of the generator data provided by the manufacture. This complicates the process.

Chapter 7

Conclusion

This chapter contains the conclusions drawn from the master thesis in relation to the objective and scope of work set in Sections 1.2 and 1.3.

The aim of the present study is to better understand why a synchronous generator connected to a battery through a diode-bridge rectifier, or multiple synchronous generator-rectifier systems connected in parallel at the DC side becomes unstable. The specific objective is to develop a simplified model that facilitates studying and aiding the understanding of this unstable phenomenon.

Previous literature have detected low frequency oscillations, 1 - 5 Hz, in the output current when diode-bridge rectifier-loaded synchronous generators operate in parallel with each other, or in parallel with a battery. Studies have suggested that transient disturbances introduced in the internal components of the generator d- and q-axis, due to rectifier, to be a part of the unstable phenomenon. The relationship $\frac{x_{\mathrm{q}}}{2x'_{\mathrm{d}}} \leq 1$ is proposed as a stability criteria for synchronous generators satisfying $x'_q = x_q$. Installing an additional q-axis damper winding on the rotor of the synchronous generator has proved to enhance the stability.

A simulation model of a synchronous generator connected to a battery through a diode bridge rectifier, able to reproduce the unstable behaviour, was implemented using Simulink/Matlab system blocks. Furthermore, based on the Simulink model, a simplified numerical average model capable of reproducing the unstable behaviour and which qualified for linear analysis was developed. This master thesis has shown that the unstable phenomenon occurs independently of an AVR and a Governor system. It has further shown that the instability occurs even though the generator is operated with the absence of a mechanical system. Thus, well-known rotor oscillations is not a part of the underlying problem and the instability is considered an electromagnetic phenomenon, not an electromechanical phenomenon.

The simplified model developed is an average value model which has eliminated the diode switching action in the rectifier, and is using two different parameters to transform between the

AC and DC currents and voltages, respectively. The simplified model is continuous and non-linear which further qualifies for linearization and small-signal analysis. The simplified model was validated and compared to the Simulink/Matlab model and has shown to follow it quite well. Based on the fact that the simplified model became unstable, despite that the dynamics associated with diode switching were removed, this indicates that the diode commutation as such is not part of the underlying problem.

Linearization of the simplified model is performed and modal analysis techniques are applied. Unstable complex pair of eigenvalues are detected and sensitivity analysis is conducted. This by the use of five different generator sets, including salient pole and round rotor structures. x'_d, x'_q and x_q resulted being the system parameters influencing the real part of the complex pair of unstable eigenvalues the most, followed by x''_d and T''_{qo}. The sensitivity analysis results did also show that the system improves stability by moving in a specific direction with respect to the d- and q-axis components, either by increasing the q-axis component and decreasing the corresponding d-axis component, or the opposite. As an example, in order to positively affect the system stability, the system wants to increase x'_d and T''_{qo} and decrease x'_q and T''_{do}, respectively. The participation factor analysis conducted for the salient pole generator SP1 indicates that the unstable pair of complex eigenvalues seem to be sensitive according to changes in the state matrix elements a_{11} and a_{33}, which contain the system parameters T'_{do}, T''_{qo}, x'_q, x''_q x''_d and r_a. Increasing x'_d such that x'_d is sufficient close to the value of x'_q, solves the challenge concerning low-frequency system oscillations.

This thesis has further shown that an unfavourable type of DC load, not contributing with sufficient damping, needs to be present for the unstable phenomenon to occur. This further indicates that the characteristics associated with the DC load, in addition to an unfavourable relationship between the d-axis and q-axis parameters in the generator, are important parts related to the instability.

To conclude, regardless of the underlying reason causing the instability, the unstable phenomenon can be considered as a transient electromagnetic phenomenon, that primarily depends on the transient reactances and time constants.

Chapter 8

Further Work

This final chapter aims to present suggestions for further work. Some of the suggestions presented here have already been presented in Chapter 6, but are restated to have them all unified.

Suggestions for further work:

- To achieve a more accurate sensitivity analysis it is recommended to transform the present system parameters into machine parameters, such as field winding resistance r_{fd}, field leakage reactance x_{lfd}, leakage reactance of the d-axis damper winding x_{l1d} etc.. Pavella presents in [78, p.353-356] a method of doing this type of generator-parameter-transformation, which also is easy to follow. Examining this analysis will be of high importance in further work.

- To improve the simplified and linearized models for avoiding the need of running the detailed simulation model in advance to obtain α, β and ϕ. In addition, the present initialization method should be improved to avoid measuring V_{dc} and I_{dc} from the detailed model in advance. Suggested methods are presented in Chapter 6.

- To explore the relationship between the corresponding system parameters in each of the generator d- and q-axis. As an example, it would be interesting to study how the relationship between X''_d and X''_q influences the system stability; Does a large or small difference between the d- and q-axis component enhance the system stability? Will the system stability improve if the ratio between the corresponding d- and q-axis becomes equal to 1?

- To study how different types of DC load influence the instability and if it is possible to recreate the unstable behaviour with the absence of a counter voltage, with only a small resistance connected to the DC side. This study can include an apparent impedance analysis, where the generator impedance seen from the output of the rectifier is extracted and compared against the impedance connected to the DC side. This analysis might contribute to gain a better understanding of which combinations of generator data and type of DC load that can be used without causing the unstable phenomenon to occur.

- To investigate the affect of locating the parallel connection of rectifier-synchronous generator at the AC side of the rectifier, rather than the DC side. So far, non of the cases conducted during the this thesis have considered the case where rectifier-synchronous generators are connected in parallel at the AC side of the rectifier, and further feeding a common DC load. A suggested method is presented in Chapter 6. This analysis will indicate whether the location of the parallel connection affects the instability.

- To study how load-dependent variables in the machine, such as power angle δ, currents and induced voltages change with respect to each other at different operating points. In other words, study their derivatives with respect to each other. Are some variables experiencing a significant change with respect to some other variables at about 33% load? This study might aid to a better understanding of why the phenomenon is a function of load and why 33% load is experienced as a worst-case load.

- To understand the combination of machine parameters that most effectively achieve a stable operation when connected to a diode-bridge rectifier and a counter voltage. Thereafter, it would be valuable to develop a detailed model that accounts for other system components connected to the generator, such as AVR, governor system, internal resistances, loads connected etc.. Such a detailed model reduces the need of being too conservative when designing the generator. This because, other components connected to the generator influence the unstable pair of complex eigenvalues, and these components might contribute with damping. Further, this model could act as a optimization model where factors such as stability margins, costs, weight and space are considered.

Bibliography

[1] E. E. A. EEA, "Transport : Increasing Oil Consumption and Greenhouse Gas Emissions Hamper EU Progress Towards Environment and Climate Objectives," *Agência Europeia do Ambiente*, p. 12, 2019. [Online]. Available: https://www.eea.europa.eu/themes/transport/term/increasing-oil-consumption-and-ghg

[2] International Maritime Organization, "Third IMO GHG Study," Tech. Rep., 2014. [Online]. Available: https://www.imo.org/en/GoogleSearch/SearchPosts/Default.aspx?q=GHGstudy

[3] International Maritime Organization, "Prevention of Air Pollution from Ships: MARPOL Annex VI - Proposal to Initiate a Revision Process," *Regulation*, vol. MEPC 53/4/, no. April, p. 12, 2005. [Online]. Available: https://www.epa.gov/sites/production/files/2016-09/documents/marpol-propose-revision-4-05.pdf

[4] International Maritime Organization, "Energy Efficiency Measures," Tech. Rep., 2011. [Online]. Available: https://www.imo.org/en/OurWork/Environment/Pages/Technical-and-Operational-Measures.aspx

[5] International Maritime Organization, "Initial IMO GHG Strategy," 2018. [Online]. Available: https://www.imo.org/en/MediaCentre/HotTopics/Pages/Reducing-greenhouse-gas-emissions-from-ships.aspx

[6] Greenport, "Norway Adopts Zero-Emissions Regulations in World Heritage Fjords," 2018. [Online]. Available: https://www.greenport.com/news101/Regulation-and-Policy/norway-adopts-zero-emissions-regulations-in-world-heritage-fjords

[7] S. Fang, Y. Wang, B. Gou, and Y. Xu, "Toward Future Green Maritime Transportation: An Overview of Seaport Microgrids and All-Electric Ships," *IEEE Transactions on Vehicular Technology*, vol. 69, no. 1, pp. 207–219, 2020.

[8] K. Kim, K. Park, G. Roh, and K. Chun, "DC-Grid System for Ships: A Study of Benefits and Technical Considerations," *Journal of International Maritime Safety,*

Environmental Affairs, and Shipping, vol. 2, no. 1, pp. 1–12, 2018. [Online]. Available: https://doi.org/10.1080/25725084.2018.1490239

[9] U. Javaid, D. Dujic, and W. Van Der Merwe, "MVDC Marine Electrical Distribution: Are we Ready?" *IECON 2015 - 41st Annual Conference of the IEEE Industrial Electronics Society*, pp. 823–828, 2015. [Online]. Available: https://ieeexplore.ieee.org/stamp/stamp.jsp?tp=&arnumber=7392201

[10] C. Nuchturee, T. Li, and H. Xia, "Energy Efficiency of Integrated Electric Propulsion for Ships – A Review," *Renewable and Sustainable Energy Reviews*, vol. 134, no. July, p. 110145, 2020. [Online]. Available: https://doi.org/10.1016/j.rser.2020.110145

[11] B. Z. Jin, G. Sulligoi, R. Cuzner, L. Meng, J. C. Vasquez, and J. M. Guerrero, "Next-Generation Shipboard DC Power System," *IEEE Electrification Magazine*, vol. 4, pp. 45–57, 2016.

[12] ABB, "Onboard DC Grid - The Step Forward in Power Generation and Propulsion," pp. 1–4, 2011.

[13] M. Chai, B. D. Reddy, S. Lingeshwaren, S. K. Panda, D. Wu, and X. Chen, "Progressing Towards DC Electrical Systems for Marine Vessels," *Energy Procedia*, vol. 143, pp. 27–32, 2017. [Online]. Available: https://doi.org/10.1016/j.egypro.2017.12.643

[14] L. Han, J. Wang, and D. Howe, "State-Space Average Modelling of 6- and 12-Pulse Diode Rectifiers," *2007 European Conference on Power Electronics and Applications, EPE*, no. 1, 2007.

[15] H. Auinger and G. Nagel, "Vom Transienten Betriebsverhalten Herrührende Schwingungen bei einem uber Gleichrichter Belasteten Synchrongenerator," *Theoretische Untersuchungen*, vol. Teil 1, 1980.

[16] H. Auinger and G. Nagel, "Vom Transienten Betriebsverhalten Herrührende Schwingungen bei einem uber Gleichrichter Belasteten Synchrongenerator," *Abhilfemassnahmen*, vol. Teil 2, 1980.

[17] M. Weiming, H. An, L. Dezhi, and Z. Gaifan, "Stability of a Synchronous Generator with Diode-Bridge Rectifier and Back-EMF Load," in *2000 IEEE Power Engineering Society Winter Meeting. Conference Proceedings (Cat. No.00CH37077)*, vol. 1, 2000, pp. 609–615 vol.1.

[18] M. J. Hoeijmakers, "The (In)stability of a Synchronous Machine with Diode Rectifier," in *Proc. Int. Conf. on Electrical Machines*, Manchester, UK, 1992, pp. 83–87.

[19] T. B. Byre, "Stability and Control of Power Systems on Ships," NTNU, Trondheim, 2020, [Unpublished project thesis. Can be requested by the author].

[20] A. Rygg, *Conversation 16.11.2020*. Siemens.

[21] T. H. Helland, "Stability Analysis of Diode Bridge Rectifier-Loaded Synchronous Generators Characterized with High Values of Reactances," NTNU, Trondheim, 2015, [Master's Thesis]. [Online]. Available: https://ntnuopen.ntnu.no/ntnu-xmlui/handle/11250/2368556

[22] J. Kirkeluten, "Stability of Synchronous Generators - Stability Analysis of Synchronous Generators Connected to Rectifiers," NTNU, Trondheim, 2016, [Master's Thesis]. [Online]. Available: https://ntnuopen.ntnu.no/ntnu-xmlui/handle/11250/2440770

[23] W. J. Bonwick, M. E., C. Eng., M.I.E.E., V. H. Jones, and B. E., "Performance of a Synchronous Generators with a Bridge Rectifier," 1972.

[24] M. J. Hoeijmakers, "A State Space Model of a Synchronous Machine with Convertor," in *Proc. Int. Aegan Conf. on Electrical Machines and Power Electronics*, Kusadasi, Turkey, 1992, pp. 592–597.

[25] J. Machowski, J. W. Bialek, and J. R. Bumby, *Power System Dynamics: Stability and Control*, 2nd ed. United Kingdom: John Wiley and Sons, Inc., 2012.

[26] N. Mohan, T. M. Undeland, and W. P. Robbins, *Power Electronics. Converters, Applications and Design*, 3rd ed. New York: John Wiley and Sons, Inc., 2003.

[27] A. Rygg, M. Amin, M. Molinas, and B. Gustavsen, "Apparent Impedance Analysis: A New Method for Power System Stability Analysis," *2016 IEEE 17th Workshop on Control and Modeling for Power Electronics, COMPEL 2016*, 2016.

[28] P. Huynh and B. Cho, "A New Methodology for the Stability Analysis of Large-Scale Power Electronics Systems," *IEEE Transactions on Circuits and Systems I: Fundamental Theory and Applications*, vol. 45, no. 4, pp. 377–385, 1998.

[29] S. Sudhoff, S. Glover, P. Lamm, D. Schmucker, and D. Delisle, "Admittance Space Stability Analysis of Power Electronic Systems," *IEEE Transactions on Aerospace and Electronic Systems*, vol. 36, no. 3, pp. 965–973, 2000.

[30] J. Huang, K. A. Corzine, and M. Belkhayat, "Small-Signal Impedance Measurement of Power-Electronics-Based AC Power Systems Using Line-to-Line Current Injection," *IEEE Transactions on Power Electronics*, vol. 24, no. 2, pp. 445–455, 2009.

[31] A. Emadi, B. Fahimi, and M. Ehsani, "On the Concept of Negative Impedance Instability in the More Electric Aircraft Power Systems with Constant Power Loads," *SAE Technical Papers*, no. 724, 1999.

[32] A. Emadi, A. Khaligh, C. H. Rivetta, and G. A. Williamson, "Constant Power Loads and Negative Impedance Instability in Automotive Systems: Definition, Modeling, Stability,

and Control of Power Electronic Converters and Motor Drives," *IEEE Transactions on Vehicular Technology*, vol. 55, no. 4, pp. 1112–1125, 2006.

[33] C. Zhang, M. Molinas, A. Rygg, J. Lyu, and X. Cai, "Harmonic Transfer-Function-Based Impedance Modeling of a Three-Phase VSC for Asymmetric AC Grid Stability Analysis," *IEEE Transactions on Power Electronics*, vol. 34, no. 12, pp. 12 552–12 566, 2019.

[34] M. Harris, A. Kelley, J. Rhode, and M. Baran, "Instrumentation for Measurement of Line Impedance," in *Proceedings of 1994 IEEE Applied Power Electronics Conference and Exposition - ASPEC'94*, 1994, pp. 887–893 vol.2.

[35] B. Palethorpe, M. Sumner, and D. Thomas, "Power System Impedance Measurement Using a Power Electronic Converter," in *Ninth International Conference on Harmonics and Quality of Power. Proceedings (Cat. No.00EX441)*, vol. 1, 2000, pp. 208–213 vol.1.

[36] G. Wang, L. Fu, X. Fan, Z. Ye, and F. Ma, "Periodic Orbit Model of Diode Rectifiers-Synchronous Machine System," *Science China Technological Sciences*, vol. 56, no. 1, p. 245–252, 2013.

[37] C. Rim, G. Joung, and G. Cho, "A State-Space Modeling of Non-Ideal DC-DC Converters," in *PESC '88 Record., 19th Annual IEEE Power Electronics Specialists Conference*, 1988, pp. 943–950 vol.2.

[38] K. Chaijarurnudomrung, K. N. Areerak, and K. L. Areerak, "Modeling of Three-Phase Controlled Rectifier Using a DQ Method," *International Conference on Applied Mathematics, Simulation, Modelling - Proceedings*, pp. 93–98, 2010.

[39] T. Sopaprim, K. N. Areerak, and K. L. Areerak, "The Averaging Model of a Six-Pulse Diode Rectifier Feeding Paralleled Buck Converters," *International Journal of Mathematics and Computers in Simulation*, vol. 6, no. 1, pp. 58–65, 2012.

[40] A. Emadi, "Modeling and Analysis of Multiconverter DC Power Electronic Systems Using the Generalized State-Space Averaging Method," *IEEE Transactions on Industrial Electronics*, vol. 51, no. 3, pp. 661–668, 2004.

[41] P. Ngamkong, P. Kochcha, K. Areerak, S. Sujitjorn, and K. Areerak, "Applications of the Generalized State-Space Averaging Method to Modelling of DC-DC Power Converters," *Mathematical and Computer Modelling of Dynamical Systems*, vol. 18, no. 3, pp. 243–260, 2012.

[42] J. Mahdavi, A. Emaadi, M. D. Bellar, and M. Ehsani, "Analysis of Power Electronic Converters Using the Generalized State-Space Averaging Approach," *IEEE Transactions on Circuits and Systems I: Fundamental Theory and Applications*, vol. 44, no. 8, pp. 767–770, 1997.

[43] A. Emadi, "Modelling of Power Electronic Loads in AC Distribution Systems Using the Generalized State Space Averaging Method," in *IECON'01. 27th Annual Conference of the IEEE Industrial Electronics Society (Cat. No.37243)*, vol. 2, 2001, pp. 1008–1014 vol.2.

[44] K. H. Chao, "Dynamic Modeling and Robust Control of Multi-Module Parallel Soft-Switching-Mode Rectifiers," *WSEAS Transactions on Systems*, vol. 8, no. 5, pp. 659–672, 2009.

[45] J. Jatskevich, S. D. Pekarek, and A. Davoudi, "Parametric Average-Value Model of Synchronous Machine-Rectifier Systems," *IEEE Transactions on Energy Conversion*, vol. 21, no. 2, pp. 435–441, 2006.

[46] J. Jatskevich and S. D. Pekarek, "Six-Phase Synchronous Generator-Rectifier Parametric Average Value Modeling Considering Operational Modes," *HAIT Journal of Science and Engineering B*, vol. 2, no. 3-4, pp. 365–385, 2005.

[47] I. Jadric, D. Borojevic, and M. Jadric, "Modeling and Control of a Synchronous Generator with an Active DC Load," *IEEE Transactions on Power Electronics*, vol. 15, no. 2, pp. 303–311, 2000.

[48] A. Baghramian and A. Forsyth, "Averaged-Value Models of Twelve-Pulse Rectifiers for Aerospace Applications," in *Second International Conference on Power Electronics, Machines and Drives (PEMD 2004).*, vol. 1, 2004, pp. 220–225 Vol.1.

[49] S. Sudhoff and O. Wasynczuk, "Analysis and Average-Value Modeling of Line-Commutated Converter-Synchronous Machine Systems," *IEEE Transactions on Energy Conversion*, vol. 8, no. 1, pp. 92–99, 1993.

[50] S. Sudhoff, K. Corzine, H. Hegner, and D. Delisle, "Transient and Dynamic Average-Value Modeling of Synchronous Machine Fed Load-Commutated Converters," *IEEE Transactions on Energy Conversion*, vol. 11, no. 3, pp. 508–514, 1996.

[51] C. Rim, D. Hu, and G. Cho, "Transformers as Equivalent Circuits for Switches: General Proofs and D-Q Transformation-Based Analyses," *IEEE Transactions on Industry Applications*, vol. 26, no. 4, pp. 777–785, 1990.

[52] C. Rim, N. Choi, G. Cho, and G. Cho, "A Complete DC and AC Analysis of Three-Phase Controlled-Current PWM Rectifier Using Circuit D-Q Transformation," *IEEE Transactions on Power Electronics*, vol. 9, no. 4, pp. 390–396, 1994.

[53] K.-N. Areerak, S. Bozhko, G. Asher, and D. Thomas, "Stability Analysis and Modelling of AC-DC System with Mixed Load Using DQ-transformation Method," in *2008 IEEE International Symposium on Industrial Electronics*, 2008, pp. 19–24.

[54] P. Kundur, J. Paserba, V. Ajjarapu, G. Andersson, A. Bose, C. Canizares, N. Hatziargyriou, D. Hill, A. Stankovic, C. Taylor, T. Van Cursem, and V. Vittal, "Definition and classification of power system stability," *IEEE Transactions on Power Systems*, vol. 19, no. 3, pp. 1387–1401, 2004.

[55] M. Basler and R. Schaefer, "Understanding Power System Stability," in *58th Annual Conference for Protective Relay Engineers, 2005.*, 2005, pp. 46–67.

[56] P. Kundur, *Power System Stability and Control*. New York: Electric Power Research Institute, McGraw-Hill, Inc., 1994.

[57] J. Persson, "Using Linear Analysis to find Eigenvalues and Eigenvectors in Power Systems," *IEEE International Symposium on Industrial Electronics*, pp. 1–4, 2002.

[58] Hedengren, John D., "Linearization of Differential Equations," 2020. [Online]. Available: https://apmonitor.com/pdc/index.php/Main/ModelLinearization

[59] M. Gibbard, N. Martins, J. Sanchez-Gasca, N. Uchida, V. Vittal, and L. Wang, "Recent applications of linear analysis techniques," *IEEE Transactions on Power Systems*, vol. 16, no. 1, pp. 154–162, 2001.

[60] I. J. Nagrath, D. P. Kothari, and R. C. Desai, *Modern Power System Analysis*. New York: Springer Science+Business Media, 2008, vol. 12, no. 1.

[61] M.-Y. Wu, "A new concept of eigenvalues and eigenvectors and its applications," *IEEE Transactions on Automatic Control*, vol. 25, no. 4, pp. 824–826, 1980.

[62] J. Sancha and I. Perez-Arriaga, "Selective Modal Analysis of Power System Oscillatory Instability," *IEEE Transactions on Power Systems*, vol. 3, no. 2, pp. 429–438, 1988.

[63] ABS American Bureau Shipping, "Guidance Notes on Control of Harmonics in Electrical Power Systems," *Control*, no. May, 2006.

[64] S. Hansen and P. Nielsen, *Power Quality and Adjustable Speed Drives*. Elsevier Inc., 2003. [Online]. Available: http://dx.doi.org/10.1016/B978-012402772-5/50013-2

[65] I. Jadric, D. Borojevic, and M. Jadric, "Simplified Model of a Variable Speed Synchronous Generator Loaded with Diode Rectifier," *PESC Record - IEEE Annual Power Electronics Specialists Conference*, vol. 1, pp. 497–502, 1997.

[66] V. H. Jones and W. J. Bonwick, "Three-Phase Bridge Rectifiers With Complex Source Impedance," *Proceedings of the Institution of Electrical Engineers*, vol. 122, no. 6, pp. 630–636, 1975.

[67] C.-M. Ong, *Dynamic Simulation of Electric Machinery : using MATLAB/SIMULINK*. New Jersey: Upper Saddle River, Prentice Hall PTR, 1998.

[68] T. Karthik and G. Raju, "New Criterion for Stator Inter Turn Fault Detection of Synchronous Generator," *17th National Power Systems Conference*, no. July, pp. 1–6, 2012.

[69] C. O'Rourke, M. Qasim, M. Overlin, and J. Kirtley, "A Geometric Interpretation of Reference Frames and Transformations: dq0, Clarke, and Park," *IEEE Transactions on Energy Conversion*, vol. 34, pp. 2070–2083, 2019.

[70] W. C. Dumper and W. J. Foley, "Recommended Phasor Diagram for Synchronous Machines," *IEEE Transactions on Power Apparatus and Systems*, vol. PAS-88, no. 11, pp. 1593–1610, 1969.

[71] MATLAB, *Version 9.7.0 (R2019b)*. Natick, Massachusetts: The MathWorks Inc., 2019.

[72] S. Documentation, *Simulation and Model-Based Design*. MathWorks, 2019. [Online]. Available: https://www.mathworks.com/products/simulink.html

[73] MathWorks, "Synchronous Machine pu Standard." [Online]. Available: https://se.mathworks.com/help/physmod/sps/powersys/ref/synchronousmachinepustandard.html

[74] MathWorks, "Simplified Synchronous Machine." [Online]. Available: https://se.mathworks.com/help/physmod/sps/powersys/ref/simplifiedsynchronousmachine.html

[75] MathWorks, "Universal Bridge." [Online]. Available: https://se.mathworks.com/help/physmod/sps/powersys/ref/universalbridge.html

[76] B. Gellert, "8 - Turbogenerators in Gas Turbine Systems," in *Modern gas turbine systems*, P. Jansohn, Ed. Woodhead Publishing, 2013, ch. 8, pp. 247–326.

[77] K. Uhlen, *Conversation 11.05.2021*. NTNU.

[78] M. Pavella and P. G. Murthy, *Transient Stability of Power Systems: Theory and Practice*. Chichester: Wiley, 1994.

Appendix A

Generator data

Table 8.1: Data for five synchronous generators.

Parameter	Symbol	Unit	Value				
			SP1	RR	SP2	SP3	SP4
Apparent power	S_{n}	MVA	3.00	1.94	1.222	0.90	2.34
Voltage	U_{n}	V	690	690	690	690	690
Frequency	f_{n}	Hz	60	66.7	50	50	60
Armature resistance	r_{a}	pu	0.0087	0.01	0.01	0.01	0.01
Direct axis synchronous reactance	x_{d}	pu	2.30	5.36	2.44	1.80	2.198
Direct axis transient reactance	x'_{d}	pu	0.40	0.49	0.233	0.09	0.438
Direct axis sub transient reactance	x''_{d}	pu	0.293	0.357	0.163	0.08	0.221
Quadrature axis synchronous reactance	x_{q}	pu	1.85	4.79	1.25	1.16	1.509
Quadrature axis transient reactance	x'_{q}	pu	1.80	4.79	1.25	1.10	1.509
Quadrature axis sub transient reactance	x''_{q}	pu	0.344	0.391	0.214	0.15	0.25
Leakage reactance	x_{l}	pu	0.178	0.076	0.10	0.03	0.18
Direct axis open-circuit transient time constant	T'_{do}	s	1.204	1.40	2.27	3.60	2.165
Direct axis open-circuit sub transient time constant	T''_{do}	s	0.01	0.05	0.029	0.02	0.036
Quadrature axis open-circuit transient time constant	T'_{qo}	s	0.95	1.04	0.20	2.00	0.90
Quadrature axis open-circuit sub transient time constant	T''_{qo}	s	0.036	0.02	0.105	0.11	0.123
Direct axis short-circuit transient time constant	T'_{d}	s	0.255	-	-	-	-
Direct axis short-circuit sub transient time constant	T''_{d}	s	0.006	-	-	-	-
Quadrature axis short-circuit transient time constant	T'_{q}	s	0.95	-	-	-	-
Quadrature axis short-circuit sub transient time constant	T''_{q}	s	0.007	-	-	-	-
Inertia	H	s	1.00	-	-	-	-
Friction factor	F_{f}		0.005	-	-	-	-
Pole pairs	P		2	-	-	-	-

Appendix B

Existing Simulink Block-Models

Disclaimer: The contents in appendix B is retrieved from [19] because the same two simulink model blocks were also used in the project work.

Synchronous Machine pu Standard

The equivalent synchronous machine model is depicted in Figure 8.1. It is presented in the rotor oriented reference frame (qd-frame). All parameters and electrical quantities are reflected from the stator. The subscripts used in the figure relates to the following:

- d,q - d- and q-axis quantity
- R,s - Rotor and stator quantity
- l,m - Leakage and magnetizing inductance
- f,k - Field and damper winding quantity

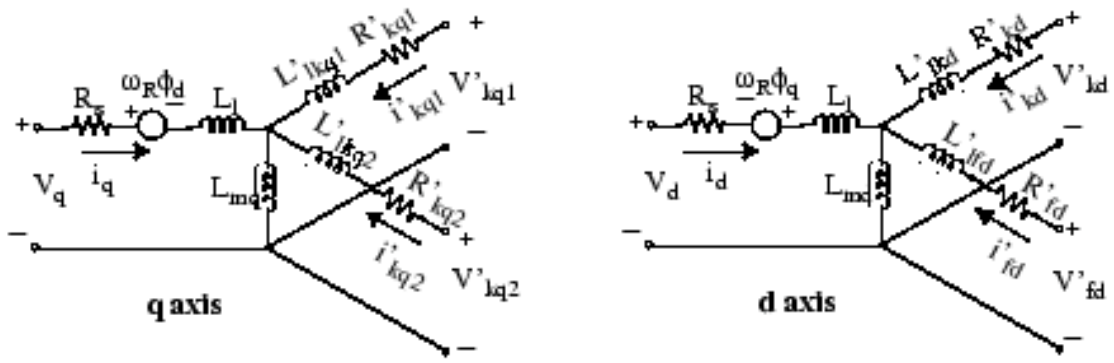

Figure 8.1: The electrical model of the synchronous machine [73]

The mechanical model of the synchronous machine is based up on Equation 8.1 and Equation 8.2 [74].

$$\Delta\omega(t) = \frac{1}{2H}\int_0^t (T_{\mathrm{m}} - T_{\mathrm{e}}) - K_{\mathrm{d}}\Delta\omega(t)\,dt \tag{8.1}$$

$$\omega(t) = \Delta\omega(t) + \omega_0 \tag{8.2}$$

where

- $\Delta\omega$ = speed variation with respect to speed of operation
- H = constant of inertia
- T_{m} = mechanical torque
- T_{e} = electrical torque
- K_{d} = damping factor representing the effect of damper windings
- $\omega(t)$ = mechanical speed of the rotor
- ω_0 = speed of operation (1 p.u.)

Three-Phase Two-Level Diode-Bridge Rectifier

The electrical circuit of the universal three-phase diode-bridge rectifier model is depicted in Figure 8.2.

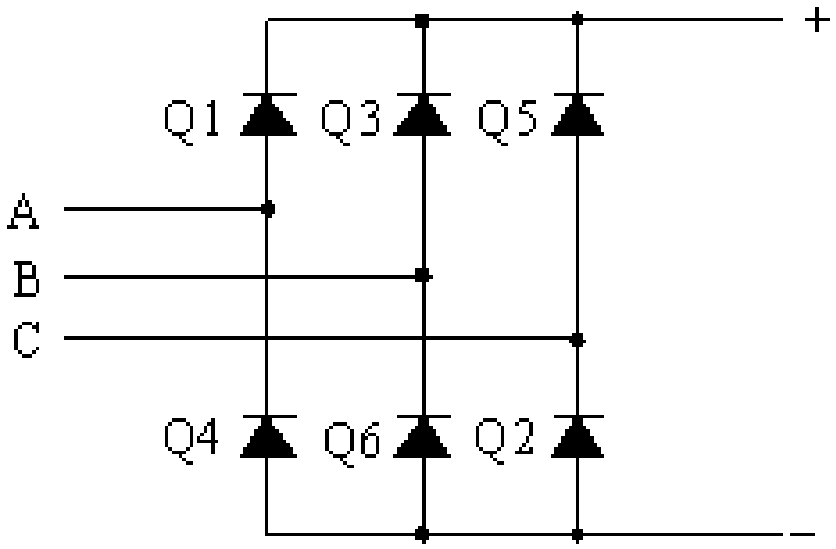

Figure 8.2: The electrical circuit of the three-phase two-level diode-bridge rectifier Simulink model [75].

Appendix C

Detailed Simulation Model

Simulation Results - Case 4

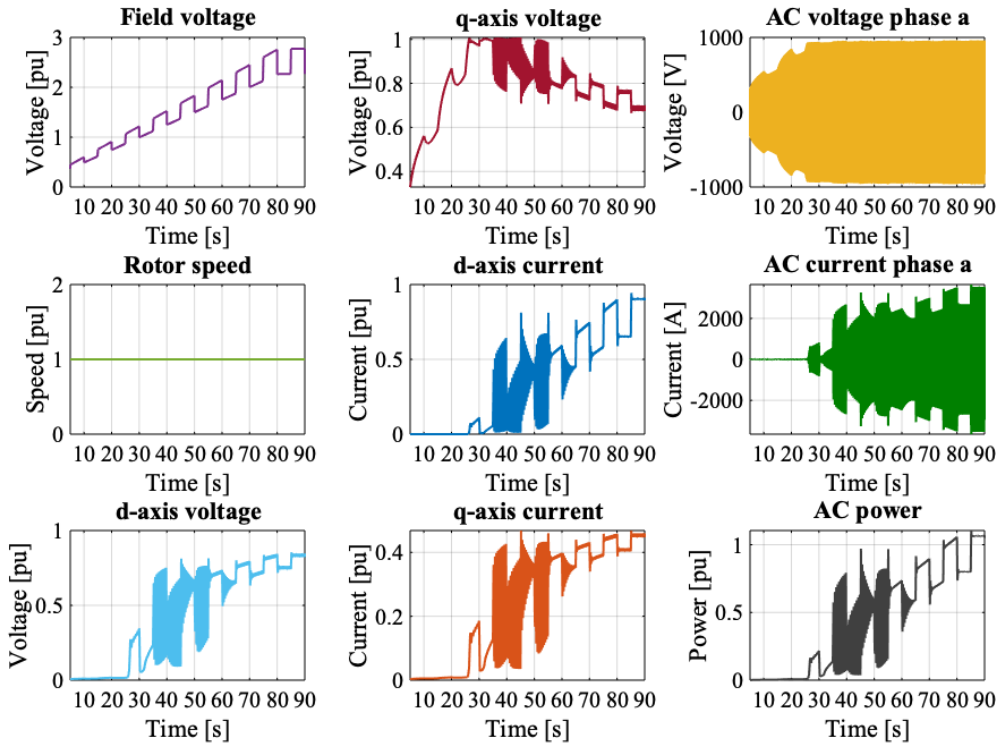

Figure 8.3: Simulation response variables when one rectifier-generator set powers a battery. The field voltage is increased linearly from 0 pu to 2.8 pu where an additional square wave with small current steps are superimposed onto the ramp.

Matlab Code - Initializing Detailed Model

```
% ------------------------------------------------------
%  Parameter tuning for the diesel-electric ship system
%                    -- Detailed Model --
% ------------------------------------------------------
clear all
close all;

%% Nominal values %%
S_n = 3000000; %3 MVA
V_n = 690;
f_n = 60; %frequency

%% Base values %%
S_b = S_n;
V_b = V_n;
V_b_dc = V_b*1.35;
Z_b = V_n^2/S_b;
I_b_ac = S_b/(sqrt(3)*V_b);
I_b_dc =S_b/V_b_dc;
Z_b_dc = V_b_dc/I_b_dc;
w_base = 2*pi*f_n ;

%% Generator parameters for SG1 [pu] %%
%K_scale = 0.770833333333333; %3
%K_scale = 0.8894230769; %2.6
%K_scale = 0.9635416667; %2.4
K_scale = 1; %2.3125
%K_scale = 1.027778; %2.25
%K_scale = 1.4453125; %1.6
%K_scale = 1.217105263157895; %1.9
%K_scale = 2.3125; %1
r_a = 0.0087;
x_d = 2.3;
x_d_t = 0.4*K_scale;
x_d_subt = 0.293;
x_q = 1.85;
x_q_t = 1.8;
x_q_subt = 0.344;
x_leak = 0.178;
```

```
40 T_do_t = 1.204;
41 T_do_subt = 0.01;
42 T_qo_t = 0.95;
43 T_qo_subt = 0.036;
44 T_d_t = 0.255;
45 T_d_subt = 0.006;
46 T_q_t = 0.95;
47 T_q_subt = 0.007;
48
49 %%inertia, friction factor and number of pole pairs
50 H = 1;
51 f_f = 0.005;
52 p_p = 2;
53
54 %% Parameters DC side %%
55 C_dc = 20e-3*S_n*1e-6; %20 mF per 1 MW
56 R_internal_bat = 20/I_b_dc;
57 V_bat = 1.35*V_b;
58 v_bat = V_bat/V_b_dc;
59 c_dc = C_dc*Z_b_dc;
60 r_internal_bat = R_internal_bat/Z_b_dc;
61
62 %% Stabilitycriteria %%
63 stability_ind = x_q/(x_d_t*2);
64
65 %% Define operating point %%
66 v_f=1.8;
67 v_bat=1*v_bat; %pu
```

Appendix D

Simplified Simulation Model

Matlab Code - Initializing Simplified Model

```
% ------------------------------------------------------
%  Parameter tuning for the diesel-electric ship system
%                    -- Simplified Model --
% ------------------------------------------------------
clear all
close all;
%% Nominal values %%
S_n = 3000000; %3 MVA
V_n = 690;
f_n = 60; %frequency
%% Set operation load %%
P_load = 1*S_n;
%% Base values %%
S_b = S_n;
V_b = V_n;
V_b_dc = V_b*1.35;
Z_b = V_n^2/S_b;
I_b_ac = S_n/(sqrt(3)*V_b);
I_b_dc =S_n/(1.35*V_b);
Z_b_dc = V_b_dc/I_b_dc;
w_sm_base = 2*pi*f_n ;
%% Generator parameters for SG1 [pu] %%
%K_scale = 0.770833333333333; %3
%K_scale = 0.8894230769; %2.6
%K_scale = 0.9635416667; %2.4
%K_scale = 1; %2.3125
%K_scale = 1.027778; %2.25
K_scale = 1.4453125; %1.6
```

```
29 %K_scale = 1.217105263157895; %1.9
30 %K_scale = 2.3125; %1
31 r_a = 0.0087;
32 x_d = 2.3;
33 x_d_t = 0.4*K_scale;
34 x_d_subt = 0.293;
35 x_q = 1.85;
36 x_q_t = 1.8;
37 x_q_subt = 0.344;
38 x_leak = 0.178;
39 T_do_t = 1.204;
40 T_do_subt = 0.01;
41 T_qo_t = 0.95;
42 T_qo_subt = 0.036;
43 T_d_t = 0.255;
44 T_d_subt = 0.006;
45 T_q_t = 0.95;
46 T_q_subt = 0.007;
47
48 %%inertia, friction factor and number of pole pairs
49 H = 3;
50 p_p = 2;
51 f_f = 0.005;
52 %% Parameters DC side %%
53 C_dc = 20e-3*S_n*1e-6; %20 mF per 1 MW
54 R_internal_bat = 20/I_b_dc;
55 V_bat = 1.35*V_b;
56 v_bat = V_bat/V_b_dc;
57 c_dc = C_dc*Z_b_dc;
58 r_internal_bat = R_internal_bat/Z_b_dc;
59 R_load_dc = (V_n*1.35)^2/S_n ;
60 r_load_dc=R_load_dc/Z_b_dc;
61 %% Parameters AC side (if reflected to the AC side) %%
62 % R_load=V_n^2/P_load;
63 % r_load=R_load/Z_b;
64 % r_tot=r_a+r_load;
65
66 %% Stabilitycriteria %%
67 stability_ind = x_q/(x_d_t*2);
68
69 %% Define operating point [pu] %%
```

```
70 %This set corresonds to 55.6% ac load
71 vf = 1.8; %set before running detailed model
72 v_bat = 1.0; %set before running detailed model
73 alpha = 1.0444; %obtained from detailed
74 beta_ = 0.9880; %obtained from detailed
75 phi = 0.2321; %[rad] %obtained from detailed
76 v_dc = 1.011433; %measured from detailed
77 i_dc = 0.5325; %measured from detailed
78 %% Initialize state variables based on alpha, beta, phi, Idc,
       Vdc %%
79 %  obtained from detailed model %
80 v_ac= v_dc*alpha;
81 i_ac_mag=i_dc/beta_;
82 i_ac=i_ac_mag*cos(phi)-i_ac_mag*sin(phi)*j;
83
84 EQ = v_ac+i_ac*(r_a+x_q*j);
85 delta=atan(imag(EQ)/real(EQ));
86 vq=cos(delta)*v_ac;
87 vd=-sin(delta)*v_ac;
88 iq=cos(delta+phi)*abs(i_ac);
89 id=-sin(delta+phi)*abs(i_ac);
90
91 %the effect of the armature reactance, ra, is neglected below
92 Eq=vq+x_d*abs(id); %Vf=Eq
93 Ed=vd+x_q*abs(iq);
94 Eq_t=vq+x_d_t*abs(id);
95 Eq_subt=vq+x_d_subt*abs(id);
96 Ed_subt=vd+x_q_subt*abs(iq);
97 %% Rename the parameters %%
98 Eq_t_val= Eq_t;
99 Eq_subt_val= Eq_subt;
100 Ed_subt_val= Ed_subt;
101 v_dc_val= v_dc;
102 delta_val= delta;
103
104 alpha_val= alpha;
105 beta_val= beta_;
106 phi_val= phi;
107 v_bat_val= v_bat;
108 vf_val= vf;
109
```

```
110 x_d_val=x_d;
111 x_d_t_val=x_d_t;
112 x_d_subt_val=x_d_subt;
113 x_q_val=x_q;
114 x_q_t_val=x_q_t;
115 x_q_subt_val=x_q_subt;
116 T_do_t_val=T_do_t;
117 T_do_subt_val=T_do_subt;
118 T_qo_subt_val=T_qo_subt;
119 r_a_val=r_a;
120 r_bat_val=r_internal_bat;
121 c_dc_val=c_dc;
122 %% Simulte the model equations to achieve better initialization
      values %%
123 %  for the state varibales (Eq ,Eq  ,Ed  ,Vdc and delta) %
124
125 Kd=1/0.01; %Kd=Kdelta=1/Tdelta
126 dt=0.000000001; %time step
127
128 for time=1:500
129     vd_val=-(v_dc_val*alpha_val)*sin(delta_val);
130     vq_val=(v_dc_val*alpha_val)*cos(delta_val);
131     id_val=(1/((r_a_val^2)+x_d_subt_val*x_q_subt_val))*(r_a_val
        *(Ed_subt_val-vd_val) -x_q_subt_val*(Eq_subt_val-vq_val)
        );
132     iq_val=(1/((r_a_val^2)+x_d_subt_val*x_q_subt_val))*(
        x_d_subt_val*(Ed_subt_val-vd_val) +r_a_val*(Eq_subt_val-
        vq_val));
133     Eq_t_dot_val=(1/T_do_t_val)*(vf_val-Eq_t_val+id_val*(
        x_d_val-x_d_t_val));
134     Eq_subt_dot_val=(1/T_do_subt_val)*(Eq_t_val-Eq_subt_val+
        id_val*(x_d_t_val-x_d_subt_val));
135     Ed_subt_dot_val=(1/T_qo_subt_val)*(-Ed_subt_val-iq_val*(
        x_q_t_val-x_q_subt_val));
136     V_dc_dot_val=(1/c_dc_val)*(beta_val*sqrt((id_val^2)+(iq_val
        ^2)) + v_bat_val/r_bat_val -v_dc_val/r_bat_val);
137     delta_dot_val=Kd*(-delta_val+asin(-id_val/(sqrt((id_val^2)
        +(iq_val^2))))-phi_val);
138     Eq_t_val=Eq_t_val+dt*Eq_t_dot_val;
139     Eq_subt_val=Eq_subt_val+dt*Eq_subt_dot_val;
140     Ed_subt_val=Ed_subt_val+dt*Ed_subt_dot_val;
```

```
141         v_dc_val=v_dc_val+dt*V_dc_dot_val;
142         delta_val=delta_val+dt*delta_dot_val;
143         eqm(time)=Eq_t_val;
144         eqdm(time)=Eq_subt_val;
145         eddm(time)=Ed_subt_val;
146         vdc(time)=v_dc_val;
147         del(time)=delta_val;
148         power(time)=iq_val*vq_val+id_val*vd_val;
149         tt(time)=time*dt;
150         plot(tt,del,tt,eqm,tt,eqdm,tt,eddm,tt,power,tt,vdc)
151 end
```

Simulation Results - Case 1

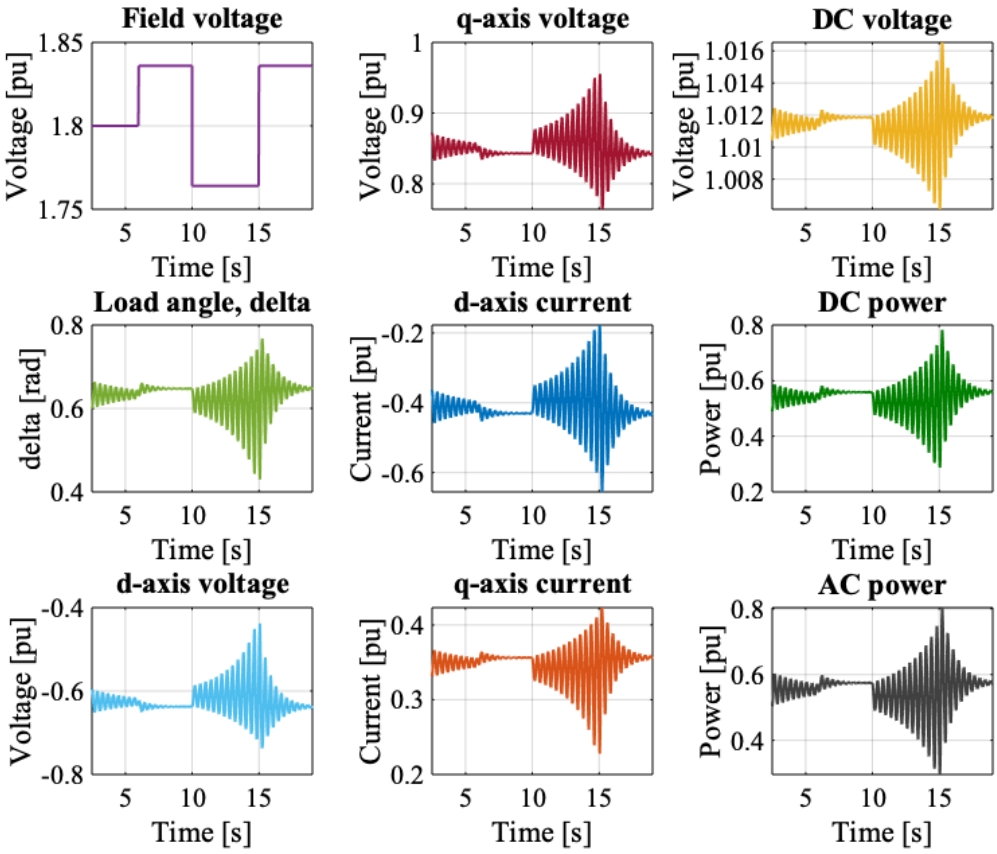

Figure 8.4: Simulation response variables when operating the simplified model at about 56% load. Small steps in the field voltage are applied (Figure 4.19). The battery voltage is set to 1 pu. The responses corresponds to the simulation case 1 presented in Table 4.3, X'_d corresponds to its original value and hence the ratio $\frac{X_q}{2X'_d}$.

Simulation Results - Case 2

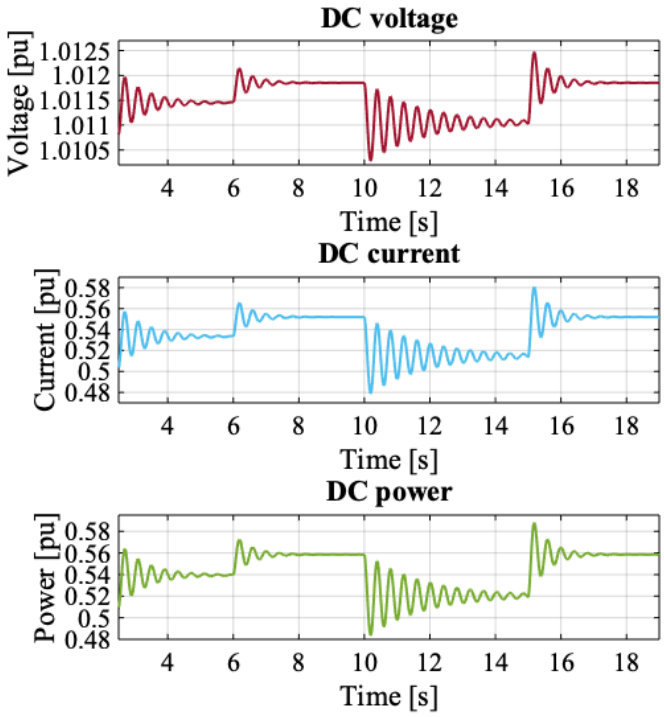

Figure 8.5: DC voltage, DC current and DC power responses for $t = 2.5$ s to $t = 19$ s. The simplified model is operated at about 56% load where small steps in the field voltage are applied (Figure 4.19). The battery voltage is set to 1 pu. The responses corresponds to the simulation case 2 presented in Table 4.3, X'_d is increased by the factor 1.027778 such that the ratio $\frac{X_q}{2X'_d}$ equalize 2.25.

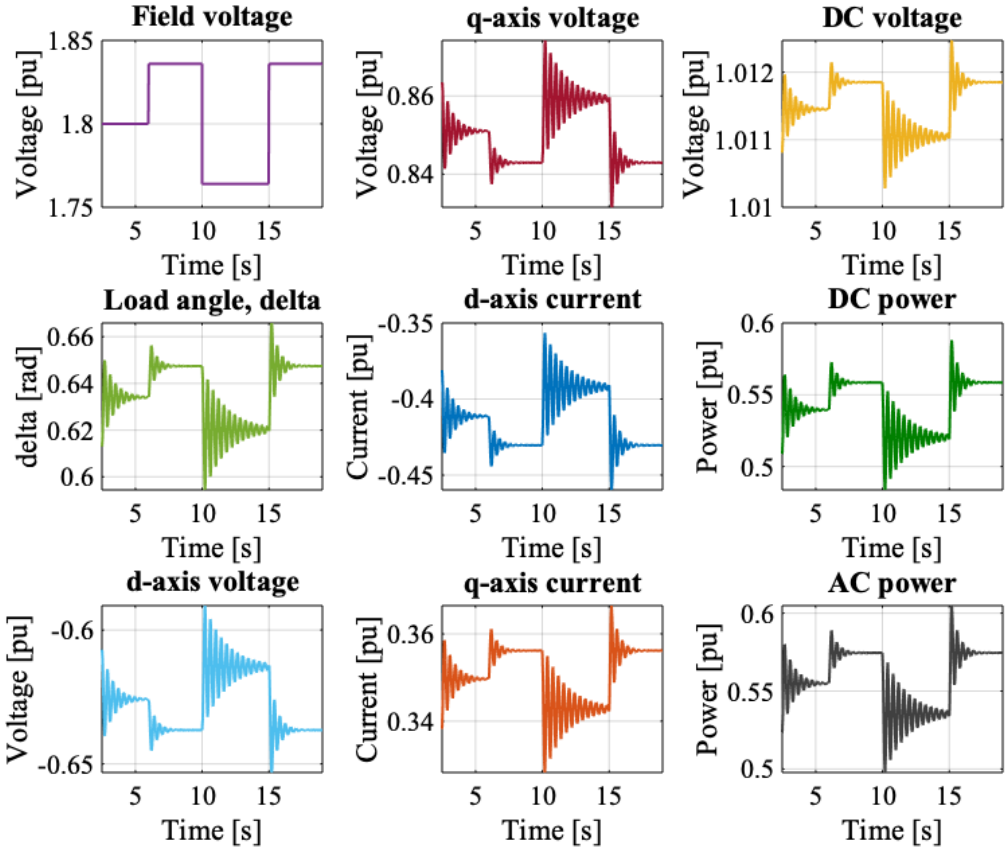

Figure 8.6: Simulation response variables when operating the simplified model at about 56% load. Small steps in the field voltage are applied (Figure 4.19). The battery voltage is set to 1 pu. The responses corresponds to the simulation case 2 presented in Table 4.3, X'_d is increased by the factor 1.027778 such that the ratio $\frac{X_q}{2X'_d}$ equalize 2.25.

Simulation Results - Case 3

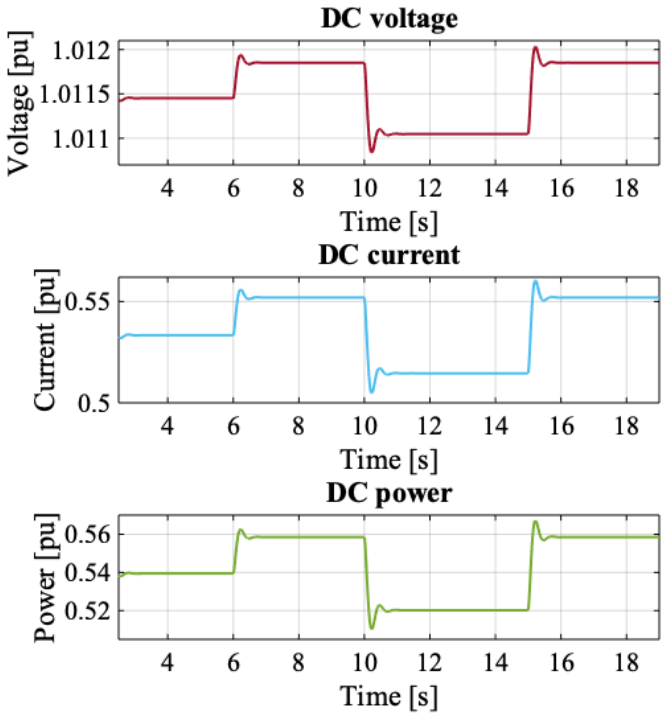

Figure 8.7: DC voltage, DC current and DC power responses for $t = 2.5$ s to $t = 19$ s. The simplified model is operated at about 56% load where small steps in the field voltage are applied (Figure 4.19). The battery voltage is set to 1 pu. The responses corresponds to the simulation case 2 presented in Table 4.3, X'_d is increased by the factor 1.217105 such that the ratio $\frac{X_q}{2X'_d}$ equalize 1.90.

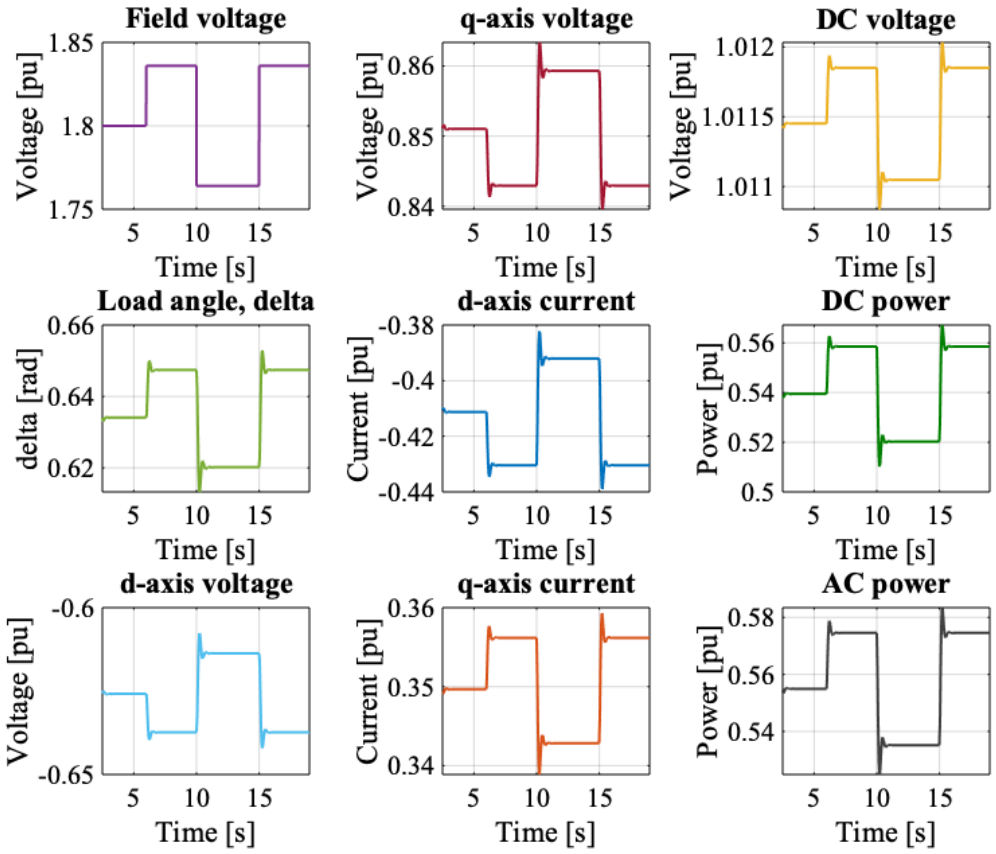

Figure 8.8: Simulation response variables when operating the simplified model at about 56% load. Small steps in the field voltage are applied (Figure 4.19). The battery voltage is set to 1 pu. The responses corresponds to the simulation case 2 presented in Table 4.3, X'_d is increased by the factor 1.217105 such that the ratio $\frac{X_q}{2X'_d}$ equalize 1.90.

Appendix E

Model Validation

Validation Case 2 - 55.5% AC Load

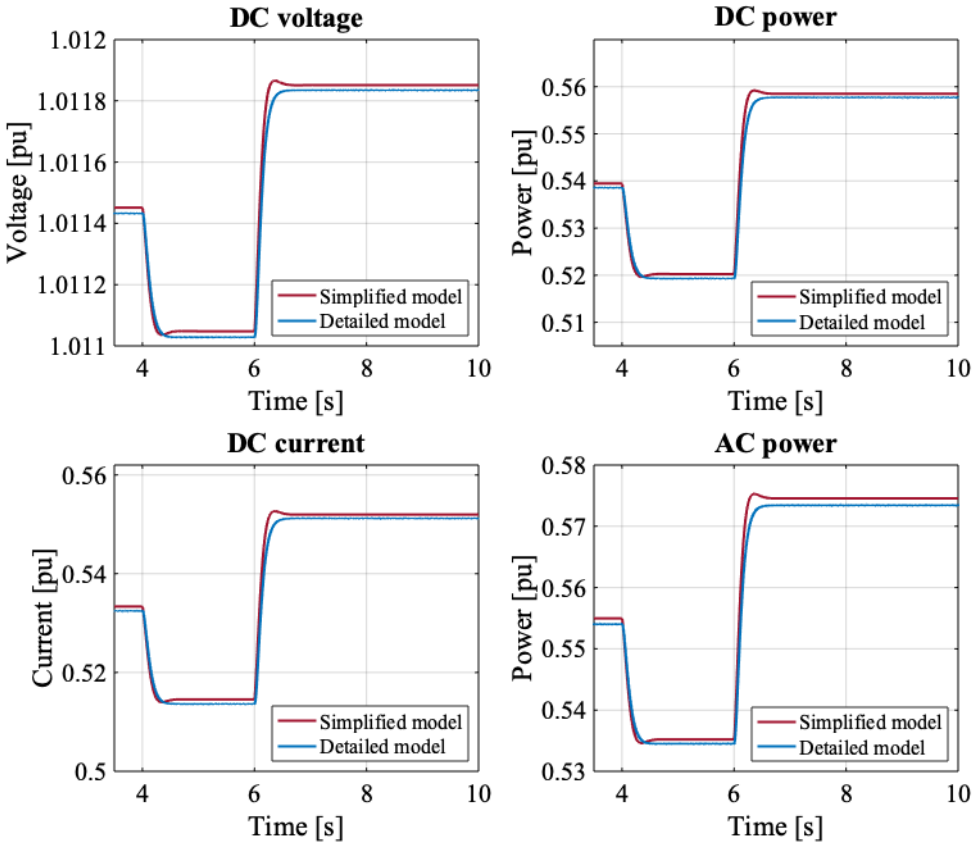

Figure 8.9: The DC Current, DC voltage, DC power and AC power responses corresponding to validation case 2, where the field voltage is stepped by $\pm 2\%$ from 1.8 pu. The applied field voltage follows the same shape as the graph shown in Figure 4.22.

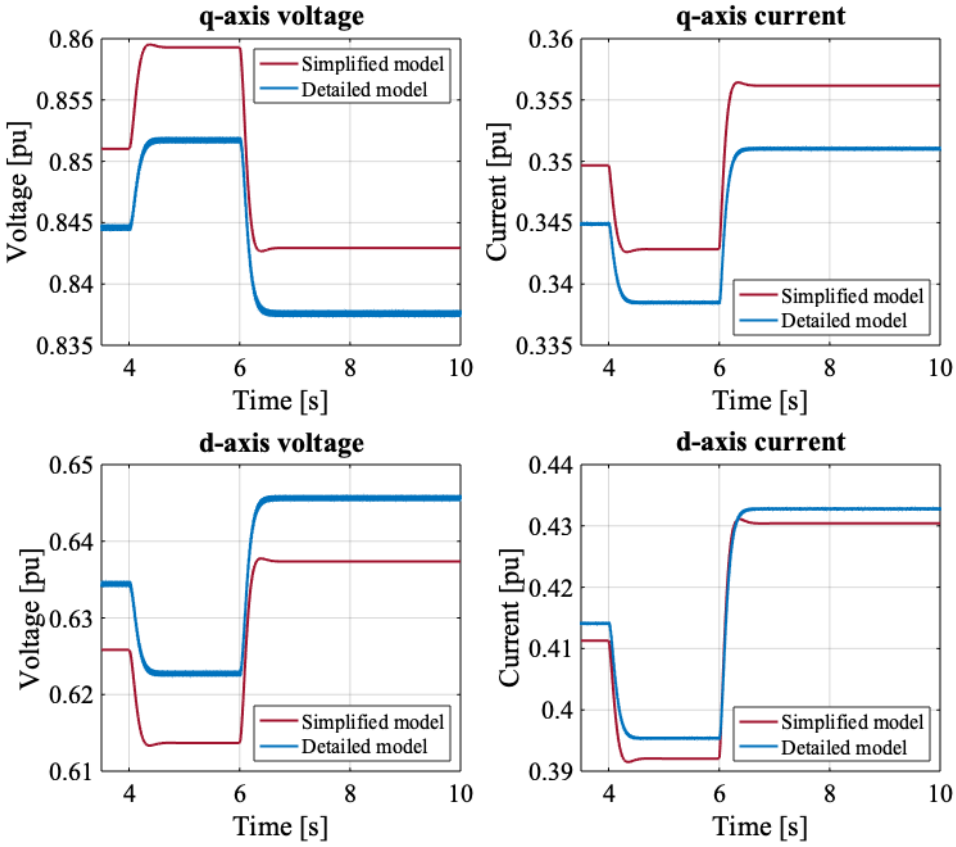

Figure 8.10: The d- and q-axis voltage and current responses corresponding to validation case 2, where the field voltage is stepped by $\pm 2\%$ from 1.8 pu. The applied field voltage follows the same shape as the graph shown in Figure 4.22.

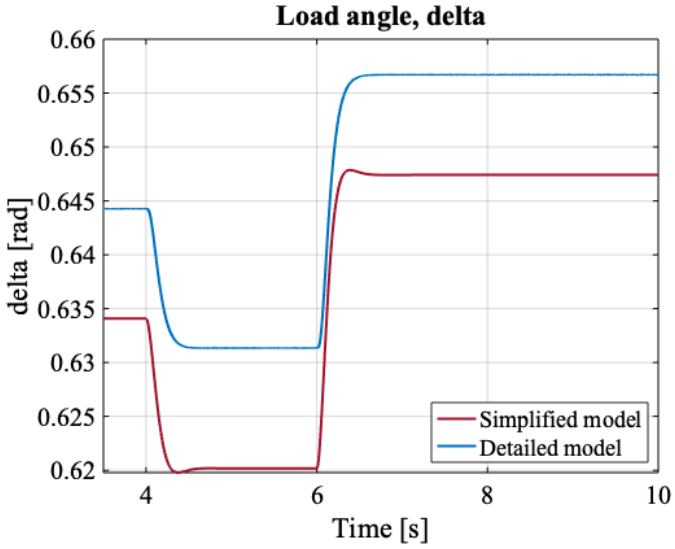

Figure 8.11: The Load angle, δ, responses corresponding to validation case 2, where the field voltage is stepped by $\pm 2\%$ from 1.8 pu. The applied field voltage follows the same shape as the graph shown in Figure 4.22.

Validation Case 3 - 33.0% AC Load

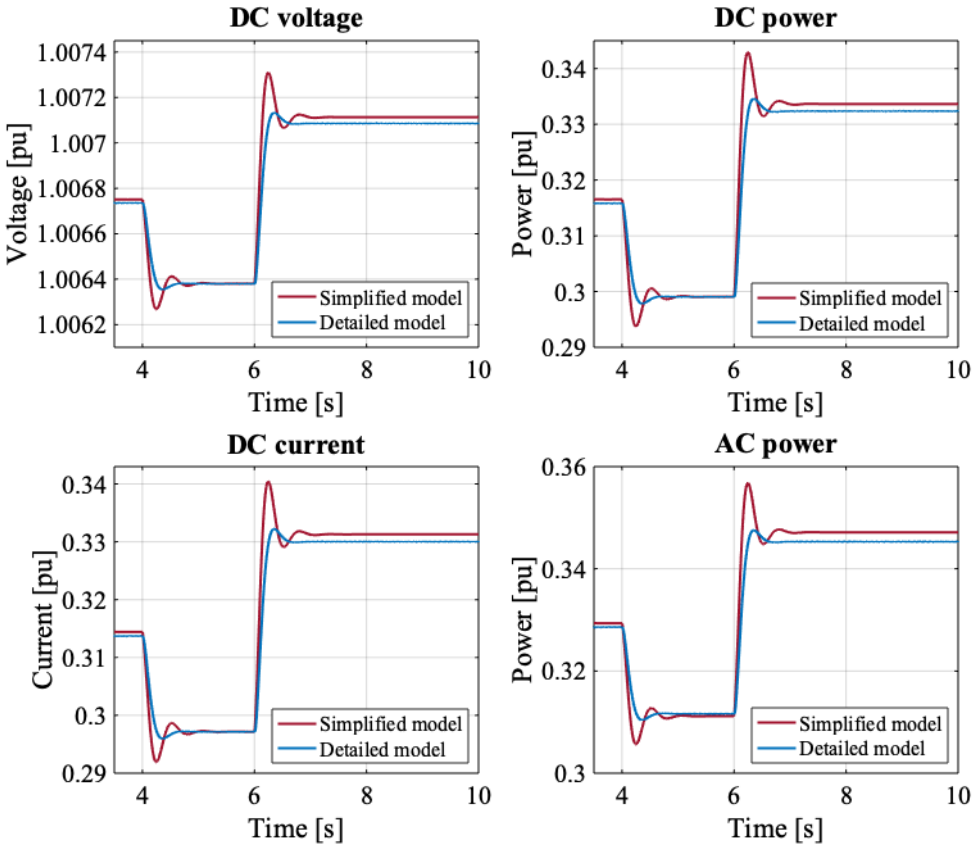

Figure 8.12: The DC Current, DC voltage, DC power and AC power responses corresponding to validation case 3, where the field voltage is stepped by $\pm 2\%$ from 1.4 pu. The applied field voltage follows the same shape as the graph shown in Figure 4.22.

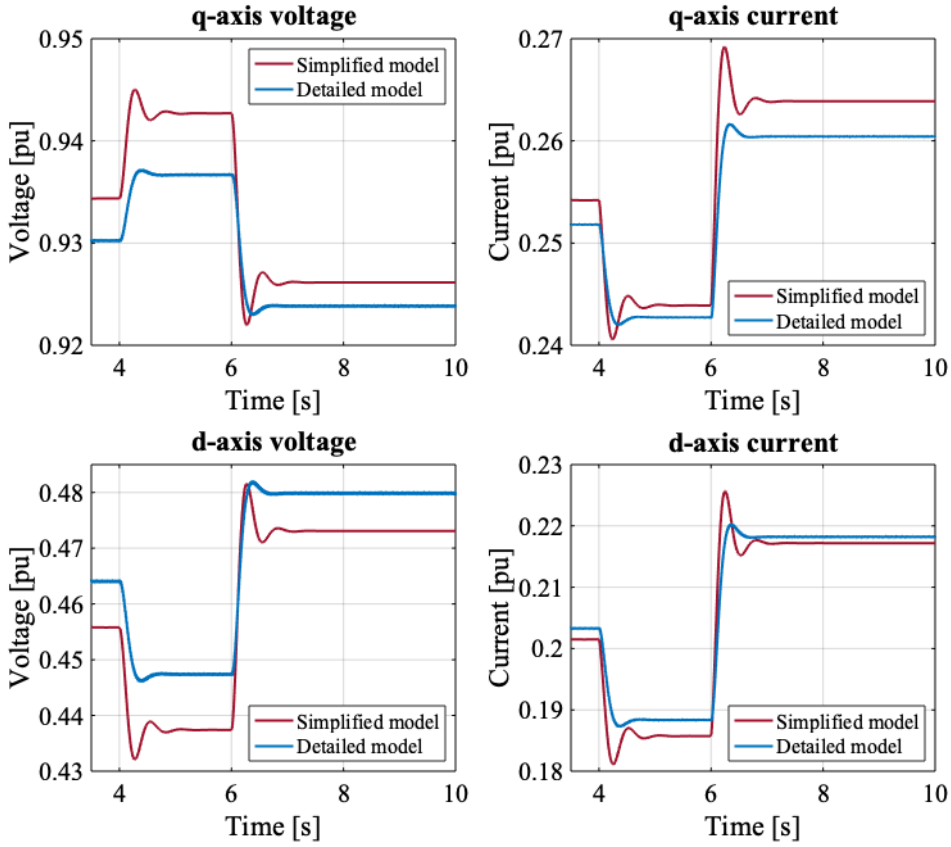

Figure 8.13: The d- and q-axis voltage and current responses corresponding to validation case 3, where the field voltage is stepped by $\pm 2\%$ from 1.4 pu. The applied field voltage follows the same shape as the graph shown in Figure 4.22.

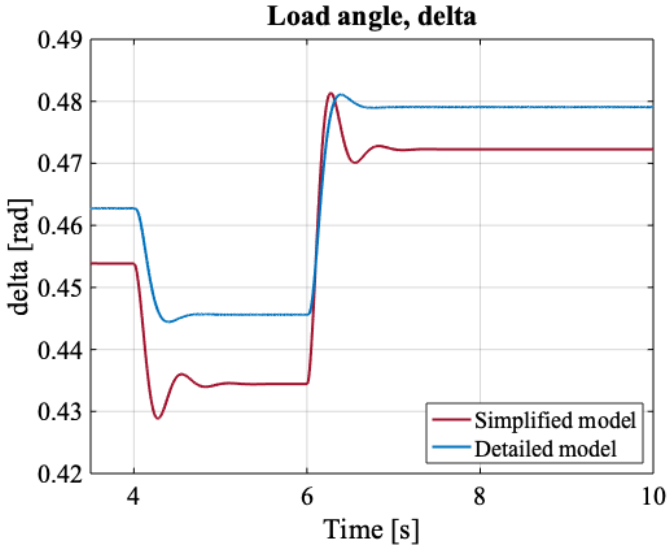

Figure 8.14: The Load angle, δ, responses corresponding to validation case 3, where the field voltage is stepped by $\pm 2\%$ from 1.4 pu. The applied field voltage follows the same shape as the graph shown in Figure 4.22.

Appendix F

Linearization of the Simplified Model

Matlab Code - Linearization and Eigenvalues Calculation

```
% ------------------------------------------
%    Linearization of the Simplified Model
%                      and
%            Eigenvalues Calculation
% ------------------------------------------
clear all
close all;
%% K_s - Scaling factor used during sensitivity analysis
%K_s = 0.90;
%K_s = 0.95;
%K_s = 1.0;
%K_s= 1.05;
%K_s = 1.10;
%% Define Symbols
syms Eq_t_dot Eq_t Eq_subt_dot Eq_subt Ed_subt_dot Ed_subt
    v_dc_dot v_dc delta_dot delta id iq vd vq;
syms alpha r_a x_d_subt x_q_subt T_do_t T_do_subt T_qo_subt x_d
     x_d_t x_q x_q_t x_q_subt c_dc beta v_bat r_bat phi vf;
%% Other equations
vd=-(v_dc*alpha)*sin(delta);
vq=(v_dc*alpha)*cos(delta);
id=(1/((r_a^2)+x_d_subt*x_q_subt))*(r_a*(Ed_subt-vd) -x_q_subt
    *(Eq_subt-vq));
iq=(1/((r_a^2)+x_d_subt*x_q_subt))*(x_d_subt*(Ed_subt-vd) +r_a
    *(Eq_subt-vq));
%% Set Kdelta
Kd=1/(0.01);
%% ODEs or f function
```

```
25 Eq_t_dot=(1/T_do_t)*(vf-Eq_t+id*(x_d-x_d_t));
26 Eq_subt_dot=(1/T_do_subt)*(Eq_t-Eq_subt+id*(x_d_t-x_d_subt));
27 Ed_subt_dot=(1/T_qo_subt)*(-Ed_subt-iq*(x_q_t-x_q_subt));
28 v_dc_dot=(1/c_dc)*(beta*sqrt((id^2)+(iq^2)) + v_bat/r_bat -v_dc
     /r_bat);
29 delta_dot=(Kd)*(-delta+asin(-id/(sqrt((id^2)+(iq^2))))-phi); %
     Kd=Kdelta=1/Tdelta
30 %% Matrix A (Jacobian)
31 A= [diff(Eq_t_dot,Eq_t) diff(Eq_t_dot,Eq_subt) diff(Eq_t_dot,
     Ed_subt) diff(Eq_t_dot,v_dc) diff(Eq_t_dot,delta)
32     diff(Eq_subt_dot,Eq_t) diff(Eq_subt_dot,Eq_subt) diff(
         Eq_subt_dot,Ed_subt) diff(Eq_subt_dot,v_dc) diff(
         Eq_subt_dot,delta)
33     diff(Ed_subt_dot,Eq_t) diff(Ed_subt_dot,Eq_subt) diff(
         Ed_subt_dot,Ed_subt) diff(Ed_subt_dot,v_dc) diff(
         Ed_subt_dot,delta)
34     diff(v_dc_dot,Eq_t) diff(v_dc_dot,Eq_subt) diff(v_dc_dot,
         Ed_subt) diff(v_dc_dot,v_dc) diff(v_dc_dot,delta)
35     diff(delta_dot,Eq_t) diff(delta_dot,Eq_subt) diff(delta_dot,
         Ed_subt) diff(delta_dot,v_dc) diff(delta_dot,delta)];
36 %% Parameter settings
37 % Nominal values %%
38 S_n = 3000000; %3 MVA
39 V_n = 690;
40 f_n = 60; %frequency
41
42 %Set operation load %%
43 P_load = 1*S_n;
44
45 % Base values %%
46 S_b = S_n;
47 V_b = V_n;
48 V_b_dc = V_b*1.35;
49 Z_b = V_n^2/S_b;
50 I_b_ac = S_n/(sqrt(3)*V_b);
51 I_b_dc =S_n/(1.35*V_b);
52 Z_b_dc = V_b_dc/I_b_dc;
53 w_sm_base = 2*pi*f_n ;
54 %% Generator parameters for SG1 [pu] %%
55 %K_scale = 0.770833333333333; %3
56 %K_scale = 0.8894230769; %2.6
```

```
%K_scale = 0.9635416667; %2.4
%K_scale = 1; %2.3125
%K_scale = 1.027778; %2.25
%K_scale = 1.4453125; %1.6
%K_scale = 1.217105263157895; %1.9
%K_scale = 2.3125; %1

r_a_val = 0.0087;
x_d_val = 2.3;
x_d_t_val = 0.4;    %K_scale;
x_d_subt_val = 0.293;
x_q_val = 1.85;
x_q_t_val = 1.8;
x_q_subt_val = 0.344;
%x_leak_val = 0.178;
T_do_t_val = 1.204;
T_do_subt_val = 0.01;
%T_qo_t_val = 0.95;
T_qo_subt_val = 0.036;
% T_d_t_val = 0.255;
% T_d_subt_val = 0.006;
% T_q_t_val = 0.95;
% T_q_subt_val = 0.007;

%%inertia, friction factor and number of pole pairs
H = 3;
p_p = 2;
f_f = 0.005;
%% Parameters DC side %%
C_dc = 20e-3*S_n*1e-6; %20 mF per 1 MW
c_dc_val = (C_dc*Z_b_dc);
R_bat = 20/I_b_dc;
r_bat_val = (R_bat/Z_b_dc);
V_bat = 1.35*V_b;
v_bat_val = V_bat/V_b_dc;
%% Stabilitycriteria %%
stability_ind = x_q_val/(x_d_t_val*2);

%% Define operating point [pu] %%

%% 1.1 - %This set corresonds to 12.5% ac load
```

```
98 % vf_val = 1.1; %set before running detailed model
99 % v_bat = 1.0; %set before running detailed model
100 % alpha_val = 1.014475; %obtained from detailed
101 % beta_val = 0.909422; %obtained from detailed
102 % phi_val = 0.17564; %obtained from detailed
103 % v_dc_val = 1.00236715; %measured from detailed
104 % i_dc_val = 0.1102275; %measured from detailed
105
106 %% 1.4 - %This set corresonds to 33% ac load
107 vf_val = 1.4; %set before running detailed model
108 v_bat_val = 1.0; %set before running detailed model
109 alpha_val = 1.03264; %obtained from detailed
110 beta_val = 0.96934; %obtained from detailed
111 phi_val = 0.2164; %obtained from detailed
112 v_dc_val = 1.006736447; %measured from detailed
113 i_dc_val = 0.313605; %measured from detailed
114
115 %% 1.8 - %This set corresonds to 55.6% ac load
116 % vf_val = 1.8; %set before running detailed model
117 % v_bat_val = 1.0; %set before running detailed model
118 % alpha_val = 1.0444; %obtained from detailed
119 % beta_val = 0.9880; %obtained from detailed
120 % phi_val = 0.2321; %obtained from detailed
121 % v_dc_val = 1.011433; %measured from detailed
122 % i_dc_val = 0.5325; %measured from detailed
123
124 %% 2.5 - %This set corresonds to 92.5% ac load
125 % vf_val = 2.5; %set before running detailed model
126 % v_bat_val = 1.0; %set before running detailed model
127 % alpha_val = 1.054975; %obtained from detailed
128 % beta_val = 1.002025; %obtained from detailed
129 % phi_val = 0.2305; %obtained from detailed
130 % v_dc_val = 1.019028449; %measured from detailed
131 % i_dc_val = 0.886167; %measured from detailed
132
133 %% Initialize state variables based on alpha, beta, phi, Idc,
    Vdc
134 %  obtained from detailed model %
135 v_ac= v_dc_val*alpha_val;
136 i_ac_mag=i_dc_val/beta_val;
137 i_ac=i_ac_mag*cos(phi_val)-i_ac_mag*sin(phi_val)*j;
```

```
138
139 EQ = v_ac+i_ac*(r_a_val+x_q_val*j);
140 delta_val=atan(imag(EQ)/real(EQ));
141 vq_val=cos(delta_val)*v_ac;
142 vd_val=-sin(delta_val)*v_ac;
143 iq_val=cos(delta_val+phi_val)*abs(i_ac);
144 id_val=-sin(delta_val+phi_val)*abs(i_ac);
145
146 %the effect of the armature reactance, ra, is neglected below
147 Eq=vq_val+x_d_val*abs(id_val); %Vf=Eq
148 Ed=vd_val+x_q_val*abs(iq_val);
149 Eq_t_val=vq_val+x_d_t_val*abs(id_val);
150 Eq_subt_val=vq_val+x_d_subt_val*abs(id_val);
151 Ed_subt_val=vd_val+x_q_subt_val*abs(iq_val);
152
153 %% simulate the model equations to avhieve better
      initialization values
154 %For the state variables (Eq , Eq   , Ed   , Vdc and delta)
      Kd=1/0.01; %Kd=Kdelta=1/Tdelta
155 dt=0.000000001; %time step
156
157 for time=1:500
158     vd_val=-(v_dc_val*alpha_val)*sin(delta_val);
159     vq_val=(v_dc_val*alpha_val)*cos(delta_val);
160     id_val=(1/((r_a_val^2)+x_d_subt_val*x_q_subt_val))*(r_a_val
          *(Ed_subt_val-vd_val) -x_q_subt_val*(Eq_subt_val-vq_val)
          );
161     iq_val=(1/((r_a_val^2)+x_d_subt_val*x_q_subt_val))*(
          x_d_subt_val*(Ed_subt_val-vd_val) +r_a_val*(Eq_subt_val-
          vq_val));
162     Eq_t_dot_val=(1/T_do_t_val)*(vf_val-Eq_t_val+id_val*(
          x_d_val-x_d_t_val));
163     Eq_subt_dot_val=(1/T_do_subt_val)*(Eq_t_val-Eq_subt_val+
          id_val*(x_d_t_val-x_d_subt_val));
164     Ed_subt_dot_val=(1/T_qo_subt_val)*(-Ed_subt_val-iq_val*(
          x_q_t_val-x_q_subt_val));
165     V_dc_dot_val=(1/c_dc_val)*(beta_val*sqrt((id_val^2)+(iq_val
          ^2)) + v_bat_val/r_bat_val -v_dc_val/r_bat_val);
166     delta_dot_val=Kd*(-delta_val+asin(-id_val/(sqrt((id_val^2)
          +(iq_val^2))))-phi_val);
167     Eq_t_val=Eq_t_val+dt*Eq_t_dot_val;
```

```
168       Eq_subt_val=Eq_subt_val+dt*Eq_subt_dot_val;
169       Ed_subt_val=Ed_subt_val+dt*Ed_subt_dot_val;
170       v_dc_val=v_dc_val+dt*V_dc_dot_val;
171       delta_val=delta_val+dt*delta_dot_val;
172       eqm(time)=Eq_t_val;
173       eqdm(time)=Eq_subt_val;
174       eddm(time)=Ed_subt_val;
175       vdc(time)=v_dc_val;
176       del(time)=delta_val;
177       power(time)=iq_val*vq_val+id_val*vd_val;
178       tt(time)=time*dt;
179       plot(tt,del,tt,eqm,tt,eqdm,tt,eddm,tt,power,tt,vdc)
180  end
181
182  V_syms=[alpha,beta,r_bat,r_a,c_dc,T_do_t,T_do_subt,T_qo_subt,
         x_d,x_d_t,x_d_subt,...
183       x_q_t,x_q_subt,Eq_subt,Ed_subt,v_dc,delta];
184  V_val=[alpha_val,beta_val,r_bat_val,r_a_val,c_dc_val,T_do_t_val
         ,T_do_subt_val,T_qo_subt_val,...
185       x_d_val,x_d_t_val,x_d_subt_val,x_q_t_val,x_q_subt_val,
             Eq_subt_val,...
186       Ed_subt_val,v_dc_val,delta_val];
187  A_mat=subs(A, V_syms, V_val);
188  A_mat_vpa=vpa(A_mat);
189  A_mat_double=double(A_mat);
190  %% Calculate eigenvalues of A (D), normalized left eigenvector
         (W) and normalized right eigenvector (V)
191  [V,D,W]=eig(A_mat_double);
192  eigVa=diag(D);
193  disp(' ')
194  disp('Eigenvalues:')
195  max_x=1;
196  min_x=0;
197  max_y=0;
198  for x=1:length(eigVa)
199       fprintf('%f%+fj\n', real(eigVa(x)), imag(eigVa(x)))
200
201       if real(eigVa(x)) > max_x
202            max_x = real(eigVa(x));
203       end
204       if real(eigVa(x)) < min_x
```

```
205             min_x = real(eigVa(x));
206         end
207         if abs(imag(eigVa(x))) > max_y
208             max_y = abs(imag(eigVa(x)));
209         end
210     end
211     figure
212     y_axis=[(-max_y-2)*j; 0j; (max_y+2)*j];
213     x_axis=[min_x-50 max_x+50];
214     plot(real(y_axis),imag(y_axis),'r','HandleVisibility','off','
        LineWidth', 1.5) %line plot
215     hold on
216     for count = 1:length(eigVa)
217         plot(real(eigVa(count)),imag(eigVa(count)),'o','LineWidth',
            2);
218         hold on;
219     end
220     axis([min_x-50 max_x+50 -max_y-2 max_y+2])
221     xlabel('Real','FontSize',20)
222     ylabel('Imaginary','FontSize',20)
223     xticks([-2700 -2500 -2000 -1500 -1000 -500 -250 -150 -50 0 50])
224     xticklabels({'-2700' '-2500' '-2000' '-1500' '-1000' '-500' '
        -250'...
225         '-150' '-50' '0' '50'})
226     grid on
227     %% %Each element in each column in W' (row in W) is scaled (
        divided) by the
228     %corresponding element in the column of diagLV.
229     %scale each left eigenvector (row) of W such that the above
        product is the identity
230     L= W';
231     diagLV=diag(L*V);
232     for k = 1:length(L)
233         L(:,k)=L(:,k)./diagLV;
234     end
235     % Equivalent method:
236     Lp = bsxfun(@rdivide,W',diag(W'*V));
237     I=L*V;
238     %% Calculating participation factors
239     %The participation factors, Pki, are used to determine how much
        the kth state variable
```

```
240 %participates in the ith mode
241 ParF=V.*L';
242 %each column in ParF should summarize to 1
243 SumColP=sum(ParF);
```

Matlab Code - Validation of State Matrix A and Eigenvalues

```
% ------------------------------------------------------
%   -- Validation of State Matrix A and Eigenvalues --

% NB! It is in advance necessary to run the Matlab code
    presented in appendix D
% ------------------------------------------------------
%clear all;
%% define the steplength dx
dx=0.000000001;

vd_val=-(v_dc_val*alpha_val)*sin(delta_val);
vq_val=(v_dc_val*alpha_val)*cos(delta_val);
id_val=(1/((r_a_val^2)+x_d_subt_val*x_q_subt_val))*(r_a_val*(
    Ed_subt-vd_val) -x_q_subt_val*(Eq_subt-vq_val));
iq_val=(1/((r_a_val^2)+x_d_subt_val*x_q_subt_val))*(
    x_d_subt_val*(Ed_subt-vd_val) +r_a_val*(Eq_subt-vq_val));
Eq_t_dot=(1/T_do_t_val)*(vf-Eq_t+id_val*(x_d_val-x_d_t_val));
Eq_subt_dot=(1/T_do_subt_val)*(Eq_t-Eq_subt+id_val*(x_d_t_val-
    x_d_subt_val));
Ed_subt_dot=(1/T_qo_subt_val)*(-Ed_subt-iq_val*(x_q_t_val-
    x_q_subt_val));
v_dc_dot=(1/c_dc_val)*(beta_val*sqrt((id_val^2)+(iq_val^2)) +
    v_bat_val/r_bat_val -v_dc_val/r_bat_val);
delta_dot=Kd*(-delta_val+asin(-id_val/(sqrt((id_val^2)+(iq_val
    ^2))))-phi_val);

Eq_t_dot0=Eq_t_dot;
Eq_subt_dot0=Eq_subt_dot;
Ed_subt_dot0=Ed_subt_dot;
v_dc_val_dot0=v_dc_dot;
delta_val_dot0=delta_dot;
%
Eq_t=Eq_t+dx;
vd_val=-(v_dc_val*alpha_val)*sin(delta_val);
vq_val=(v_dc_val*alpha_val)*cos(delta_val);
id_val=(1/((r_a_val^2)+x_d_subt_val*x_q_subt_val))*(r_a_val*(
    Ed_subt-vd_val) -x_q_subt_val*(Eq_subt-vq_val));
iq_val=(1/((r_a_val^2)+x_d_subt_val*x_q_subt_val))*(
    x_d_subt_val*(Ed_subt-vd_val) +r_a_val*(Eq_subt-vq_val));
```

```
Eq_t_dot=(1/T_do_t_val)*(vf-Eq_t+id_val*(x_d_val-x_d_t_val));
Eq_subt_dot=(1/T_do_subt_val)*(Eq_t-Eq_subt+id_val*(x_d_t_val-
    x_d_subt_val));
Ed_subt_dot=(1/T_qo_subt_val)*(-Ed_subt-iq_val*(x_q_t_val-
    x_q_subt_val));
v_dc_dot=(1/c_dc_val)*(beta_val*sqrt((id_val^2)+(iq_val^2)) +
    v_bat_val/r_bat_val -v_dc_val/r_bat_val);
delta_dot=Kd*(-delta_val+asin(-id_val/(sqrt((id_val^2)+(iq_val
    ^2))))-phi_val);
Amat(1,1)=(Eq_t_dot-Eq_t_dot0)/dx;
Amat(2,1)=(Eq_subt_dot-Eq_subt_dot0)/dx;
Amat(3,1)=(Ed_subt_dot-Ed_subt_dot0)/dx;
Amat(4,1)=(v_dc_dot-v_dc_val_dot0)/dx;
Amat(5,1)=(delta_dot-delta_val_dot0)/dx;
Eq_t=Eq_t-dx;
%
Eq_subt=Eq_subt+dx;
vd_val=-(v_dc_val*alpha_val)*sin(delta_val);
vq_val=(v_dc_val*alpha_val)*cos(delta_val);
id_val=(1/((r_a_val^2)+x_d_subt_val*x_q_subt_val))*(r_a_val*(
    Ed_subt-vd_val) -x_q_subt_val*(Eq_subt-vq_val));
iq_val=(1/((r_a_val^2)+x_d_subt_val*x_q_subt_val))*(
    x_d_subt_val*(Ed_subt-vd_val) +r_a_val*(Eq_subt-vq_val));
Eq_t_dot=(1/T_do_t_val)*(vf-Eq_t+id_val*(x_d_val-x_d_t_val));
Eq_subt_dot=(1/T_do_subt_val)*(Eq_t-Eq_subt+id_val*(x_d_t_val-
    x_d_subt_val));
Ed_subt_dot=(1/T_qo_subt_val)*(-Ed_subt-iq_val*(x_q_t_val-
    x_q_subt_val));
v_dc_dot=(1/c_dc_val)*(beta_val*sqrt((id_val^2)+(iq_val^2)) +
    v_bat_val/r_bat_val -v_dc_val/r_bat_val);
delta_dot=Kd*(-delta_val+asin(-id_val/(sqrt((id_val^2)+(iq_val
    ^2))))-phi_val);
Amat(1,2)=(Eq_t_dot-Eq_t_dot0)/dx;
Amat(2,2)=(Eq_subt_dot-Eq_subt_dot0)/dx;
Amat(3,2)=(Ed_subt_dot-Ed_subt_dot0)/dx;
Amat(4,2)=(v_dc_dot-v_dc_val_dot0)/dx;
Amat(5,2)=(delta_dot-delta_val_dot0)/dx;
Eq_subt=Eq_subt-dx;
%
Ed_subt=Ed_subt+dx;
vd_val=-(v_dc_val*alpha_val)*sin(delta_val);
```

```
vq_val=(v_dc_val*alpha_val)*cos(delta_val);
id_val=(1/((r_a_val^2)+x_d_subt_val*x_q_subt_val))*(r_a_val*(
    Ed_subt-vd_val) -x_q_subt_val*(Eq_subt-vq_val));
iq_val=(1/((r_a_val^2)+x_d_subt_val*x_q_subt_val))*(
    x_d_subt_val*(Ed_subt-vd_val) +r_a_val*(Eq_subt-vq_val));
Eq_t_dot=(1/T_do_t_val)*(vf-Eq_t+id_val*(x_d_val-x_d_t_val));
Eq_subt_dot=(1/T_do_subt_val)*(Eq_t-Eq_subt+id_val*(x_d_t_val-
    x_d_subt_val));
Ed_subt_dot=(1/T_qo_subt_val)*(-Ed_subt-iq_val*(x_q_t_val-
    x_q_subt_val));
v_dc_dot=(1/c_dc_val)*(beta_val*sqrt((id_val^2)+(iq_val^2)) +
    v_bat_val/r_bat_val -v_dc_val/r_bat_val);
delta_dot=Kd*(-delta_val+asin(-id_val/(sqrt((id_val^2)+(iq_val
    ^2))))-phi_val);
Amat(1,3)=(Eq_t_dot-Eq_t_dot0)/dx;
Amat(2,3)=(Eq_subt_dot-Eq_subt_dot0)/dx;
Amat(3,3)=(Ed_subt_dot-Ed_subt_dot0)/dx;
Amat(4,3)=(v_dc_dot-v_dc_val_dot0)/dx;
Amat(5,3)=(delta_dot-delta_val_dot0)/dx;
Ed_subt=Ed_subt-dx;
%
v_dc_val=v_dc_val+dx;
vd_val=-(v_dc_val*alpha_val)*sin(delta_val);
vq_val=(v_dc_val*alpha_val)*cos(delta_val);
id_val=(1/((r_a_val^2)+x_d_subt_val*x_q_subt_val))*(r_a_val*(
    Ed_subt-vd_val) -x_q_subt_val*(Eq_subt-vq_val));
iq_val=(1/((r_a_val^2)+x_d_subt_val*x_q_subt_val))*(
    x_d_subt_val*(Ed_subt-vd_val) +r_a_val*(Eq_subt-vq_val));
Eq_t_dot=(1/T_do_t_val)*(vf-Eq_t+id_val*(x_d_val-x_d_t_val));
Eq_subt_dot=(1/T_do_subt_val)*(Eq_t-Eq_subt+id_val*(x_d_t_val-
    x_d_subt_val));
Ed_subt_dot=(1/T_qo_subt_val)*(-Ed_subt-iq_val*(x_q_t_val-
    x_q_subt_val));
v_dc_dot=(1/c_dc_val)*(beta_val*sqrt((id_val^2)+(iq_val^2)) +
    v_bat_val/r_bat_val -v_dc_val/r_bat_val);
delta_dot=Kd*(-delta_val+asin(-id_val/(sqrt((id_val^2)+(iq_val
    ^2))))-phi_val);
Amat(1,4)=(Eq_t_dot-Eq_t_dot0)/dx;
Amat(2,4)=(Eq_subt_dot-Eq_subt_dot0)/dx;
Amat(3,4)=(Ed_subt_dot-Ed_subt_dot0)/dx;
Amat(4,4)=(v_dc_dot-v_dc_val_dot0)/dx;
```

```
91  Amat(5,4)=(delta_dot-delta_val_dot0)/dx;
92  v_dc_val=v_dc_val-dx;
93  %
94  delta_val=delta_val+dx;
95  vd_val=-(v_dc_val*alpha_val)*sin(delta_val);
96  vq_val=(v_dc_val*alpha_val)*cos(delta_val);
97  id_val=(1/((r_a_val^2)+x_d_subt_val*x_q_subt_val))*(r_a_val*(
        Ed_subt-vd_val) -x_q_subt_val*(Eq_subt-vq_val));
98  iq_val=(1/((r_a_val^2)+x_d_subt_val*x_q_subt_val))*(
        x_d_subt_val*(Ed_subt-vd_val) +r_a_val*(Eq_subt-vq_val));
99  Eq_t_dot=(1/T_do_t_val)*(vf-Eq_t+id_val*(x_d_val-x_d_t_val));
100 Eq_subt_dot=(1/T_do_subt_val)*(Eq_t-Eq_subt+id_val*(x_d_t_val-
        x_d_subt_val));
101 Ed_subt_dot=(1/T_qo_subt_val)*(-Ed_subt-iq_val*(x_q_t_val-
        x_q_subt_val));
102 v_dc_dot=(1/c_dc_val)*(beta_val*sqrt((id_val^2)+(iq_val^2)) +
        v_bat_val/r_bat_val -v_dc_val/r_bat_val);
103 delta_dot=Kd*(-delta_val+asin(-id_val/(sqrt((id_val^2)+(iq_val
        ^2))))-phi_val);
104 Amat(1,5)=(Eq_t_dot-Eq_t_dot0)/dx;
105 Amat(2,5)=(Eq_subt_dot-Eq_subt_dot0)/dx;
106 Amat(3,5)=(Ed_subt_dot-Ed_subt_dot0)/dx;
107 Amat(4,5)=(v_dc_dot-v_dc_val_dot0)/dx;
108 Amat(5,5)=(delta_dot-delta_val_dot0)/dx;
109 delta_val=delta_val-dx;
110 %
111 disp('State matrix A and corresponding eigenvalues:')
112 disp('')
113 disp(Amat)
114 eig(Amat)
```

State Matrix A

```
%% A matrix represented with syms variables column by column

%% First Column
    A(:,1)=

    -1/T_do_t,

    1/T_do_subt,

    0,

    0,

    0,


%% Second Column
    A(:,2)=

    -(x_q_subt*(x_d - x_d_t))/(T_do_t*(r_a^2 + x_d_subt*
       x_q_subt)),

    -((x_q_subt*(x_d_t - x_d_subt))/(r_a^2 + x_d_subt*x_q_subt)
        + 1)/T_do_subt,

    -(r_a*(x_q_t - x_q_subt))/(T_qo_subt*(r_a^2 + x_d_subt*
       x_q_subt)),

    (beta*((2*r_a*(r_a*(Eq_subt - alpha*v_dc*cos(delta)) +
       x_d_subt*(Ed_subt + alpha*v_dc*sin(delta))))/(r_a^2 +
       x_d_subt*x_q_subt)^2 + (2*x_q_subt*(x_q_subt*(Eq_subt -
       alpha*v_dc*cos(delta)) - r_a*(Ed_subt + alpha*v_dc*sin(
       delta))))/(r_a^2 + x_d_subt*x_q_subt)^2))/(2*c_dc*((r_a
       *(Eq_subt - alpha*v_dc*cos(delta)) + x_d_subt*(Ed_subt +
        alpha*v_dc*sin(delta)))^2/(r_a^2 + x_d_subt*x_q_subt)^2
        + (x_q_subt*(Eq_subt - alpha*v_dc*cos(delta)) - r_a*(
       Ed_subt + alpha*v_dc*sin(delta)))^2/(r_a^2 + x_d_subt*
       x_q_subt)^2)^(1/2)),
```

```
28
29      (100*(x_q_subt/(((r_a*(Eq_subt - alpha*v_dc*cos(delta)) +
           x_d_subt*(Ed_subt + alpha*v_dc*sin(delta)))^2/(r_a^2 +
           x_d_subt*x_q_subt)^2 + (x_q_subt*(Eq_subt - alpha*v_dc*
           cos(delta)) - r_a*(Ed_subt + alpha*v_dc*sin(delta)))^2/(
           r_a^2 + x_d_subt*x_q_subt)^2)^(1/2)*(r_a^2 + x_d_subt*
           x_q_subt)) - ((x_q_subt*(Eq_subt - alpha*v_dc*cos(delta)
           ) - r_a*(Ed_subt + alpha*v_dc*sin(delta)))*((2*r_a*(r_a
           *(Eq_subt - alpha*v_dc*cos(delta)) + x_d_subt*(Ed_subt +
            alpha*v_dc*sin(delta))))/(r_a^2 + x_d_subt*x_q_subt)^2
           + (2*x_q_subt*(x_q_subt*(Eq_subt - alpha*v_dc*cos(delta)
           ) - r_a*(Ed_subt + alpha*v_dc*sin(delta))))/(r_a^2 +
           x_d_subt*x_q_subt)^2))/(2*((r_a*(Eq_subt - alpha*v_dc*
           cos(delta)) + x_d_subt*(Ed_subt + alpha*v_dc*sin(delta))
           )^2/(r_a^2 + x_d_subt*x_q_subt)^2 + (x_q_subt*(Eq_subt -
            alpha*v_dc*cos(delta)) - r_a*(Ed_subt + alpha*v_dc*sin(
           delta)))^2/(r_a^2 + x_d_subt*x_q_subt)^2)^(3/2)*(r_a^2 +
            x_d_subt*x_q_subt))))/(1 - (x_q_subt*(Eq_subt - alpha*
           v_dc*cos(delta)) - r_a*(Ed_subt + alpha*v_dc*sin(delta))
           )^2/(((r_a*(Eq_subt - alpha*v_dc*cos(delta)) + x_d_subt
           *(Ed_subt + alpha*v_dc*sin(delta)))^2/(r_a^2 + x_d_subt*
           x_q_subt)^2 + (x_q_subt*(Eq_subt - alpha*v_dc*cos(delta)
           ) - r_a*(Ed_subt + alpha*v_dc*sin(delta)))^2/(r_a^2 +
           x_d_subt*x_q_subt)^2)*(r_a^2 + x_d_subt*x_q_subt)^2))
           ^(1/2),
30
31
32
33  %% Third Column
34      A(:,3)=
35
36      (r_a*(x_d - x_d_t))/(T_do_t*(r_a^2 + x_d_subt*x_q_subt)),
37
38      (r_a*(x_d_t - x_d_subt))/(T_do_subt*(r_a^2 + x_d_subt*
           x_q_subt)),
39
40      -((x_d_subt*(x_q_t - x_q_subt))/(r_a^2 + x_d_subt*x_q_subt)
            + 1)/T_qo_subt,
41
42      -(beta*((2*r_a*(x_q_subt*(Eq_subt - alpha*v_dc*cos(delta))
           - r_a*(Ed_subt + alpha*v_dc*sin(delta))))/(r_a^2 +
```

```
        x_d_subt*x_q_subt)^2 - (2*x_d_subt*(r_a*(Eq_subt - alpha
        *v_dc*cos(delta)) + x_d_subt*(Ed_subt + alpha*v_dc*sin(
        delta))))/(r_a^2 + x_d_subt*x_q_subt)^2))/(2*c_dc*((r_a
        *(Eq_subt - alpha*v_dc*cos(delta)) + x_d_subt*(Ed_subt +
         alpha*v_dc*sin(delta)))^2/(r_a^2 + x_d_subt*x_q_subt)^2
         + (x_q_subt*(Eq_subt - alpha*v_dc*cos(delta)) - r_a*(
        Ed_subt + alpha*v_dc*sin(delta)))^2/(r_a^2 + x_d_subt*
        x_q_subt)^2)^(1/2)),
43
44      -(100*(r_a/(((r_a*(Eq_subt - alpha*v_dc*cos(delta)) +
        x_d_subt*(Ed_subt + alpha*v_dc*sin(delta)))^2/(r_a^2 +
        x_d_subt*x_q_subt)^2 + (x_q_subt*(Eq_subt - alpha*v_dc*
        cos(delta)) - r_a*(Ed_subt + alpha*v_dc*sin(delta)))^2/(
        r_a^2 + x_d_subt*x_q_subt)^2)^(1/2)*(r_a^2 + x_d_subt*
        x_q_subt)) - ((x_q_subt*(Eq_subt - alpha*v_dc*cos(delta)
        ) - r_a*(Ed_subt + alpha*v_dc*sin(delta)))*((2*r_a*(
        x_q_subt*(Eq_subt - alpha*v_dc*cos(delta)) - r_a*(
        Ed_subt + alpha*v_dc*sin(delta))))/(r_a^2 + x_d_subt*
        x_q_subt)^2 - (2*x_d_subt*(r_a*(Eq_subt - alpha*v_dc*cos
        (delta)) + x_d_subt*(Ed_subt + alpha*v_dc*sin(delta))))
        /(r_a^2 + x_d_subt*x_q_subt)^2))/(2*((r_a*(Eq_subt -
        alpha*v_dc*cos(delta)) + x_d_subt*(Ed_subt + alpha*v_dc*
        sin(delta)))^2/(r_a^2 + x_d_subt*x_q_subt)^2 + (x_q_subt
        *(Eq_subt - alpha*v_dc*cos(delta)) - r_a*(Ed_subt +
        alpha*v_dc*sin(delta)))^2/(r_a^2 + x_d_subt*x_q_subt)^2)
        ^(3/2)*(r_a^2 + x_d_subt*x_q_subt))))/(1 - (x_q_subt*(
        Eq_subt - alpha*v_dc*cos(delta)) - r_a*(Ed_subt + alpha*
        v_dc*sin(delta)))^2/(((r_a*(Eq_subt - alpha*v_dc*cos(
        delta)) + x_d_subt*(Ed_subt + alpha*v_dc*sin(delta)))
        ^2/(r_a^2 + x_d_subt*x_q_subt)^2 + (x_q_subt*(Eq_subt -
        alpha*v_dc*cos(delta)) - r_a*(Ed_subt + alpha*v_dc*sin(
        delta)))^2/(r_a^2 + x_d_subt*x_q_subt)^2)*(r_a^2 +
        x_d_subt*x_q_subt)^2))^(1/2),
45
46
47  %% Fourth Column
48      A(:,4)=
49
50      ((alpha*x_q_subt*cos(delta) + alpha*r_a*sin(delta))*(x_d -
        x_d_t))/(T_do_t*(r_a^2 + x_d_subt*x_q_subt)),
51
```

```
52      ((alpha*x_q_subt*cos(delta) + alpha*r_a*sin(delta))*(x_d_t
          - x_d_subt))/(T_do_subt*(r_a^2 + x_d_subt*x_q_subt)),
53
54      -((alpha*x_d_subt*sin(delta) - alpha*r_a*cos(delta))*(x_q_t
          - x_q_subt))/(T_qo_subt*(r_a^2 + x_d_subt*x_q_subt)),
55
56      -(1/r_bat - (beta*((2*(r_a*(Eq_subt - alpha*v_dc*cos(delta)
          ) + x_d_subt*(Ed_subt + alpha*v_dc*sin(delta)))*(alpha*
          x_d_subt*sin(delta) - alpha*r_a*cos(delta)))/(r_a^2 +
          x_d_subt*x_q_subt)^2 - (2*(x_q_subt*(Eq_subt - alpha*
          v_dc*cos(delta)) - r_a*(Ed_subt + alpha*v_dc*sin(delta))
          )*(alpha*x_q_subt*cos(delta) + alpha*r_a*sin(delta)))/(
          r_a^2 + x_d_subt*x_q_subt)^2))/(2*((r_a*(Eq_subt - alpha
          *v_dc*cos(delta)) + x_d_subt*(Ed_subt + alpha*v_dc*sin(
          delta)))^2/(r_a^2 + x_d_subt*x_q_subt)^2 + (x_q_subt*(
          Eq_subt - alpha*v_dc*cos(delta)) - r_a*(Ed_subt + alpha*
          v_dc*sin(delta)))^2/(r_a^2 + x_d_subt*x_q_subt)^2)^(1/2)
          ))/c_dc,
57
58      -(100*((alpha*x_q_subt*cos(delta) + alpha*r_a*sin(delta))
          /(((r_a*(Eq_subt - alpha*v_dc*cos(delta)) + x_d_subt*(
          Ed_subt + alpha*v_dc*sin(delta)))^2/(r_a^2 + x_d_subt*
          x_q_subt)^2 + (x_q_subt*(Eq_subt - alpha*v_dc*cos(delta)
          ) - r_a*(Ed_subt + alpha*v_dc*sin(delta)))^2/(r_a^2 +
          x_d_subt*x_q_subt)^2)^(1/2)*(r_a^2 + x_d_subt*x_q_subt))
           + ((x_q_subt*(Eq_subt - alpha*v_dc*cos(delta)) - r_a*(
          Ed_subt + alpha*v_dc*sin(delta)))*((2*(r_a*(Eq_subt -
          alpha*v_dc*cos(delta)) + x_d_subt*(Ed_subt + alpha*v_dc*
          sin(delta)))*(alpha*x_d_subt*sin(delta) - alpha*r_a*cos(
          delta)))/(r_a^2 + x_d_subt*x_q_subt)^2 - (2*(x_q_subt*(
          Eq_subt - alpha*v_dc*cos(delta)) - r_a*(Ed_subt + alpha*
          v_dc*sin(delta)))*(alpha*x_q_subt*cos(delta) + alpha*r_a
          *sin(delta)))/(r_a^2 + x_d_subt*x_q_subt)^2))/(2*((r_a*(
          Eq_subt - alpha*v_dc*cos(delta)) + x_d_subt*(Ed_subt +
          alpha*v_dc*sin(delta)))^2/(r_a^2 + x_d_subt*x_q_subt)^2
          + (x_q_subt*(Eq_subt - alpha*v_dc*cos(delta)) - r_a*(
          Ed_subt + alpha*v_dc*sin(delta)))^2/(r_a^2 + x_d_subt*
          x_q_subt)^2)^(3/2)*(r_a^2 + x_d_subt*x_q_subt))))/(1 - (
          x_q_subt*(Eq_subt - alpha*v_dc*cos(delta)) - r_a*(
          Ed_subt + alpha*v_dc*sin(delta)))^2/(((r_a*(Eq_subt -
          alpha*v_dc*cos(delta)) + x_d_subt*(Ed_subt + alpha*v_dc*
```

```
        sin(delta)))^2/(r_a^2 + x_d_subt*x_q_subt)^2 + (x_q_subt
        *(Eq_subt - alpha*v_dc*cos(delta)) - r_a*(Ed_subt +
        alpha*v_dc*sin(delta)))^2/(r_a^2 + x_d_subt*x_q_subt)^2)
        *(r_a^2 + x_d_subt*x_q_subt)^2))^(1/2),
59
60
61  %% Fifth Column
62      A(:,5)=
63
64      ((alpha*r_a*v_dc*cos(delta) - alpha*v_dc*x_q_subt*sin(delta
            ))*(x_d - x_d_t))/(T_do_t*(r_a^2 + x_d_subt*x_q_subt)),
65
66      ((alpha*r_a*v_dc*cos(delta) - alpha*v_dc*x_q_subt*sin(delta
            ))*(x_d_t - x_d_subt))/(T_do_subt*(r_a^2 + x_d_subt*
            x_q_subt)),
67
68      -((alpha*v_dc*x_d_subt*cos(delta) + alpha*r_a*v_dc*sin(
            delta))*(x_q_t - x_q_subt))/(T_qo_subt*(r_a^2 + x_d_subt
            *x_q_subt)),
69
70      (beta*((2*(alpha*v_dc*x_d_subt*cos(delta) + alpha*r_a*v_dc*
            sin(delta))*(r_a*(Eq_subt - alpha*v_dc*cos(delta)) +
            x_d_subt*(Ed_subt + alpha*v_dc*sin(delta))))/(r_a^2 +
            x_d_subt*x_q_subt)^2 - (2*(alpha*r_a*v_dc*cos(delta) -
            alpha*v_dc*x_q_subt*sin(delta))*(x_q_subt*(Eq_subt -
            alpha*v_dc*cos(delta)) - r_a*(Ed_subt + alpha*v_dc*sin(
            delta))))/(r_a^2 + x_d_subt*x_q_subt)^2))/(2*c_dc*((r_a
            *(Eq_subt - alpha*v_dc*cos(delta)) + x_d_subt*(Ed_subt +
             alpha*v_dc*sin(delta)))^2/(r_a^2 + x_d_subt*x_q_subt)^2
             + (x_q_subt*(Eq_subt - alpha*v_dc*cos(delta)) - r_a*(
            Ed_subt + alpha*v_dc*sin(delta)))^2/(r_a^2 + x_d_subt*
            x_q_subt)^2)^(1/2)),
71
72      -(100*((alpha*r_a*v_dc*cos(delta) - alpha*v_dc*x_q_subt*sin
            (delta))/(((r_a*(Eq_subt - alpha*v_dc*cos(delta)) +
            x_d_subt*(Ed_subt + alpha*v_dc*sin(delta)))^2/(r_a^2 +
            x_d_subt*x_q_subt)^2 + (x_q_subt*(Eq_subt - alpha*v_dc*
            cos(delta)) - r_a*(Ed_subt + alpha*v_dc*sin(delta)))^2/(
            r_a^2 + x_d_subt*x_q_subt)^2)^(1/2)*(r_a^2 + x_d_subt*
            x_q_subt)) + (((2*(alpha*v_dc*x_d_subt*cos(delta) +
            alpha*r_a*v_dc*sin(delta))*(r_a*(Eq_subt - alpha*v_dc*
```

```
cos(delta)) + x_d_subt*(Ed_subt + alpha*v_dc*sin(delta))
))/(r_a^2 + x_d_subt*x_q_subt)^2 - (2*(alpha*r_a*v_dc*
cos(delta) - alpha*v_dc*x_q_subt*sin(delta))*(x_q_subt*(
Eq_subt - alpha*v_dc*cos(delta)) - r_a*(Ed_subt + alpha*
v_dc*sin(delta))))/(r_a^2 + x_d_subt*x_q_subt)^2)*(
x_q_subt*(Eq_subt - alpha*v_dc*cos(delta)) - r_a*(
Ed_subt + alpha*v_dc*sin(delta))))/(2*((r_a*(Eq_subt -
alpha*v_dc*cos(delta)) + x_d_subt*(Ed_subt + alpha*v_dc*
sin(delta)))^2/(r_a^2 + x_d_subt*x_q_subt)^2 + (x_q_subt
*(Eq_subt - alpha*v_dc*cos(delta)) - r_a*(Ed_subt +
alpha*v_dc*sin(delta)))^2/(r_a^2 + x_d_subt*x_q_subt)^2)
^(3/2)*(r_a^2 + x_d_subt*x_q_subt))))/(1 - (x_q_subt*(
Eq_subt - alpha*v_dc*cos(delta)) - r_a*(Ed_subt + alpha*
v_dc*sin(delta)))^2/(((r_a*(Eq_subt - alpha*v_dc*cos(
delta)) + x_d_subt*(Ed_subt + alpha*v_dc*sin(delta)))
^2/(r_a^2 + x_d_subt*x_q_subt)^2 + (x_q_subt*(Eq_subt -
alpha*v_dc*cos(delta)) - r_a*(Ed_subt + alpha*v_dc*sin(
delta)))^2/(r_a^2 + x_d_subt*x_q_subt)^2)*(r_a^2 +
x_d_subt*x_q_subt)^2))^(1/2) - 100,
```

Appendix G

The Impact of a Counter Voltage

The Absence of a Counter voltage

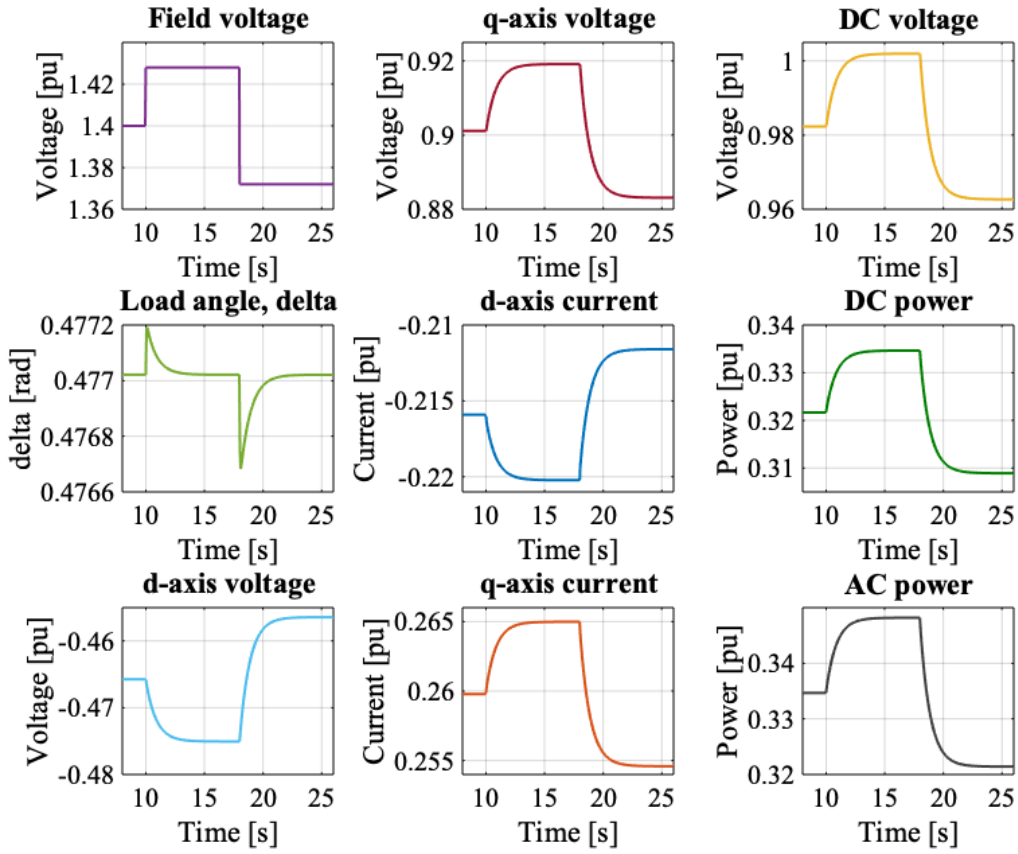

Figure 8.15: Simulation response variables corresponding to examination of case 2 presented in Section 4.7, studying the impact of a counter voltage. This figure represents the outputs measured when the simplified model operates with the absence of a counter voltage.

The Presence of a Counter voltage

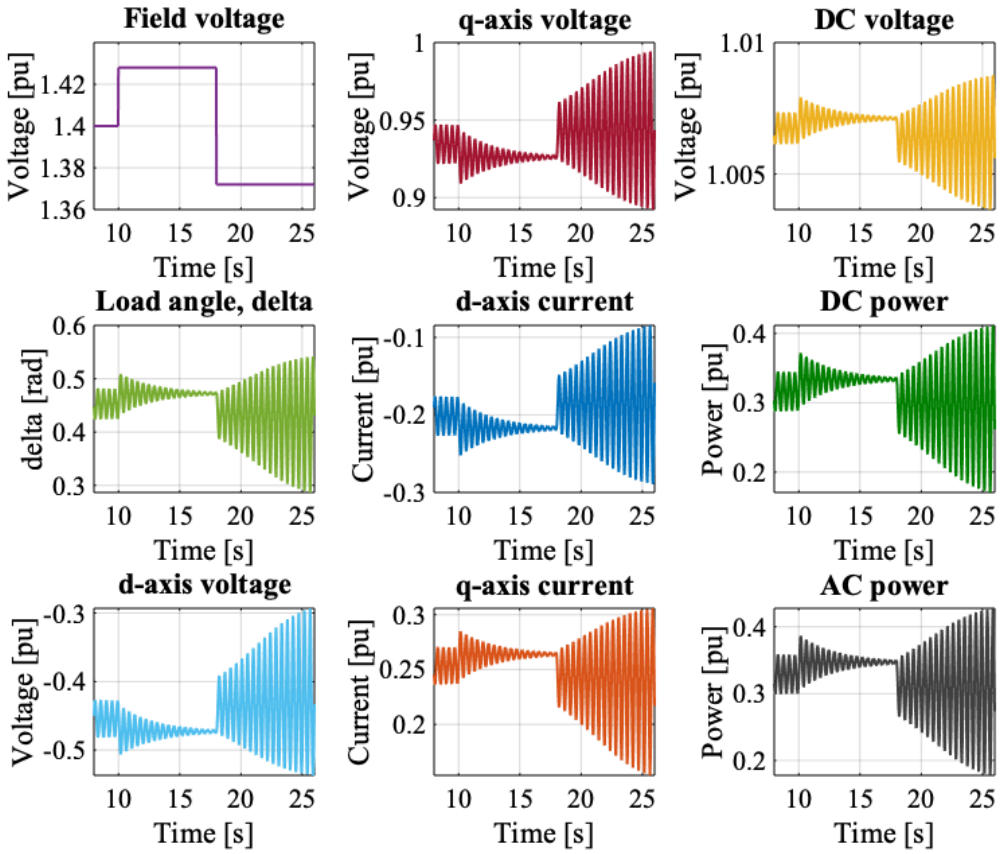

Figure 8.16: Simulation response variables corresponding to examination of case 2 presented in Section 4.7, studying the impact of a counter voltage. This figure represents the outputs measured when the simplified model operates with the presence of a counter voltage.

Appendix H

The Impact of a Three-Phase Diode-Bridge Rectifier

The Absence of a Three-Phase Diode-Bridge Rectifier

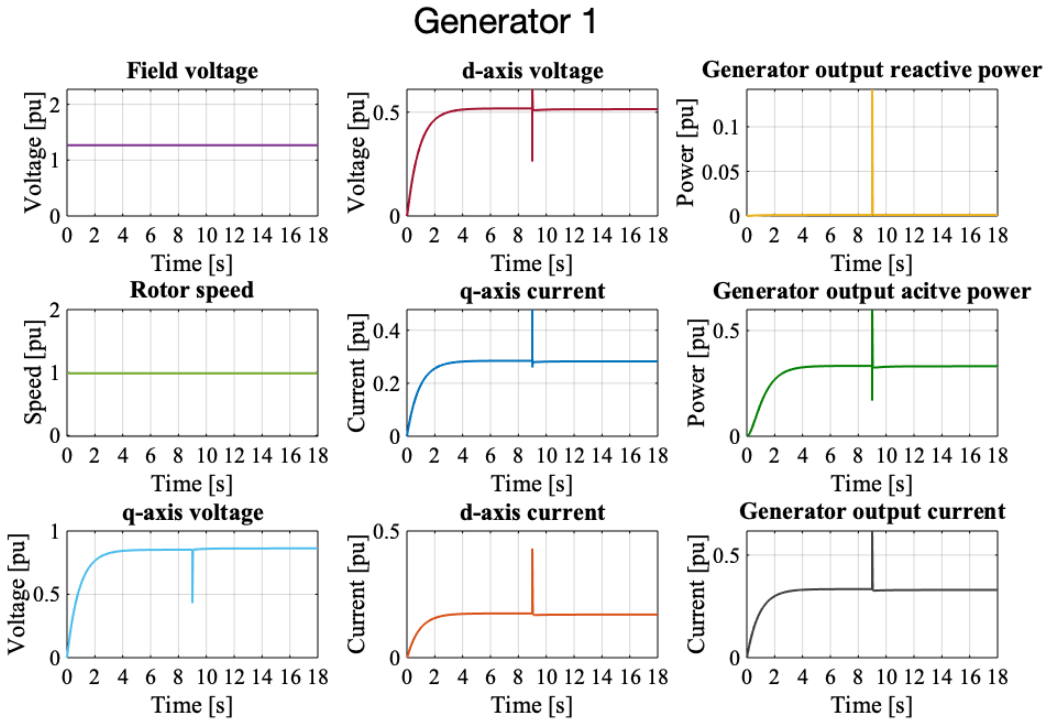

Figure 8.17: Simulation response variables corresponding to the first part of simulation case 3, for the first generator variables. The generators power a common resistive three-phase AC load and the system operates with the absence of three-phase diode bridge rectifiers. A negative 2% step in load is applied at $t = 9$ s.

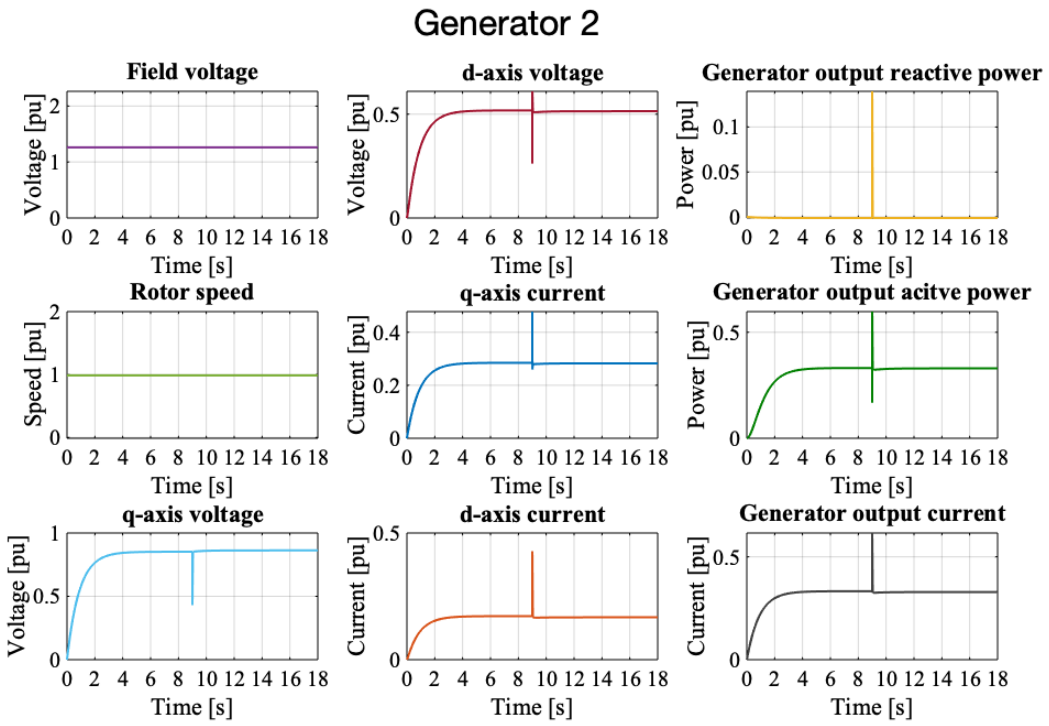

Figure 8.18: Simulation response variables corresponding to the first part of simulation case 3, for the second generator variables. The generators power a common resistive three-phase AC load and the system operates with the absence of three-phase diode bridge rectifiers. A negative 2% step in load is applied at $t = 9$ s.

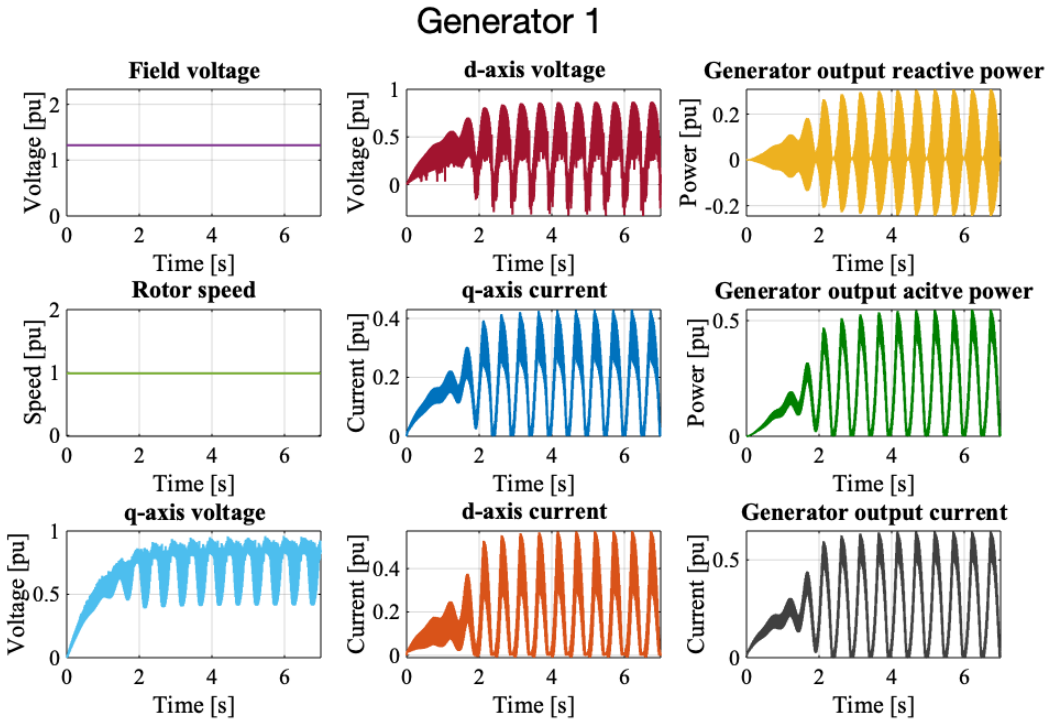

Figure 8.19: Simulation response variables corresponding to the second part of simulation case 3, for the first generator variables. Each of the generators are connected to a three-phase diode-bridge rectifier which further powers a common resistive DC load.

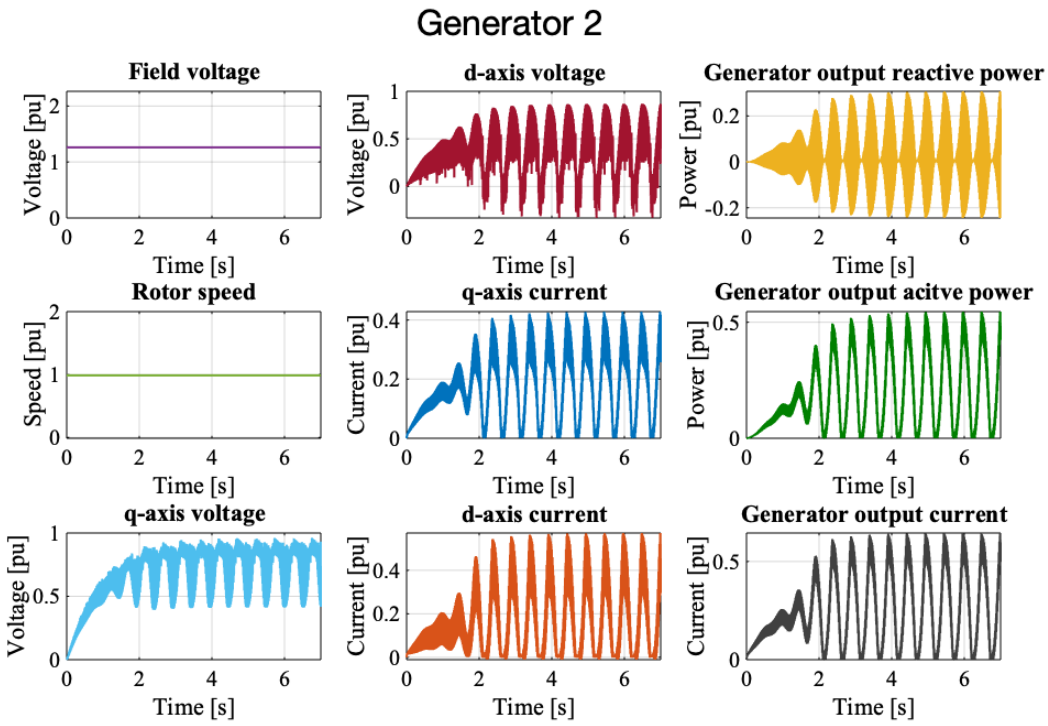

Figure 8.20: Simulation response variables corresponding to the second part of simulation case 3, for the second generator variables. Each of the generators are connected to a three-phase diode-bridge rectifier which further powers a common resistive DC load.

Trude Birgitte Byre

Modelling and Stability Analysis of Diode-Bridge Rectifier-Synchronous Generator Systems

NTNU
Norwegian University of
Science and Technology